Modeling and analyzing the effects and feedbacks of irrigation on land-atmosphere interaction
-
Using a regional climate model up to convection-permitting scale

Dissertation

zur Erlangung des Doktorgrades
an der Fakultät für Mathematik, Informatik und
Naturwissenschaften Fachbereich Erdsystemwissenschaften
der Universität Hamburg

vorgelegt von
Christina Pop, geb. Asmus
aus Primalkinskoje, Russland

30. September 2025

Fachbereich Erdsystemwissenschaften

Datum der Disputation:	11.09.2025
Gutachter/innen der Dissertation:	Prof. Dr. Jürgen Böhner
	Dr. Diana Rechid
Zusammensetzung der Prüfungskommission:	Prof. Dr. Jürgen Böhner
	Dr. Diana Rechid
	Prof. Dr. Udo Schickhoff
	Prof. Dr. Johanna Baehr
	Prof. Dr. Bernd Leitl
Vorsitzender des Fach-Promotionsausschusses Erdsystemwissenschaften:	Prof. Dr. Hermann Held
Dekan der Fakultät MIN:	Prof. Dr. Ing. Norbert Ritter

Acknowledgments

On the long journey of this thesis, I faced multiple challenges which ones might not have been feasible without the support and help of many people, to whom I want to express my deepest gratitude.

First of all and foremost, I would like to express my deepest gratitude to both of my supervisors, *Diana Rechid* and *Jürgen Böhner*. Thank you both for your exceptional scientific and personal guidance, your availabilities, constant support and patience.

I am also sincerely grateful to *Joni Pekka-Pietikäinen* for all the technical help, moral support, and answering patiently all my questions about the model. Many thanks go also to *Peter Hoffmann*, my project colleague, for the scientific advice, the many fruitful discussions, and the constant support. I further want to thank *Lars Buntemeyer* for the preparation of data and the support in publishing code and data. I also thank *Annika Nolte* for our energizing lunch and coffee breaks at the Chilehaus that brightened my days. I am also grateful to my former project colleague *Vanessa Reinhart* for introducing me to all the GERICS workflows. I want to express my gratitude to my former professor *Heinke Schlünzen* for introducing me to the world of science already early during my studies and laying the foundation for my understanding of climate modeling.

Many thanks go also to my friends and family! Thank you *Gisa Trautmann, Ge Cheng, Vivien Voss* and *Sonja Deckwart* for your companionship and being a welcome source of distraction and always helping me find a peace of mind. Thank you *Anastasia, Regina, Mom*, *Dad* and *Auntie Lydia* for believing in me and for your endless support.

Above all, a special thanks goes to my husband, *Corin Pop* for enduring my unavailabilities, panicked moments, and countless frustrations throughout this journey. Your endless patience, encouragement, and emotional strength carried me through the hardest times. Thank you for always knowing how to cheer me up when I needed it most.

Abstract

With land use practices humans alter the biophysical and biogeochemical properties of the land surface. A widely applied land use practices in agriculture is irrigation, which aims for improved growth conditions of crops by increasing the soil moisture. Multiple studies have investigated irrigation effects on both the global and regional scale. Often these studies focus on large-scale irrigated areas such as in India, China or in the US. However, there is a lack of studies investigating the effects of small-scale irrigation, particularly in regions with heterogeneous land cover such as Europe. Here, regional climate models (RCMs) have the advantage of their high spatial resolution. Within the last decade, various RCMs have received irrigation parameterizations, which are governed by the model's characteristics.

Against this background, this cumulative dissertation targets at the development, implementation and application of a novel irrigation parameterization for the new version of the RCM REMO2020, interactively coupled to its vegetation module iMOVE. This model setup enables the interaction of irrigation effects and feedbacks between soil, atmosphere and vegetation processes. With the advancements in climate modeling towards higher resolutions, the parameterization should be applicable to high resolution. Therefore, a subgrid-scale approach with a separate irrigated fraction is realized, which represents the heterogeneous soil moisture distribution caused by irrigation. The newly developed parameterization increases the soil moisture directly if irrigation is required during the growing season. Irrigation requirement is assessed based on a user-defined irrigation threshold. For the water application three different schemes can be selected, depending on the research aim.

The irrigation parameterization is applied and evaluated in two consecutive, largely complementary simulation studies. In the first study, the newly developed irrigation parameterization is applied at 0.11° horizontal resolution for the case study area of South-Western Europe, with a focus on the Po Valley in Northern Italy as one of the most irrigated areas in Europe. Reanalysis-driven simulations are conducted for the year 2017, a year characterized by multiple heatwaves, with and without the irrigation parameterization. The application

of the irrigation parameterization with the consequent increase of soil moisture causes effects and feedbacks on land, atmosphere and vegetation. For example, the surface energy balance shows an increased latent heat flux and a decreased sensible heat flux. Furthermore, higher evapotranspiration rates increase the 2 m relative humidity and lowers the 2 m mean temperature. The results indicate that irrigation has the ability to reduce the intensity of heatwaves. Vegetation processes strongly depend on the soil moisture and the 2 m temperature. The results show the LAI responds to irrigation with a slower growth, but a higher LAI peak.

The second study employs the non-hydrostatic version of REMO2020-iMOVE with the irrigation parameterization at convection-permitting scale (0.0275°) for a case study around the Po Valley. The simulations are nested into the simulations at 0.11° horizontal resolution from the first study, using the same irrigation settings and the same period, making them comparable. The higher resolution at 0.0275° allows for a more accurate representation of land surface features, such as topography and irrigated areas, resulting in more grid cells with higher irrigated fractions. This leads to more localized and more pronounced air temperature effects at 0.0275° horizontal resolution. Irrigation effects on vegetation develop similarly at both resolutions. However, the interactive coupling makes them sensitive to changes in atmospheric conditions due to the different resolutions. In particular, precipitation is represented differently at both resolutions. The diurnal cycle of precipitation is improved at convection-permitting resolution compared to observational values. Furthermore, irrigation effects on precipitation develop very different at 0.11° and at 0.0275° horizontal resolution. While at 0.11° horizontal resolution, irrigation leads to precipitation increase at the border of the Alps, but inhibits convection above irrigated areas, at 0.0275° the effects on precipitation are characterized with small-scale features and mixed signals. In total, at convection-permitting scale irrigation leads to a precipitation reduction.

Zusammenfassung

Der Mensch verändert durch Landnutzung die biophysikalischen und biogeochemischen Eigenschaften der Landoberfläche. Bewässerung ist solch eine Landnutzung, die global weit verbreitet ist und auf verbesserte Wachstumsbedingungen abzielt. Dabei erhöht Bewässerung die Bodenfeuchte. Einige Studien untersuchen den Effekt von Bewässerung auf globaler sowie auf regionaler Skala. Hierbei liegt oftmals der Fokus auf großflächig bewässerten Regionen wie in Indien, China oder den USA. Jedoch ist beispielsweise Europa von kleinflächigeren bewässerten Anbauflächen geprägt, deren Bewässerungseffekte bisher in nur wenigen Studien analysiert wurden. Hierfür eignen sich insbesondere regionale Klimamodelle, da sie eine hohe Auflösung erreichen. Im letzten Jahrzehnt wurden verschiedene Bewässerungsparametrisierungen in regionale Klimamodelle implementiert. Diese sind vor allem von den individuellen Modellcharakteristika abhängig.
Vor diesem Hintergrund soll in dieser kumulativen Dissertation die Entwicklung, Implementierung und Anwendung einer neuen Bewässerungsparametrisierung für die das regionale Klimamodell REMO2020 durchgeführt werden. REMO2020 ist dabei mit dem Vegetationsmodul iMOVE interaktiv gekoppelt, um so Bewässerungseffekte und mögliche Rückwirkungen zwischen dem Boden, der Vegetation und der Atmosphäre zu qunatifizieren. Zudem soll die Bewässerungsparametrisierung auch für hochaufgelöste Studien geeignet sein. Daher wurde sie mit einem subskaligen Ansatz verwirklicht, der einen separaten, bewässerten Gitterzellenanteil in das Modell implementiert. Die Parametrisierung erhöht die Bodenfeuchte während der Wachstumsperiode, wenn Bewässerung notwendig ist. Dieses wird über die Nutzer-spezifische Einstellung der Bewässerungsgrenze für Bodenfeuchte definiert. Weiterhin besteht die Parametrisierung aus drei verschiedenen Wasserverteilungsschemen, die für unterschiedliche Bewässerungsstudien verwendet werden können.
Die neu-entwickelte Parametrisierung wird in zwei aufeinander aufbauenden Studien angewandt. In der ersten Studie werden Simulationen für Südwest-Europa, mit dem Fokus auf das Po-Tal in Norditalien als eine der am intensivsten bewässerten Anbauregionen Europas, auf einer horizontalen Auflösung von 0.11°

durchgeführt. Die Simulationen werden von Reanalysedaten angetrieben und simulieren das Jahr 2017, das von mehreren Hitzewellen geprägt war. Um den Effekt von Bewässerung zu quantifizieren, werden Simulationen mit und ohne Bewässerungsparametrisierung durchgeführt. Die erhöhte Bodenfeuchte durch Bewässerung führt zu Effekten und Rückwirkungen zwischen Boden, Vegetation und Atmosphäre. So verändert Bewässerung die Bodenenergiebilanz durch einen erhöhten latenten, turbulenten Wärmefluss und einen verringerten fühlbaren, turbulenten Wärmefluss. Die verstärkte Evapotranspiration führt zu einem Anstieg der 2 m relativen Luftfeuchte und einem Kühlungseffekt der 2 m Temperatur. Der Kühlungseffekt birgt Mitigationspotential für Hitzewellen. In REMO2020-iMOVE sind Vegetationsprozesse stark Bodenfeuchte- und Lufttemperatur-abhängig. Durch den Abkühlungseffekt entwickelt sich daher der LAI langsamer in den Simulationen mit Bewässerung, erreicht jedoch einen höheren Maximalwert.
In der zweiten Studie wird die nicht-hydrostatische Version von REMO2020-iMOVE mit der Bewässerungsparametrisierung auf konvektionsauflösender Skala (0.0275°) angewandt. Der Fokus liegt auf dem Po-Tal. Die Simulationen werden in die Simulationen auf 0.11° Auflösung aus der ersten Studie eingebunden und verwenden die gleichen Bewässerungseinstellungen. Damit sind die beide Studien vergleichbar. Die höhere Auflösung von 0.0275° führt zu einer realistischeren Abbildung der Topografie sowie der bewässerten Flächen, die mit einer erhöhten Anzahl an Gitterzellen mit einem erhöhten Bewässerungsanteil auffällt. Dieser Effekt führt zu lokalisierten und stärker ausgeprägten Bewässerungseffekten auf 0.0275° horizontaler Auflösung verglichen zu 0.11°. Bewässerungseffekte auf die Vegetation entwickeln sich auf beiden Auflösungen ähnlich. Die interaktive Kopplung führt jedoch dazu, dass sich Unterschiede in atmosphärischen Prozessen auch auf die Vegetationsprozesse auswirken. Insbesondere der Niederschlag zeigt große Unterschiede, wie beispielsweise im Tagesgang, der in den konvektionsauflösenden Simulationen näher an den Beobachtungen liegt als der Tagesgang auf 0.11°. Weiterhin sind die Bewässerungseffekte auf den Niederschlag stark auflösungsabhängig. So erhöht sich der Niederschlag an den Alpenrändern auf 0.11° horizontaler Auflösung, wohingegen er sich über dem Po-Tal in den konvektionsauflösenden Simulationen verringert.

Content Of The Unifying Essay

List of Figures

Acronyms

CAPE	Convective Available Potential Energy
CIN	Convective Inhibition
CORDEX	Coordinated Downscaling Experiments
ESA CCI	European Space Agency Climate Change Initiative
FPS	Flagship Pilot Study
GAR	Greater Alpine Region
GCM	General Circulation Model
GERICS	Climate Service Center Germany
GMIA	Global Map of Irrigated Areas
HICSS	Helmholtz Institute for Climate Service Science
iMOVE	interactive MOsaic-based VEgetation module
IPCC	Intergovernmental Panel on Climate Change
LAI	Leaf Area Index
LIAISE	Land Surface Interactions with the Atmosphere over the Iberian Semi-arid Environme
LSM	Land Surface Model
LT	Local Time
LUCAS	Land Use and Climate Across Scales
LULCC	Land Use and Land Cover Change
NPP	Net Primary Production
PFT	Plant Functional Type
RAPID	Regional Advection Perturbations in an Irrigated Desert
RCM	Regional Climate Model
REMO	REgional Climate MOdel
RG	Research Gap
RQ	Research Question
SGAR	Smaller Greater Alpine Region

1 Introduction

1.1 Motivation

In 2019, the IPCC released the "Special Report on Climate Change and Land" highlighting the crucial role of land in the context of climate change (IPCC, 2019). Land use and land cover change (LULCC) is considered an anthropogenic forcing, which affects the regional climate through biogeochemical and biophysical effects (IPCC, 2019). Through energy and mass exchange, anthropogenic modifications of the land surface cause effects and feedbacks in the climate system. Modeling studies on different scales aim to quantify LULCC effects and feedbacks. It was shown that at local and regional scale, LULCC effects can be of comparable magnitude to the greenhouse gas forcing (de Noblet-Ducoudré et al., 2012). However, there is still large uncertainty in the sign and the magnitude of these effects between models, underlining the need for further research and improvement in modeling LULCC (de Noblet-Ducoudré et al., 2012). LULCC can be divided into land use change, referring to land surface modifications within the same land cover including various agricultural land use practices, and into land cover change, referring to conversions of the land cover (Luyssaert et al., 2014). While numerous studies focus on combined effects of LULCC or exclusively on land cover changes, research revealed that land use practices can affect climate variables in the same magnitude as land cover changes and therefore, need to be considered in earth system studies (Luyssaert et al., 2014). Many land use practices have the potential to be implemented into Earth system models (Pongratz et al., 2018), and incorporate not just another physical process in the model, but a human activity and an additional anthropogenic forcing. Through land use practices, humans adapt agriculture to unsuitable climatic conditions. Multiple studies analyzed the role of different land use practices as adaptation measures to climate change (Cotera et al., 2024, Martínez-Mena et al., 2020, Smith et al., 2020). Moreover, the effects and feedbacks of land use practices might have a potential to contribute to climate change mitigation (Sha et al., 2022, Shukla et al., 2019, Smith et al., 2020), which emphasizes the urgent need to understand the physical processes driving these interactions.
regional climate models (RCMs) are a valuable tool to investigate land-atmosphere

interactions at high resolution focusing on regional and local effects and feedbacks. Their ability to couple land and atmospheric processes and to resolve regionally and locally specific features enable the quantification of alterations in the regional climate system. For contributing to a better understanding of the effects and feedbacks of LULCCs in the regional climate system, the Flagship Pilot Study (FPS) Land Use and Climate Across Scales (LUCAS) was endorsed by the World Climate Research Program (WCRP) Coordinated Regional Climate Downscaling Experiments (CORDEX) (Rechid et al., 2017), conducting coordinated, high-resolution simulations with multiple RCMs for different LULCC scenarios in Europe. Closely linked to LUCAS is the project "Modelling human LAND surface modifications and its feedbacks on local and regional cliMATE" (LANDMATE), in which this thesis is embedded. LANDMATE was carried out by the Helmholtz Institute for Climate Service Science (HICSS), a cooperation between the Climate Service Center Germany (GERICS) and the Universität Hamburg. The goal of LANDMATE was to address research gaps in modeling LULCC with the focus on RCM studies. While the human influence on aerosols and GHG are well represented in RCM studies with suitable, harmonized datasets and parameterizations (e.g. MACv2-SP, a parameterization for aerosol forcing by Stevens et al. (2017)), the implementation of harmonized LULCC in RCMs received less attention. Therefore, LANDMATE aims for improving the representation of the land surface in regional climate modeling by developing tailored and evaluated datasets for RCMs (Hoffmann et al., 2023, Reinhart et al., 2022) and by developing parameterizations for representing land use practices in regional climate modeling. Implementing land use practices in an RCM has the potential to reduce biases in heavily managed regions and, thereby, enhances the accuracy of the simulation results. The analysis and quantification of the effects and feebacks of these land use practices provide insight in their role in the regional climate system and their potential as mitigation measure.

One of the most widely applied land use practices is irrigation. More than 20% of the global cultivated area is irrigated, contributing to approximately 40% of the total food production (Siebert and Doell, 2010). These numbers underline the crucial role of irrigation not only for our earth system, but also for society. Irrigation is a vast research topic. It is studied on different scales and by different

disciplines. Global studies underline the regional differences of irrigation effects (Puma and Cook, 2010, Singh et al., 2018, Thiery et al., 2017) and possible remote effects (de Vrese et al., 2016). Often large-scale irrigated areas in India (Chou et al., 2018, de Vrese et al., 2016, Saeed et al., 2009, Tuinenburg et al., 2014), the North China Plain (Kang and Eltahir, 2018, Wu et al., 2018, Yuan et al., 2023), or the Great Plains in the US (Huber et al., 2014, Yang et al., 2019) are selected case study areas. However, the effects of small-scale irrigation in heterogeneous agricultural areas such as in Europe received only little attention. Different studies implemented irrigation parameterizations into RCMs, for instance Branch et al. (2014), Kueppers et al. (2007), Saeed et al. (2009), Valmassoi et al. (2020*a*), Wu et al. (2018). However, the soil and surface heterogeneity was often neglected (McDermid et al., 2023), as many parameterizations operate at grid cell level. While for large-scale irrigation areas this approach is suitable, small-scale irrigation areas are characterized by heterogeneous soil moisture conditions, leading to subsequently highly variable effects between soil-surface-atmosphere and if included vegetation. Accounting for this heterogeneity provides an opportunity to capture small-scale effects and feedbacks of irrigation within the regional climate system.

Another challenge in modeling irrigation is the inclusion of interactive vegetational processes (McDermid et al., 2023), which enable the investigation of interactions between vegetation, soil and atmosphere. Irrigation is applied to improve growth conditions of plants, and has therefore a direct effect on vegetational processes. Multiple vegetational processes are highly dependent on water availability (Brouwer and Heibloem, 1986) and respond immediately to water conditions. Furthermore, vegetational processes, for instance transpiration and plant growth, subsequently influence atmospheric processes with biophysical and biogeochemical effects, leading to feedbacks between the soil, vegetation and atmosphere (Brovkin, 2002). While irrigation studies with LSMs link irrigation closely to the crop cycle and to crop development (de Vrese et al., 2016, Ozdogan et al., 2010, e.g.), there is a lack of irrigation studies with RCMs, which incorporate interactive vegetation schemes, although irrigation is applied to improve the growth conditions of plants.

With the advances in regional climate modeling to increase the horizontal reso-

lution up to convection-permitting scale (< 4 km), a new modeling setup is established, which applies the benefits of explicitly resolved convection to climate time scales (Ban et al., 2021). Modeling irrigation at convection-permitting scale with RCMs enables the investigation of irrigation effects on resolved convection processes, which were parameterized on coarser resolution leading to uncertain feedback, particularly in precipitation. Additionally, the high resolution of the convection-permitting scale represents topographic and land surface features with higher precision compared to the coarse resolution, and therefore, influences directly the modeling of irrigation areas and land-atmosphere interactions.
Summarized the research gaps (RG) addressed in this work are

- *RG1*: There is a lack of irrigation modeling studies addressing small-scale irrigation in heterogeneous areas such as in Europe with irrigation parameterizations.

- *RG2*: In irrigation studies with RCMs, interactive vegetational processes are not sufficiently represented.

- *RG3*: There are just a few RCM studies investigating irrigation effects and feedbacks at convection-permitting scale.

1.2 Objectives

In line with the aims of LUCAS and LANDMATE, the overall objective of this work is to improve the land surface representation in RCMs by including human land surface modifications. This work focuses on irrigation as example for land use practice. While multiple RCMs received an irrigation parameterization in recent years (e.g. WRF by Valmassoi et al. (2020*a*), RegCM by Marcella and Eltahir (2014)), the REgional CLimate model REMO lacks a suitable irrigation parameterization. REMO is the RCM hosted by GERICS ((Jacob and Podzun, 1997), section 2.3). Previously, irrigation was tested with REMO by Saeed et al. (2009) for a case study in South Asia. However, in the past years, major effort has been made to develop REMO further (Pietikäinen et al., 2025) and allow for more sophisticated parameterization approaches, which address the research

gaps identified in section 1.1. For instance, REMO received a dedicated vegetation module named iMOVE, which can be interactively coupled (Wilhelm et al., 2014). Furthermore, REMO received a non-hydrostatic dynamical core, which is able to explicitly resolve convection (Goettel, 2009). In this context, the first objective of this work is to develop a new irrigation parameterization for REMO2020-iMOVE suitable for high-resolution studies, its implementation and its tests. The second objective aims to quantify irrigation effects and feedbacks on soil-vegetation-atmosphere interactions affecting the regional and local climate, and to investigate their interconnected physical processes. The third objective is the application of the irrigation parameterization in simulations at convection-permitting scale, the highest resolution of the RCM REMO2020, and to assess the role of resolution in representing irrigation effects in a fully coupled soil-vegetation-atmosphere system.

1.3 Research questions

Governed by the research gaps identified in section 1.1 and the research objectives from section 1.2 three research questions (RQ) emerge for this dissertation:

RQ1: How can irrigation be represented in a regional climate model for high-resolution studies?
Based on the knowledge of existing irrigation parameterizations, a new irrigation parameterization should be developed for the RCM REMO2020. For incorporating vegetational processes, REMO2020 will be interactively coupled to its vegetation module iMOVE. For the development of an irrigation parameterization, it has to be assessed, which components of the regional climate system are addressed by irrigation, which additional data is required and how it has to be processed, and how the irrigation process can be represented in the RCM. Moreover, the irrigation parameterization should be applicable for high-resolution studies in heterogeneous areas.

RQ2: What are the effects and feedbacks of irrigation on soil-vegetation-atmosphere interaction and can they influence climate extreme events?

For a selected case study the newly developed irrigation parameterization is applied, and the effects and feedbacks of irrigation on soil-vegetation-atmosphere interactions are investigated. Analyzing the effects and feedbacks on land-atmosphere interaction under extreme climatic conditions, such as heatwaves, quantifies the mitigation potential of irrigation.

RQ3: What is the role of resolution in modeling irrigation effects up to convection-permitting scale using a coupled regional climate model system?
The irrigation parameterization is applied to simulations at convection-permitting scale (< 4 km) using REMO2020-iMOVE with the non-hydrostatic dynamical core. The resulting irrigation effects on soil, atmosphere and vegetation at convection-permitting scale are compared to those from simulations at convection-parameterized scale with the hydrostatic version of REMO2020-iMOVE. Resolution-dependent processes and differences of irrigation effects and feedbacks will be investigated.

1.4 Structure of the thesis

To answer previous research questions (section 1.3), this thesis is structured as followed: The design of this research is described in chapter 2 by starting with an overview of modeling irrigation (section 2.1). Section 2.2 introduces the case study area Northern Italy and the Po Valley, and section 2.3 describes the relevant characteristics of the employed RCM REMO2020-iMOVE. The research approach of developing a new irrigation parameterization for REMO2020-iMOVE, its implementation and first application is described in section 2.4. In section 2.5, the application of the newly developed irrigation parameterization to a convection-permitting modeling setup is elaborated. Section 2.6 highlights the novelty and the unique selling point of this research approach. An overview of related publications, including the publication of created data and code as well as co-authorships and conference publications, is given in chapter 3. Chapter 4 assesses and discusses the research findings, and provides answer to the research questions (section 4.1). Striking results in the simulations is given more

attention in section 4.2, and reflections and limitations are discussed in section 4.3. Chapter 5 summarizes the research findings of this work (section 5.1) and assesses the advancements and added values (section 5.2). The implications of this work for climate services are discussed in section 5.3, before section 5.4 gives an outlook in future research directions.

2 Research Design and Model Development

2.1 Irrigation parameterizations in land and climate modeling

Irrigation is represented with parameterizations in different RCMs respectively in their coupled LSMs. The parameterizations are governed by the model's physics schemes, as well as by the model setup. While former irrigation studies transformed whole model grid cells to irrigated grid cells (Branch et al., 2014, Marcella and Eltahir, 2014), newer stduies implemented an irrigated subgrid land surface fraction(de Vrese et al., 2016, Oleson et al., 2010, Tuinenburg et al., 2014, Valmassoi et al., 2020*a*, Wu et al., 2018), based on maps of irrigated areas from e.g. Siebert et al. (2013) or Ozdogan and Gutman (2008). The irrigation schemes vary considerably in how they represent the irrigation process. Saeed et al. (2009) implemented irrigation into REMO2009 studying irrigation effects in South Asia by increasing the soil moisture to 75% of the maximum water-holding capacity, which in REMO represents the field capacity, for every time step(Saeed et al., 2009). Marcella and Eltahir (2014) simulated irrigation in Western Africa using RegCM3-IBIS by setting the root zone soil moisture to its relative field capacity considering different saturation levels in different soil moisture levels. Irrigation is carried out every timestep from May to September (Marcella and Eltahir, 2014). For studies with WRF multiple irrigation parameterizations were developed (Branch et al., 2014, Qian et al., 2013, Valmassoi et al., 2020*a*, Wu et al., 2018, Yang et al., 2016). In various studies, WRF was coupled to the LSM Noah (Branch et al., 2014, Qian et al., 2013, Wu et al., 2018, Yang et al., 2016). Qian et al. (2013) and Yang et al. (2016) base their irrigation parameterization on Ozdogan et al. (2010). Ozdogan et al. (2010) developed a parameterization for sprinkler irrigation which applies irrigation as precipitation in the LSM Noah. The irrigation amount is defined as the difference of the root-zone soil moisture and the field capacity, weighted by the fraction of irrigated area of cropland in the grid cell. By using WRF coupled to Noah-MP, Wu et al. (2018) further included interactive vegetation and idealized groundwater processes for irrigation, limiting the available irrigation water, which is defined as the difference of

the current soil moisture and the saturated soil moisture in the upper two soil layers weighted to their depths. The irrigation amount is then applied as effective precipitation to grid cells with cropland as dominant land cover class and an irrigation fraction larger than 20% (Wu et al., 2018). Branch et al. (2014) developed a parameterization for one specific plantation in Israel, analyzing irrigation effects at a high resolution of 2 km with the non-hydrostatic WRF-ARW coupled to Noah. As subsurface irrigation is addressed for this case study, the soil moisture of the second and third soil layer is increased every seven days, until the defined soil moisture target is reached. The newest parameterization for WRF was developed by Valmassoi et al. (2020*a*), and applied for a case study in Northern Italy. Valmassoi et al. (2020*a*) investigated multiple irrigation parameterization approaches with different levels of evapotranspiration. The first option increases the effective precipitation, the second applies irrigation water right above the canopy including interception, and the last option applies the irrigation water to the lowest level of the atmosphere in a form of artificial rain, allowing for evaporation and advection while irrigating (Valmassoi et al., 2020*a*). The irrigation water amount is defined by the model user and weighted with the irrigated fraction in one grid cell (Valmassoi et al., 2020*a*). Tuinenburg et al. (2014) compared the irrigation response of three RCMs, HIRHAM, HADRM3, RAMS and the LSM JSBACH by implementing similar irrigation schemes. In each of the models the soil moisture of the top layer was increased to 90 % of the maximum field capacity and stayed constant. An irrigated subgrid land surface fraction was implemented, where it was not available yet, except for HIRHAM where irrigation was applied to grid cells with the irrigated area exceeding 20 % of the grid cell (Tuinenburg et al., 2014).

LSMs incorporate sophisticated vegetation and soil schemes, which allow for more detailed representation of the irrigation process. de Vrese et al. (2016) built on the irrigation scheme from Tuinenburg et al. (2014) for JSBACH, but extends the maintenance of an increased soil moisture to the dependence on the dynamic vegetation ratio. Irrigation is applied to the whole grid cell, which considers a vegetated and non-vegetated fraction (de Vrese et al., 2016). de Vrese et al. (2016) conducted two experiments. One with maximum irrigation, resembling flooding, and setting the soil moisture target to the field capacity while allowing

for bare soil evapotranspiration in the grid cell. And the second one with minimum irrigation, setting the soil moisture target to 0.75 field capacity. Oleson et al. (2010) implemented irrigation in the LSM CLM and partly builds on the parameterization of Ozdogan et al. (2010). However, Oleson et al. (2010) implemented a separate irrigated cropland fraction. The irrigation process is then carried out for the irrigated fraction, when water limits the photosynthesis rate. The irrigation amount is defined by the difference of the current soil moisture and a soil moisture target different soil layers (Oleson et al., 2010).

2.2 Case study areas: South-Western Europe and Northern Italy

The analysis of the modeled irrigation effects focuses mainly on the Po Valley in Northern Italy. For the development of the irrigation parameterization and the first application case in publication I (section 3.1), a larger model domain was selected covering South-Western Europe representing the heterogeneity of intensely irrigated areas such as the Po Valley and the Ebro Basin as well as non-irrigated areas. The selected case study area adjusted the model domain Greater Alpine Region (GAR) used by the CORDEX FPS Convection (Coppola et al., 2020) to a resolution of 0.11°. In this work GAR refers to the case study area of South-Western Europe at 0.11° horizontal resolution. The central position of the Po Valley in GAR enables the nesting of the smaller, higher resolution domain named Smaller Greater Alpine Region (SGAR) (Figure 1), representing the Po Valley at 0.0275° horizontal resolution and used for the convection-permitting simulations in publication 2 (section 3.4).

The Po Valley represents the plain of the Po River Basin in Northern Italy. It spans across the regions Piemonte, Valle d'Aosta, Lombardia, Veneto, Liguria, Emilia-Romagna and the Autonomous Province of Trento (Agenzia Interregionale per il fiume Po (AIPo), 2025), and is inhabited by around a third of the Italian population (Joint Research Centre. European Commission, 2018). Geographically it is located between the Alps in the north and the Apennines

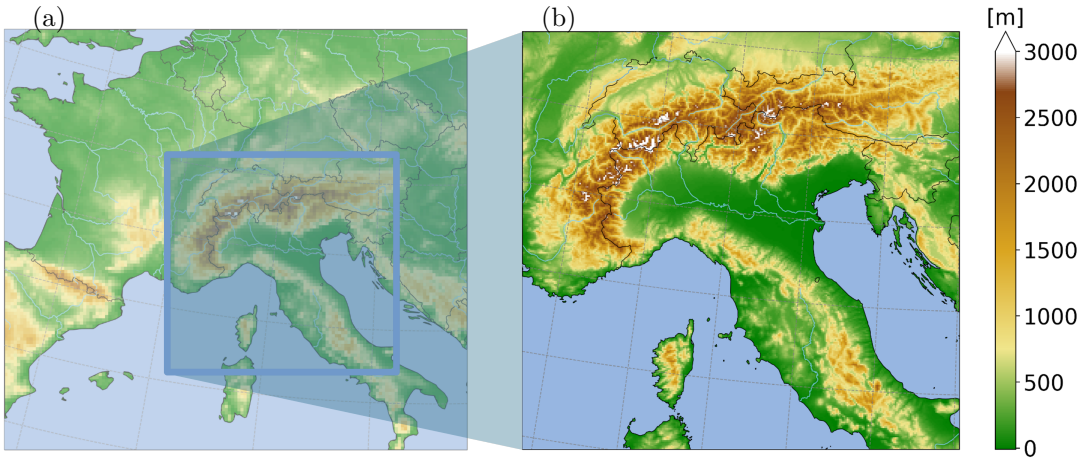

Figure 1: Orography of case study areas focusing on the Po Valley, a) GAR at 0.11° horizontal resolution, and b) SGAR at 0.0275° horizontal resolution. Blue square and trapezium represent the nesting approach.

in the south. The Po river flows eastwards from the Pian del Re of Monte Viso to the Adriatic Sea, receiving water from multiple tributaries originating in the Alps and Apennines (Boyko et al., 2022, Joint Research Centre. European Commission, 2018). The Po Valley is characterized by a long tradition of agriculture (Marchetti, 2002), which accounts for around 41 % of the Po Valley's surface in 2023 (Joint Research Centre. European Commission, 2018). The main agricultural goods are crops such as maize and rice, vegetables and orchards (Massari et al., 2021). Due to its intensive agriculture, the Po Valley is one of the most irrigated areas in Europe (Siebert and Doell, 2010). Historical processes have determined the size and spatial extent of irrigated agricultural areas, resulting in small-scale, heterogeneous patterns (Massari et al., 2021).
In recent years, the Po Valley faced multiple droughts with large effects on agriculture. Multiple studies expect an increase of droughts with climate change causing a thread to water availability and water use for agriculture in the Po Valley (Avanzi et al., 2024, Bozzola and Swanson, 2014, Montanari et al., 2023, Monteleone and Borzí, 2024). The climate of the Po Valley follows the description of a humid, subtropical climate (Cfa) in the Köppen-Geiger climate zone classification. The orographic differences nearby the plain of Po Valley and its

surrounding mountainous areas of the Alps and the Apennines cause favorable conditions for convective activities (Boyko et al., 2022).

2.3 The model: REMO2020-iMOVE

For the developments and the experiments of this research, the new version of the REgional climate MOdel REMO is employed. REMO is developed as a three-dimensional, hydrostatic, atmospheric circulation model by Jacob and Podzun (1997). Based on the primitive equations of the atmosphere, it is built from the dynamical core of the Europa Model (EM), the former numerical weather prediction model of the German Weather Service (Majewski, 1991), and multiple physical parameterizations from the global circulation model ECHAM4 (Roeckner et al., 1996). The prognostic variables are surface pressure, temperature, horizontal wind components, water vapor content, and cloud water content. The horizontal discretization uses the Arakawa-C grid, which defines mass-related variables in the center of a model grid cell and wind vectors at its boundaries (Arakawa and Lamb, 1977). The vertical discretization uses a hybrid sigma-pressure coordinate system following the orography in lower atmospheric levels and becoming more independent with height (Pfeifer, 2006). The model grid cells in REMO are projected onto a rotated coordinate system, ensuring equally sized areas of the model grid cells. For the temporal discretization, REMO uses the leap-frog scheme with a semi-implicit correction and Asselin filter (Asselin, 1972).

Over the years, REMO received multiple developments improving the representation of atmospheric processes such as cloud processes (Pfeifer, 2006), a chemistry module (Teichmann, 2010), aerosols (Pietikäinen et al., 2012), as well as a non-hydrostatic extension of the dynamical core (Goettel, 2009). Additionally, the land processes were improved by introducing tiles for land, water and sea ice (Semmler, 2002), implementing a vegetation cycle (Rechid and Jacob, 2006, Rechid et al., 2009), glaciers (Kotlarski, 2007), lake physics (Pietikäinen et al., 2018) and a vegetation module, which can be interactively coupled, named iMOVE (Wilhelm et al., 2014). Newest developments improved various parameterizations and rebuilt REMO with a modular approach enabling a facilitated

coupling of various features (Pietikäinen et al., 2025).
For this research, the representation of the land and of land-atmosphere exchange processes are of particular interest. The tile approach in REMO introduced by Semmler (2002) treats surface heterogeneity by enabling the representation of land, water and sea ice in one grid cell. Each of these subgrid tiles is defined by individual parameters and processes, leading to separate surface energy fluxes, which are averaged in the lowest atmosphere level with respect to their fraction in the grid cell. The turbulent fluxes in the surface energy balance are calculated with a bulk transfer parameterization using transfer coefficients based on the Monin-Obukhov similarity theory (Kotlarski, 2007). For a more detailed representation of the land surface, the land tile is further separated into a fraction with vegetation cover and a bare soil fraction, distinguishing the different radiation and water exchange processes. The vegetation cover is determined by the seasonal cycle, which is represented with variations of the vegetation ratio, the leaf area index (LAI) and the background albedo (Rechid and Jacob, 2006).
In REMO, the soil's heat budget is represented with five temperature layers, reaching a total depth of around 10 m. The layer's thickness increase with depth. The heat transfer between these layers is solved with diffusion equations, assuming a zero heat flux at the lowest boundary (Kotlarski, 2007). The heat conductivity and heat capacity are determined by the soil types from Zobler (1986). The hydrology of the land surface and the soil consists of three water reservoirs: the snow on the land surface, the skin reservoir, describing interception of rain and melted snow, and soil moisture. The soil moisture reservoir is represented with a simple one bucket scheme (Manabe, 1969). Soil moisture processes are driven by the field capacity, which is represented as the maximum water-holding capacity from the global dataset of land surface parameters by Hagemann et al. (1999). Precipitation increases the soil moisture. Based on the improved Arno scheme, precipitation is separated into one part that is infiltrated and the part that flows off as surface runoff considering the subgrid heterogeneity of the field capacity (Dümenil and Todini, 1992). The infiltration leads to subsurface drainage for soil moisture levels above 5% of the field capacity. Between 5% and 90% of the field capacity, fast drainage appears, while for field capacities above 90% the drainage is slow. Soil moisture decreases by evapotranspiration

driven by atmospheric conditions. From the bare soil fraction of one grid cell, evaporation occurs from the upper 10 cm. At the surface, runoff occurs once the soil moisture reaches the level of the field capacity indicating saturation. As there are no lateral flows between the grid cells, runoff leaves the water balance in REMO (Kotlarski, 2007).

As irrigation is directly influencing vegetation, surface and soil processes, this study makes use of the interactive MOsaic-based VEgetation module iMOVE (Wilhelm et al., 2014). Interactively coupled to the standard REMO version, iMOVE overlays the land tile with a mosaic of 16 plant functional types (PFTs) described in Table 1.

Table 1: PFTs in iMOVE.

1	Tropical broadleaf evergreen trees
2	Tropical deciduous trees
3	Temperate broadleaf evergreen
4	Temperate deciduous trees
5	Evergreen coniferous trees
6	Deciduous coniferous trees
7	Coniferous shrubs
8	Deciduous shrubs
9	C3 grass
10	C4 grass
11	Tundra
12	Swamp
13	C3 crops
14	C4 crops
15	Urban
16	Bare land

PFTs group plant species based on shared phenological and physiological traits and functions (Bonan et al., 2002, Wullschleger et al., 2014), and have been frequently utilized in Earth system modeling (Poulter et al., 2015). In iMOVE, the PFT distribution incorporates land cover information with climate information based on the Holdrige life zone concept (Holdridge, 1967). Holdridge life zones are described by near-surface temperature and precipitation (Wilhelm et al., 2014). While the original approach of iMOVE was based on the land cover of the GLOBCOVER2000 dataset with a resolution of 1 km (Bartholomé and and, 2005) , Reinhart et al. (2022) applied the original approach to the recent European Space Agency Climate Change Initiative (ESA CCI) land cover maps with a resolution of 300 m ESA (2017), creating the LANDMATE PFT dataset, which is suitable for high-resolution studies. Hoffmann et al. (2023) based the LUCAS LUC dataset on LANDMATE PFTs and extended it by an annual time dimension, thereby, enabling the use of LULC data for a specific year. PFTs are characterized by individual parameters and processes. The values and the parameterizations of iMOVE are based on the LSM JSBACH (Reick et al., 2013, Wilhelm et al., 2014) and determine plant processes such as photosynthesis, growing and wilting, and a possible harvest individually for PFTs. Due to the coupling of REMO and iMOVE, the individual PFT developments are driven by soil and atmospheric conditions, more precisely by soil moisture, 2 m temperature, surface and near-surface humidity, radiation, pressure, and atmospheric CO_2 concentration (Figure 2). For this research the soil moisture-dependent processes are of interest. In iMOVE, soil moisture influences the actual canopy conductance ($g^{H_2O}_{C,stress}$), which refers to the stomatal conductance applied to canopies. The canopy conductance drives the photosynthesis process. In iMOVE, the photosynthesis is calculated with the Farquhar model (Farquhar et al., 1980) and follows the approach of the Biosphere Energy Transfer Hydrology (BETHY) model by Knorr (1997). The canopy conductance depends on the soil moisture. In cases where the normalized available soil moisture falls below the soil moisture at the critical point (ws_{crit}) but is above the wilting point (ws_{pwp}) soil moisture (ws) decreases the optimal canopy conductance with a scaling factor (equation 1 and 2). This scaling factor is also referred to as "water stress" in the model (Reick et al., 2013, Wilhelm et al., 2014).

$$g_{C,stress}^{H_2O} = \begin{cases} f_{ws} g_C^{H_2O} & \text{for } q_a \leq q_s \\ 0 & \text{otherwise} \end{cases} \tag{1}$$

$$f_{ws} = \begin{cases} 0 & \text{for } ws \leq ws_{pwp} \\ \frac{ws - ws_{pwp}}{ws_{crit} - ws_{pwp}} & \text{for } ws_{pwp} < ws < ws_{crit} \\ 1 & \text{otherwise} \end{cases} \tag{2}$$

with q_a as air humidity, q_s as surface humidity.

The canopy conductance under water stress is applied to the photosynthesis process, which calculates the net primary production (NPP) and drives the LAI growth or decline. Here, it has to be noted, that soil moisture does not only affect the LAI indirectly through the canopy conductance and the NPP, but LAI growth is additionally directly dependent on the soil moisture, and grows only when the soil moisture is above the wilting point. Otherwise, it declines, which is represented with leaf shedding. The LAI affects the albedo as well as the vegetation ratio, which both are variables transferred from iMOVE to REMO2020 (Figure 2). Additionally, the canopy conductance is transferred to REMO2020 as well and influences the evapotranspiration, and, consequently, the turbulent latent heat flux. The coupling process, as well as the soil moisture-dependent processes are shown in Figure 2.

The parameters and calculated variables of the 16 PFTs are averaged with respect to their fraction in the model grid cell to a combined land value, before being further aggregated with the subgrid tiles of water and sea ice, and transferred to the atmosphere. Compared to the standard REMO2020 version, REMO2020-iMOVE improves the representation the surface heterogeneity. The interactive coupling enables the response of the individual plant processes to the soil and atmospheric conditions, which in turn feed back to the atmosphere. This leads to interactive albedo, LAI, vegetation ratio, and canopy conductance (Figure 2). A detailed description of REMO2020-iMOVE can be found in Wilhelm et al. (2014).

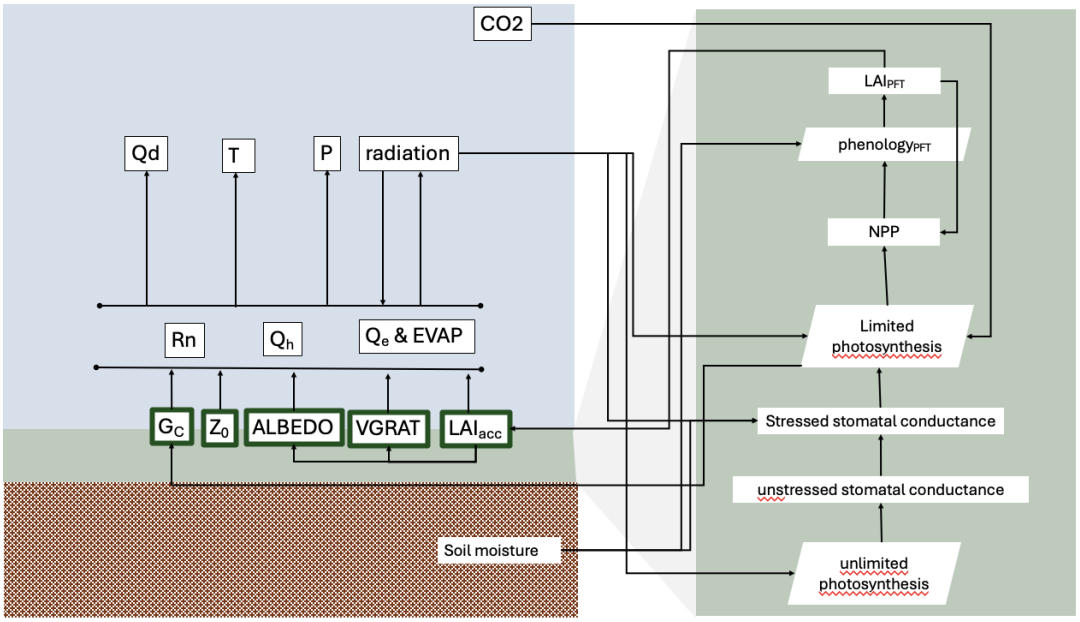

Figure 2: Coupling process of REMO2020 and iMOVE. The green shaded processes represent the calculations in iMOVE, while the blue shaded processes and variables the ones from REMO2020. Thick frames underline the variables transferred from iMOVE to REMO2020. This graphic is based on Wilhelm et al. (2014) with further adjustments.

Another important model characteristic for this research is the use of the non-hydrostatic, dynamical core of REMO. In the last two decades, there have been substantial advancements in data storage and growth in computing power, enabling higher resolutions paired with long-term simulations for RCMs (Ban et al., 2021, Kendon et al., 2021, Prein et al., 2015). However, with the increasing resolution, the hydrostatic approximation, which assumes a balance of the pressure gradient force and the gravitational force, since the vertical velocity is negligible, is no longer valid (Holton and Hakim, 2013, Prein et al., 2015). The hydrostatic approximation is applied to simplify the vertical momentum equation and is valid for large-scale atmospheric systems with horizontal scales around 10 km (Holton and Hakim, 2013). Small-scale atmospheric systems and processes such as convection are represented with parameterizations in these hydrostatic

models. For the cumulus convection, REMO uses the Tiedtke scheme (Tiedtke, 1989) with modifications after Nordeng (1994), which is based on the mass flux approach and separates convection depending on the moisture convergence into shallow, penetrative, and mid-level convection. Increasing the spatial resolution to convection-permitting scale (higher than 4 km) enables the explicit resolution of the convective process (Prein et al., 2015), and can make convection parameterizations obsolete. REMO with its non-hydrostatic core was recently successfully applied in convection-permitting studies by the FPS Convection (Ban et al., 2021, Coppola et al., 2020).

2.4 Development, implementation and evaluation of the irrigation parameterization

In RCMs, irrigation is usually represented with a parameterization, as the spatial scale of irrigation practices is smaller than that of the model grid cells. For representing irrigation in REMO2020-iMOVE a new parameterization should be developed, which is applicable for high-resolution studies in heterogeneous. The goal of irrigation is to provide sufficient soil moisture to plants for growth. Therefore, the interactive coupling of REMO2020 with the vegetation module iMOVE has the advantage of not only representing irrigation effects on land and atmosphere, but additionally incorporating the direct effects of irrigation on vegetation processes as well as their feedback mechanisms. The soil moisture increase through irrigation is carried out by different irrigation methods, depending on the region, the crop or plant type, and the investment possibilities (McDermid et al., 2023). These different irrigation methods affect different parts of the climate system, and therefore require individual parameterizations. For instance, channel or surface irrigation are steady systems increasing the soil moisture through transporting water to the agricultural area through open channels (Brouwer et al., 1988). Sprinkler irrigation applies water through often mobile sprinkler systems increasing soil moisture in a form of artificial precipitation, which includes interception of water on leaves and infiltration of water in the soil (Brouwer et al., 1988). Flooding is carried out for instance for rice paddies, covering the agricultural area with water by oversaturating the soil moisture

(Brouwer et al., 1988). For this study, channel irrigation, as predominant irrigation method in the Po Valley (Zucaro, 2014), was selected to be parameterized. The small scale of the irrigation practice compared to the resolution of RCMs, as well as the fact that irrigation is carried out often for selected agricultural areas, results in a heterogeneous distribution of soil moisture. Transferring this information to suitable information for an RCM implies that, depending on the resolution, only a fraction of the model grid cell is affected by irrigation. Following previous land surface parameterizations developed for REMO, for instance the parameterization for glaciers (Kotlarski, 2007) or for lakes (Pietikäinen et al., 2018), a parameterization at subgrid scale with a separate irrigated fraction is addressing the heterogeneity of the land surface. As irrigation affects the soil, the subgrid scale does not only refer to the land surface, but also to the underlying soil, creating a separate soil column. In REMO2020-iMOVE, all PFTs are linked to the land fraction of one model grid cell. Therefore, as first step of the irrigation parameterization, a new irrigated land fraction was implemented into REMO2020-iMOVE, exclusively for irrigated PFTs with a separate irrigated land surface energy balance. This procedure has the advantage that irrigation effects can be studied separately without being overlayed by other processes. As iMOVE represents land use and land cover with PFTs, a new PFT "irrigated cropland" was introduced to the new irrigated fraction, being so far, the only irrigated PFT and therefore, correspond to the size of the whole irrigated fraction. This approach leads to twice calculation of land processes: The first time for the not irrigated land fraction and its PFTs, and the second time for the irrigated land fraction. Consequently, land surface, soil, and vegetation variables are duplicated: Once for the not irrigated fraction and another time for the irrigated fraction. The irrigated fraction is based on the Global Map of Irrigated Areas (GMIA) version 5 by (Siebert et al., 2013), which provides the area equipped for irrigation at 5 arcmin and is used in various irrigation studies (Valmassoi et al., 2020*a*, Wu et al., 2018, Yang et al., 2019). For implementing the data from GMIA and the new PFT, a new preprocessor was developed, which interpolates GMIA to the target grid of the model domain and checks for the land-sea-mask as well as for the cropland PFT of the not irrigated fraction.

The second part of the parameterization is an irrigation module implemented as

extension of iMOVE. The irrigation module defines the requirements and properties of the irrigation process, and depends strongly on the soil and land surface parameterizations of the model. For simulating irrigation, the soil moisture is directly increased. During the growing season, irrigation is triggered once the soil moisture falls below a user-defined soil moisture value. The irrigation target, also user-defined, defines the end of the irrigation process. Irrigation is carried out explicitly during the growing season and explicitly for the newly defined "irrigated cropland" PFT on the irrigated fraction. During the development process of the parameterization different water application schemes were tested, which can be used for different purposes. The irrigation parameterization with the new fraction and the irrigation module follow the new developments of REMO2020 (Pietikäinen et al., 2025).
The development and the first application of the irrigation parameterization were accomplished for the GAR model domain (section 2.2) at 0.11° horizontal resolution, a well-established spatial resolution for regional climate models also applied by the EURO-CORDEX modeling community (Jacob et al., 2020). To investigate the behavior of the parameterization throughout the year, a one year simulation was conducted. The simulation is driven by ERA5 reanalysis data, allowing for evaluation against observational data. Irrigation effects are analyzed mainly for months with activated irrigation and delayed irrigation effects in summertime. As irrigation is particularly important for warm and dry months, irrigation effects are assessed for the year 2017, which was characterized by multiple heatwaves (Copernicus Climate Change Service, 2022). The irrigation effects are analyzed and evaluated in terms of their physical consistency, and additionally compared to observational data.

2.5 Modeling and evaluating irrigation effects and feedbacks up to convection-permitting scale

The newly developed irrigation parameterization is employed for convection-permitting simulations. The convection-permitting scale represents a key focus and a major future direction in regional climate modeling (Giorgi, 2019). Employing the irrigation parameterization in convection-permitting simulations

gives the chance to investigate irrigation effects and feedbacks on the physical processes leading to convection and precipitation. Furthermore, the added value of convection-permitting simulations in capturing extreme events, such as heatwaves and maximum temperatures (Hohenegger et al., 2009, Sangelantoni et al., 2025), aligns with the optimal conditions for representing irrigation effects and feedbacks. Furthermore, employing the coupled model system REMO2020-iMOVE to convection-permitting scale enables the investigation of vegetation processes at high resolution, a test case that was until now never realized with REMO2020-iMOVE. As due to the coupling, vegetation processes are highly dependent on atmospheric and soil moisture processes, differences in the effects and feedbacks of irrigation can be expected. Moreover, the higher resolution serves as an important sensitivity test for the irrigation parameterization at a resolution different from its original scale. The higher resolution affects directly the land surface features such as the irrigated fraction of model grid cells. The irrigated fraction data from GMIA by Siebert et al. (2013) had to be interpolated to the resolution of 0.0275°. Due to the higher resolution, more grid cells with higher irrigated fraction are created. Special attention is also required to the preparation of the model domain. Due to the high computational and storage demand, the model domain for the convection-permitting simulations is adjusted to a minium for analyzing irrigation effects in the Po Valley resulting in SGAR (section 2.2). The model domain SGAR is nested into the processed, non-irrigated simulation of GAR (Figure 1), which serves as driving conditions and downscales ERA5 data. This procedure refers to as double nesting and avoids large resolution jumps (Matte et al., 2016, 2017). The convection-permitting simulations are conducted by using the non-hydrostatic model version and turning off the convection parameterization (section 2.3), enabling the explicit resolution of convection development.

2.6 Research approach and novelty

This research aims for the improvement of the representation of land processes in RCMs, in form of the development and implementation of a new irrigation parameterization into the RCM system REMO2020-iMOVE. Compared to a pre-

viously developed irrigation parameterization for REMO2009 by Saeed et al. (2009), which was applied to studies with large-scale irrigation in South Asia, the new parameterization should be designed for small-scale irrigation in heterogeneous areas such as in Europe. Therefore, the parameterization includes a separate irrigated fraction, an approach used in irrigation studies by LSMs (Oleson et al., 2010). To the knowledge of the author, there is only one recent irrigation study with the RCM WRF implementing irrigation on a separate irrigated fraction (Wu et al., 2022), which was developed in the same time as the parameterization in this work. Another key characteristic of this research work is the modeling setup with the use of the interactive vegetation module iMOVE. Incorporating vegetational processes interactively adds a crucial component to the climate system, especially when analyzing land-atmosphere interactions. The development of the irrigation parameterization for REMO2020-iMOVE creates the foundation for this thesis (Figure 3), upon which the subsequent studies are built. In addition to the parameterization development and implementation, the modeling tasks include the preparation of the model input data. Particularly, the data for the irrigated fraction requires the development of a preprocessor. After multiple tests and finding suitable model settings, the parameterization is employed in one-year long simulations at 0.11° horizontal resolution. Simulations are conducted with and without the irrigation parameterization and their difference is defines as irrigation effect.

The results of the simulations at 0.11° horizontal resolution serve as boundary forcing data for the high-resolution simulations at convection-permitting scale (0.0275°), for which the input data has to prepared at the higher resolution. It is the first time, that REMO2020-iMOVE is employed at such high resolution, and therefore, requires multiple tests of the model settings. The combination of the high-resolution of convection-permitting scale and the incorporation of interactive vegetational processes create an advanced modeling setup towards a more realistic and complex regional climate modeling system. The interactive coupling enables the analysis of irrigation effects and feedbacks on soil, vegetation and atmosphere. Furthermore, this study analyzes and compares the effects of irrigation across different resolutions. By using spatial resolutions up to convection-permitting scale, this study provides new insights into how the resolu-

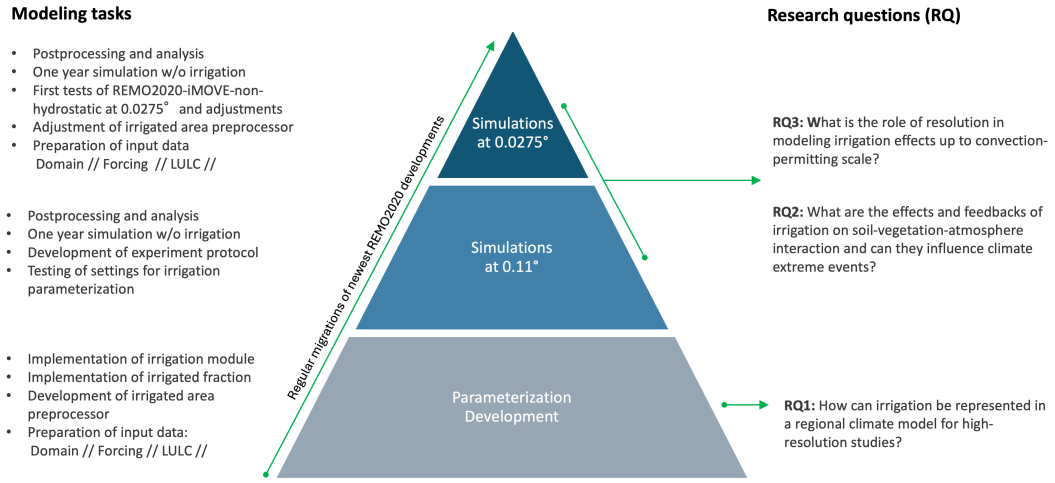

Figure 3: Structure of modeling tasks of this thesis with research questions.

tion of RCMs influences the representation of irrigation effects. This comparison contributes to the understanding of resolution-dependent features of irrigation effects.

3 Publication Overview

This section includes two research articles with leading authorship, which contribute to the research objectives. In addition, the simulation results and the analysis code created for these publications are published supporting high transparency and open access science according to the "Findability, Accessibility, Interoperability, and Reuseable" (FAIR) principles (Wilkinson et al., 2016). Further contributions as co-author and conference participations are listed under section 3.7.

3.1 Publication I

Asmus, C., Hoffmann, P., Pietikäinen, J.-P., Böhner, J., and Rechid, D.: Modeling and evaluating the effects of irrigation on land–atmosphere interaction in southwestern Europe with the regional climate model REMO2020–iMOVE using a newly developed parameterization, Geosci. Model Dev., 16, 7311–7337, https://doi.org/10.5194/gmd-16-7311-2023, 2023.

Received: 03 May 2023 – Discussion started: 14 Jul 2023 – Revised: 20 Oct 2023 – Accepted: 22 Oct 2023 – Published: 19 Dec 2023

Abstract. Irrigation is a crucial land use practice to adapt agriculture to unsuitable climate and soil conditions. Aiming to improve the growth of plants, irrigation modifies the soil condition, which causes atmospheric effects and feedbacks through land–atmosphere interaction. These effects can be quantified with numerical climate models, as has been done in various studies. It could be shown that irrigation effects, such as air temperature reduction and humidity increase, are well understood and should not be neglected on local and regional scales. However, there is a lack of studies including the role of vegetation in the altered land–atmosphere interaction. With the increasing resolution of numerical climate models, these detailed processes have a chance to be better resolved and studied. This study aims to analyze the effects of irrigation on land–atmosphere interaction, including the effects and feedbacks of vegetation. We developed a new parameterization for irrigation, implemented it into the REgional climate MOdel (REMO2020), and coupled it with the interactive MOsaic-based VEgetation module (iMOVE). Following this new approach of a separate irrigated fraction, the parameterization is suitable as a subgrid parameterization for high-resolution studies and resolves irrigation effects on land, atmosphere, and vegetation. Further, the parameterization is designed with three different water application schemes in order to analyze different parameterization approaches and their influence on the representation of irrigation effects. We apply the irrigation parameterization for southwestern Europe including the Mediterranean region at a 0.11 ◦ horizontal resolution for hot extremes. The simulation results are evaluated in terms of the consistency of physical processes. We found di-

rect effects of irrigation, like a changed surface energy balance with increased latent and decreased sensible heat fluxes, and a surface temperature reduction of more than -4 K as a mean during the growing season. Further, vegetation reacts to irrigation with direct effects, such as reduced water stress, but also with feedbacks, such as a delayed growing season caused by the reduction of the near-surface temperature. Furthermore, the results were compared to observational data, showing a significant bias reduction in the 2 m mean temperature when using the irrigation parameterization.

Contribution: CA developed the experiments in coordination with DR, JB and PH. CA processed the irrigation data and developed the irrigation module. CA and JPP implemented the parameterization in the model code of REMO2020-iMOVE, which included additionally various migrations of different model versions as REMO2020 was in the same time under development. CA created the visualizations and conducted the analysis under the supervision of DR and JB. CA prepared the initial paper. All authors reviewed the paper draft and contributed to the final paper.

3.2 Software Publication I

Asmus, C. & Buntemeyer, L.: Analysis scripts supporting "Modeling and evaluating the effects of irrigation on land-atmosphere interaction in southwestern Europe with the regional climate model REMO2020-iMOVE using a newly developed parameterization" (v1.1). Zenodo. https://doi.org/10.5281/zenodo.10017312, 2023.

Contribution: CA wrote the analysis code. LB implemented the setup for using the analysis code.

3.3 Data Publication I

Asmus, C.: Data supporting "Modeling and evaluating the effects of irrigation on land-atmosphere interaction in southwestern Europe with the regional climate model REMO2020-iMOVE using a newly developed parameterization" [Data set]. Zenodo. https://doi.org/10.5281/zenodo.10014915, 2023.

Contribution: CA conducted the simulations with REMO2020-iMOVE which created the data. CA analyzed the data in terms of its physical meaning.

3.4 Publication II

Pop, C., Böhner, J., Hoffmann, P., Pietikäinen, J.-P., and Rechid, D. (2025). The role of horizontal resolution in modeling irrigation effects with a coupled regional climate model system up to convection-permitting scale.

Submitted to JGR Atmospheres. This version is the revised version after first major revisions, which was resubmitted to the journal.

Note: The inital version, submitted to JGR Atmospheres, was published as preprint and is available in ESS Open Archive. [preprint] https://doi.org/10.22541/essoar.173655443.36008527/v1. The final version of the paper was published on 20 September 2025, and is available under https://doi.org/10.1029/2024JD043227.

Abstract. Increasing the resolution of regional climate models up to convection-permitting scales enables explicitly resolved convection and finer resolved surface features. In this work, we use the benefits of the high resolution climate model and apply it to model irrigation effects and feedbacks on the local and regional climate, focusing on the interaction of irrigation with soil, surface, atmosphere, and vegetation processes. We employ the regional climate model REMO2020 interactively coupled to its vegetation module iMOVE and incorporate our newly developed irrigation parameterization. We conduct two simulations sets with and without the irrigation parameterization. In the first set, we employ the hydrostatic model version at 0.11° horizontal resolution for Southwestern Europe. For the second set, we repeat the experiment employing the non-hydrostatic model version at convection-permitting resolution of 0.0275° for Northern Italy. Our results indicate that improved vegetation conditions due irrigation, such as an increased canopy conductance, lead to effects in the atmosphere. For the atmosphere, we find more distinct and localized irrigation effects for the simulations at convection-permitting resolution with enhanced near-surface cooling of up to -2 K compared to the simulations at 0.11°. In the boundary layer, irrigation effects are highly influenced by turbulences, transporting the irrigation effect in higher levels. The largest differences in representing irrigation effects on the two

resolutions were found in precipitation. While at 0.11° horizontal resolution, precipitation increases due to favorable convection conditions, explicitly resolving convection leads to rather mixed effects with a decrease of precipitation above irrigated areas, where the convection inhibition increased.

Contribution: CP developed the experiments in coordination with DR and JB. CP processed the irrigation data on convection-permitting scale. CP run the simulations with guidance of JPP. CP created the visualizations and conducted the analysis under the supervision of DR and JB, and in close cooperation with PH and JPP. CP prepared the initial paper. All authors reviewed the paper draft and contributed to the final paper.

3.5 Software Publication II

Pop, C. (2025). Scripts supporting the analysis of "The role of horizontal resolution in modeling irrigation effects with a coupled regional climate model system up to convection-permitting scale" (v1.0). Zenodo. https://doi.org/10.5281/zenodo.15156272.

Contribution: CP wrote the analysis scripts and created the visualizations.

3.6 Data Publication II

Pop, C. (2025). Data supporting "The role of horizontal resolution in modeling irrigation effects with a coupled regional climate model system up to convection-permitting scale" (v1.0) [Data set]. Zenodo. https://doi.org/10.5281/zenodo.15144005.

Contribution: CP conducted the simulations with REMO2020-iMOVE and REMO2020-nh-iMOVE, which created the data. CP analyzed the data.

3.7 Further Publications

Co-authorships

Hoffmann, P., Reinhart, V., Rechid, D., de Noblet-Ducoudré, N., Davin, E. L., **Asmus, C.**, Bechtel, B., Böhner, J., Katragkou, E., and Luyssaert, S.: High-resolution land use and land cover dataset for regional climate modelling: historical and future changes in Europe, Earth Syst. Sci. Data, 15, 3819–3852, https://doi.org/10.5194/essd-15-3819-2023, 2023.

Contribution: CA wrote the sections on analysis of irrigated cropland (sections 3.2.2 and 3.1.2) and prepared Table A2. All the co-authors reviewed the paper draft and contributed to the final manuscript.

Pietikäinen, J.-P., Sieck, K., Buntemeyer, L., Frisius, T., Nam, C., Hoffmann, P., Pop, C., Rechid, D., and Jacob, D.: REMO2020: a modernized modular regional climate model, EGUsphere [preprint], https://doi.org/10.5194/egusphere-2025-1586, 2025.

Contribution: CP wrote the paragraph on iMOVE and supported the analysis of the results of REMO2020-iMOVE. As co-author CP reviewed the paper.

Conference Publications

Asmus, C., Hoffmann, P., Rechid, D., and Böhner, J.: Modeling the effects and feedbacks of irrigation on the regional climate in Northern Italy, EGU General Assembly 2020, Online, 4–8 May 2020, EGU2020-8913, https://doi.org/10.5194/egusphere-egu2020-8913, 2020.

Asmus, C., Hoffmann, P., Böhner, J., and Rechid, D.: Parametrisierung unterschiedlicher Bewässerungsmethoden in einem regionalen Klimamodell und deren Effekte auf das regionale Klima in der „Greater Alpine Region“ , 12. Deutsche Klimatagung, online, 15–18 Mar 2021, DKT-12-11, https://doi.org/10.5194/dkt-12-11, 2021.

Asmus, C., Hoffmann, P., Pietikäinen, J.-P., Böhner, J., and Rechid, D.: Modeling irrigation effects on the regional climate in the "Greater Alpine Region" using a newly developed parameterization, EMS Annual Meeting 2021, online, 6–10 Sep 2021, EMS2021-176, https://doi.org/10.5194/ems2021-176, 2021.

Asmus, C., Hoffmann, P., Pietikäinen, J.-P., Böhner, J., and Rechid, D.: Analyzing the influence of irrigation on convection – Case study for Northern Italy using convection-permitting simulations, EMS Annual Meeting 2022, Bonn, Germany, 5–9 Sep 2022, EMS2022-275, https://doi.org/10.5194/ems2022-275, 2022.

Asmus, C., Hoffmann, P., Pietikäinen, J.-P., Böhner, J., and Rechid, D.: Analyzing simulated irrigation effects on convection-permitting scale – Does irrigation in northern Italy affect convective processes? ICRC 2023, Trieste, Italy, 25-29 September 2023. https://indico.ictp.it/event/10212/material/9/2.pdf, last accessed: 20.05.2025.

4 Synthesis and Discussion

4.1 Assessment and synthesis of research results

Within this work, a new irrigation parameterization was developed and implemented into REMO2020-iMOVE as well as applied at 0.11° and at 0.0275° horizontal resolution, reaching the convection-permitting scale. The parameterization development is the foundation of this work. Together with the selected model setup, it answers RQ1 (section 1.3) and addresses RG1 and RG2, which were identified in section 1.1. The parameterization builds on characteristics from state-of-the-art parameterizations, such as from Oleson et al. (2010), de Vrese and Hagemann (2018) and Saeed et al. (2009), but adjusts and extends them to align with REMO2020-iMOVE's physics. In the following, the main characteristics of the new irrigation parameterization are summarized:

Subgrid-scale parameterization with a separate irrigated fraction:
Implementing the irrigation parameterization into REMO2020-iMOVE as subgrid-scale parameterization with a dedicated irrigated fraction ensures that irrigation is applied exclusively to the irrigated fraction of the model grid cell, which is based on the GMIA by Siebert et al. (2013). The subgrid-scale approach with a separate irrigated fraction facilitates the development of separate, irrigated surface fluxes, and therefore, increases the land surface and the soil moisture heterogeneity within one model grid cell. The separate surface fluxes are consequently averaged with respect to the fraction of the model grid cell. According to Giorgi and Avissar (1997), this approach is not only capable of considering non-linear processes, but is one of the most accurate and efficient in climate modeling, when aggregating surface heterogeneity. Therefore, a subgrid-scale approach with a separate irrigated fraction is in particular important for modeling small-scale irrigation in heterogeneous areas such as Europe and improves the representation of the land characteristics in RCMs. A similar subgrid-scale approach for an irrigation parameterization was implemented in the LSM CLM by Oleson et al. (2010). For RCMs the subgrid-scale approach for irrigation is rare. It was recently implemented in WRF coupled to the LSM Noah by Wu et al. (2022), however, without fully coupling the vegetation processes.

A new parameterization as extension of the interactively coupled vegetation module iMOVE:
The new irrigation parameterization is implemented as an extension of REMO-2020's vegetation module iMOVE. Employing REMO2020 interactively coupled to iMOVE was shown to improve the representation of surface parameters such as the LAI and albedo, which affect the surface energy balance and, for instance, improve the 2 m mean temperature in summer in Northern Europe (Pietikäinen et al., 2025). For studying irrigation effects and feedbacks, iMOVE has multiple advantages. Firstly, this setup incorporates the interaction between atmosphere, soil and vegetation. Irrigation is a process aiming for improved growth conditions of plants. Therefore, including interactive vegetation enables the investigation of the irrigation effects on vegetational processes and of consequent feedbacks in the regional climate system. In iMOVE, soil moisture is a driving factor for plant processes. It influences the stomatal conductance, which in turn affects photosynthesis, and consequently NPP and LAI growth (section 2.3). Through the interactive coupling of REMO2020 and iMOVE, these changes affect evapotranspiration as well as the vegetation ratio of a model grid cell, thereby contributing to the altered surface energy balance and affecting climatic processes. Secondly, incorporating iMOVE enhances the representation of land surface heterogeneity in one model grid cell by using a mosaic of PFTs (Wilhelm et al., 2014). Last, the irrigation parameterization is linked to the phenological dynamics of cropland, which are characterized by a growing season and a harvest event, and define the implemented irrigation period.

Direct soil moisture increase:
The irrigation parameterization directly increases the soil moisture, aiming for the representation of channel irrigation. This irrigation method affects exclusively the soil and surface, and does not result in interception on leaves nor in direct effects on the atmosphere. Irrigation effects develop through an altered surface energy balance and soil moisture dependent processes in the model such as e.g. evapotranspiration and plant growth, which consequently cause various feedbacks. Irrigation water loss through e.g. open-channel evapotranspiration

are not considered, neither are different irrigation methods, which require individual parameterizations and can lead to different effects in the climate system (Leng et al., 2017, Valmassoi et al., 2020*a*).

Different water application schemes:
During the development process of the irrigation parameterization, three different water application schemes were tested. The water application schemes distribute the water amount across the time steps defined by the model user. The first scheme applies prescribed irrigation water linearly to the soil moisture. As REMO2020-iMOVE represents the soil hydrology with a one bucket scheme, prescribing suitable irrigation water amounts is not trivial. Therefore, water application schemes based on soil moisture targets are implemented. The second water application scheme applies irrigation linearly until a user-defined soil moisture target is reached. The last water application scheme uses a non-linear, time-dependent relaxation approach for reaching the soil moisture target. The differences in the effects of the three water application schemes are negligible, when using a similar irrigation water amount. However, the most suitable scheme is the time-dependent relaxation water application scheme, as the irrigation target is reached in the specified irrigation duration.

Adjustable irrigation threshold, soil moisture target, irrigation water amount, irrigation duration:
Key parameters for irrigation studies such as irrigation threshold, which defines the soil moisture level for the irrigation start, soil moisture target, irrigation water amount, irrigation duration, or the choice of the water application scheme are adjustable by the model user through the namelist. This feature enhances the usability of the irrigation module and gives the opportunity to investigate various irrigation scenarios.

Employing the newly developed irrigation parameterization in model simulations enables the analysis of irrigation effects with a focus on the Po Valley and provides an answer to RQ2. In the coupled model system, the irrigation effects interact between soil, vegetation and atmospheric processes and develop

feedback mechanisms in between each other. Increasing soil moisture through irrigation alters the surface energy balance by increasing the latent heat flux due to increased evapotranspiration, while reducing the sensible heat flux. The sensible heat flux reaches negative values of up to -15 Wm^{-2} in the early afternoon of the mean diurnal cycle during the irrigation period in the irrigated simulations at both resolution, meaning that it is directed towards the surface (section 4.2). This effect appeared as well during the Land Surface Interactions with the Atmosphere over the Iberian Semi-arid Environment (LIAISE) measurement campaign in the Ebro basin in Spain in June 2021, however, with a stronger intensity reaching -150 Wm^{-2} (Boone et al., 2025, Udina et al., 2024). The surface and the soil temperatures decrease in the irrigated simulations with a delayed cooling effect for deeper soil layers. The altered surface fluxes decrease the 2 m mean temperature by up to -2.5 K at 0.11° horizontal resolution and up to -2.8 K at 0.0275° as mean effect of a single grid cell in June 2017. This cooling effect on the 2 m mean temperature decreases the warm model bias compared to station data in months with activated irrigation. Irrigation particularly affects the daily 2 m maximum temperature by inducing a cooling effect up to -4.2 K at 0.11° horizontal resolution and up to -5.7 K at 0.0275° horizontal resolution as monthly mean effect for a single grid cell in June 2017. Comparable studies such as by Valmassoi et al. (2020*b*) found a 2 m maximum temperature decrease of up to -3 K in single grid cells of the Po Valley as monthly mean effect in July 2015 in simulations at 3 km horizontal resolution. The more pronounced effects of this work might be caused by the setup using the maximal water-holding capacity as irrigation target and irrigation threshold, which cause everyday irrigation. According to Valmassoi and Keller (2022), the irrigation amount is a driving factor of the magnitude of irrigation effects. Furthermore, higher temperatures cause a stronger development of irrigation effects as shown in Thiery et al. (2017). This thesis further pointed out the importance of the size of the irrigated fraction, which correlates with the irrigation effects on the 2 m maximum temperature, while it shows a lower correlation with the 2 m minimum temperature. Irrigation effect on the 2 m minimum temperature can be either increasing or decreasing. This finding aligns with studies by (Chen and Jeong, 2018, Li et al., 2022). Furthermore, this study shows delayed irrigation effects, which occur when irrigation

is not active. For instance, due to the high soil moisture caused by irrigation, the cooling effect on temperature remained and reduced the intensity of a heatwave in August 2017 in Northern Italy, revealing the mitigation potential of irrigation. In the coupled model system, the effects in the soil and atmosphere feed back with the vegetation. As described above, iMOVE's plant physiology is influenced by the state of soil moisture, as well as by the 2 m temperature. The increase in soil moisture through irrigation, and the absence of water stress lead to a more productive photosynthesis with higher NPP in the irrigated simulations than in the not irrigated simulations. Furthermore, the LAI development is influenced. At both resolutions, due to the lower temperature, the LAI develops slower in irrigated simulations. However, irrigation leads to a slight increase of the LAI peak and an extension of the growing season, which is ending with the harvest event. This extension results from a lower 2 m temperature caused by irrigation, as the timing of the harvest event is defined with a temperature sum (Wilhelm et al., 2014). The study by Wu et al. (2018) in the Northern Plains of China shows a more pronounced LAI increase than in this work. Also, an extension of the growing season could not be found (Wu et al., 2018), indicating that both features are very model-specific and might need improvement. The influenced vegetation processes contribute to the alterations of the surface energy balance. The changes in LAI affect the vegetation ratio, and therefore, the albedo and the evapotranspiration processes of plants, which in turn drive land-atmosphere exchange processes.

Employing the newly developed irrigation parameterization in the coupled model setup with interactions between soil, vegetation and atmospheric processes at convection-permitting resolution is one of the novelties of this work and addresses RQ2 and RQ3. In recent years, multiple studies investigated irrigation at convection-permitting scale Liu et al. (2023), Qian et al. (2020), Udina et al. (2024), Valmassoi et al. (2020*b*), Wang et al. (2024), Zhang et al. (2025). However, all these studies employ the RCM WRF with different irrigation parameterization, and except for Zhang et al. (2025), vegetation processes are neglected. The role of convection-permitting scale becomes clear when comparing the convection-permitting simulations to the simulations at 0.11° horizontal res-

olution (convection-parameterized scale). The higher resolution increases the heterogeneity of the land surface. For the irrigated fraction, it leads to more grid cells with a higher irrigated fraction, causing more localized and distinct irrigation effects on the 2 m maximum temperature and 2 m mean temperature. These effects feedback with the vegetational processes, e.g. with the length of the growing season due to the temperature-dependent harvest event. However, overall the vegetational processes develop similarly at both resolutions. The advantages of a higher resolution - particularly of the convection-permitting scale - become evident in atmospheric processes. As a resolution effect, the representation of the diurnal cycle of precipitation in the convection-permitting simulations is improved compared to station data. This improvement in convection-permitting simulations was observed in Ban et al. (2021), Kendon et al. (2021), Prein et al. (2015). Precipitation is the variable in this work, which shows the largest differences between irrigation effects at the convection-parameterized and the convection-permitting scale, represented by a change of sign in the two resolutions. While at 0.11° horizontal resolution precipitation increases mainly at the border to the Alps, at 0.0275° the irrigation effect on precipitation shows a divers small-scale response. In total, precipitation slightly decreases in the analysis region due to irrigation in the convection-permitting simulations (-4 %). While at both resolution the convective available potential energy (CAPE) increases, convective inhibition (CIN) increases in multiple areas at 0.0275° horizontal resolution, while it rather decreases at 0.11°. These different effects on precipitation were also found by Udina et al. (2024) for the Ebro basin in simulations with WRF. However, in the study by Valmassoi et al. (2020*b*), precipitation increases up to +9.5 % above the Po Valley in July 2015.

4.2 On the role of a negative sensible heat flux

In this work a negative sensible heat flux refers to the direction of the sensible heat flux from the atmosphere towards the surface. The implemented, separate irrigated fraction of the irrigation parameterization enables the analysis of a separate, irrigated energy surface balance. The application of the irrigation parameterization causes a negative sensible heat flux for the irrigated fraction from

the early afternoon (section 3.1, section 3.4), while in the simulations without irrigation a negative heat flux develops during the evening and nighttime. Since a negative sensible heat flux affects the energy partition of the whole surface energy balance, it requires a more detailed analysis.

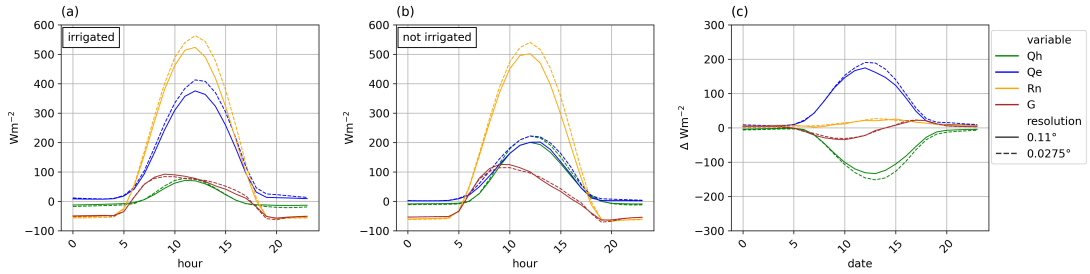

Figure 4: Mean diurnal cycle of the surface energy balance in the irrigated month MAMJJ for a) the irrigated simulations and b) not irrigated simulations. c) shows the irrigation effect as difference between the simulations with and without irrigation for the grid cell with an irrigated fraction > 0.7.

The negative sensible heat flux, directed from the atmosphere towards the surface, implies a warmer atmosphere in the lower levels compared to the surface. It establishes for instance during nighttime, due to the absent solar radiation and the faster cooling of the land surface compared to the atmosphere (Oke, 1988). Further, a negative sensible heat flux occurs with seasonal variability over lakes and water bodies (Potes et al., 2017). In our experiments, irrigation increases the soil moisture until the maximal water-holding capacity of the soil. This high soil moisture enhances evapotranspiration resulting in a surface energy balance of the irrigated fraction dominated by the latent heat flux (section 3.1, section 3.4). In the afternoon, the latent heat flux exceeds even the solar radiation, which marks the shift from a positive to a negative sensible heat flux (Figure 4a). It follows, that the energy for the evapotranspiration, which is necessary for the phase transition of the water droplets into water vapor, is absorbed by the surroundings causing the evaporative cooling effect. As a result, the irrigated surface temperature is decreasing by up to -5.8 K in the simulations at 0.11° horizontal resolution and -4.9 K at 0.0275° during the irrigated months MAMJJ

with the strongest decrease at noon. The 2 m temperature is decreasing by up to -2.8 K at 0.11° horizontal resolution and -3.5 K at 0.0275° horizontal resolution with the strongest decrease in the afternoon from 15:00 LT (Figure 5c). This temperature reduction leads to a smaller range of the diurnal surface temperature and of the 2 m temperature in the averaged diurnal cycle in MAMJJ (Figure 5a) compared to the development of these temperatures in the not irrigated simulations (Figure 5b). From 14:00 LT at 0.11° horizontal resolution and from 11:00 LT at 0.0275° the surface temperature of the irrigated fraction is cooler than the 2 m temperature in the irrigated simulations, while in the not irrigated simulations this feature occurs from 18:00 LT at 0.11° horizontal resolution and from 16:00 LT at 0.0275° caused by the decrease of solar radiation. These temperature developments lead to the negative sensible heat flux in the surface energy balance of the irrigated fraction.

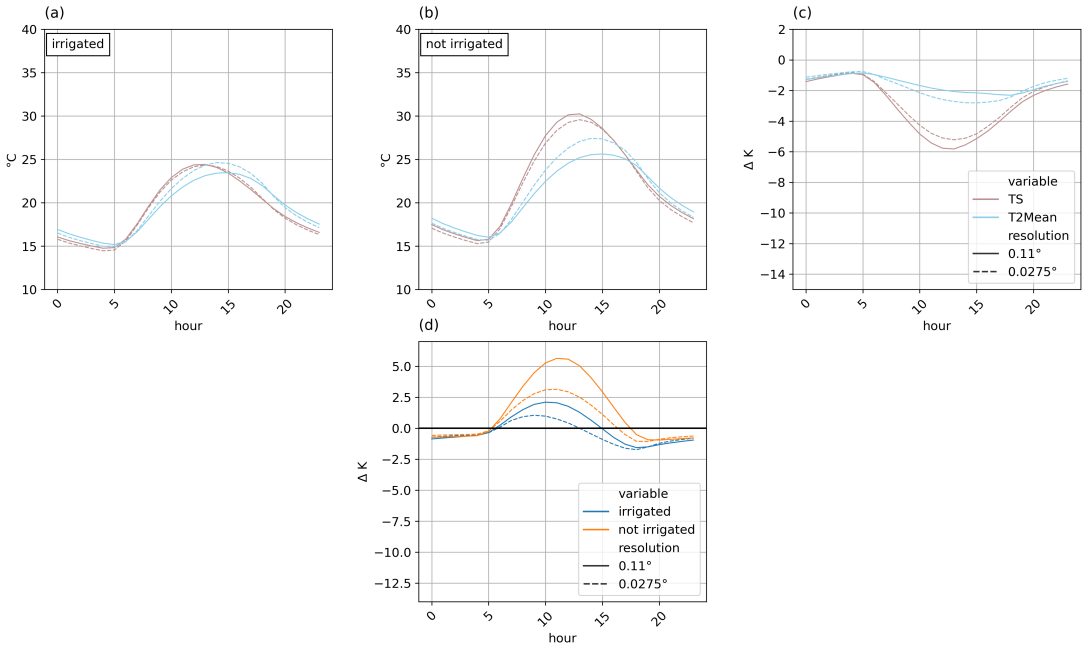

Figure 5: Diurnal cycle of differences of surface temperature and 2 m temperature in June 2017 for irrigated fraction > 0.7.

A negative sensible heat flux above irrigated areas was observed in multiple

measurement campaigns, such as in the LIAISE campaign in Spain measured by a flux tower at an irrigated location of a homogeneous area (Udina et al., 2024). In the Regional Advection Perturbations in an Irrigated Desert (RAPID) experiment the sensible heat flux turned negative for a number of days in Idaho, US (De Bruin et al., 2004). The negative sensible heat flux was correlated with the wind speeds above 3 ms^{-1} advecting dry, warm air from not-irrigated areas to the measurement site (De Bruin et al., 2004). A similar result was found by Uddin et al. (2013) measuring the Bowen ratio under advective conditions at an irrigated cotton field in Australia. The derived negative sensible heat flux during irrigation hours occurred as net radiation was too low to sustain high evapotranspiration from the irrigated fields. The resulting reversed temperature characteristics cause stable near-surface atmospheric conditions, preventing mixing.

4.3 Reflections and limitations

In this work a new irrigation parameterization for the coupled regional climate model system REMO2020-iMOVE was developed, enabling the investigation of irrigation effects on land, atmosphere and vegetation. For the first time, REMO2020-iMOVE was applied to convection-permitting scale using the non-hydrostatic dynamical core of REMO2020.

While this study provides physically reasonable results, its limitations should be addressed. With the new irrigation parameterization unrealistically large amounts of irrigation water are used. This disadvantage is linked to the current soil parameterization of REMO2020-iMOVE. REMO2020-iMOVE represents the soil moisture with a one bucket scheme (Manabe, 1969). It attributes the same soil moisture to the entire soil depth, which is a significant simplification of the soil hydrology. Consequently, for modeling irrigation unrealistically large amounts of irrigation water are required, making observational data unsuitable for use. Multiple RCMs include layers for the soil hydrology (Branch et al., 2014, Marcella and Eltahir, 2014, Oleson et al., 2010, Valmassoi et al., 2020*a*). This allows to irrigate specific layers, and to consider, for instance, the root depth of vegetation (Oleson et al., 2010). A layer scheme influences among others the evapotranspiration processes (Abel, 2023) and would affect the representation of

irrigation effects. However, the implementation of layers or the migration of the layer scheme developed by Abel (2023) for REMO2015 into REMO2020-iMOVE goes beyond the aim of this work.

The use of observational data as irrigation water amount is crucial for the estimation of a realistic magnitude of irrigation effects. Irrigation effects depend strongly on the irrigation water amount (Valmassoi and Keller, 2022). The studies presented in this work are extreme experiments with maximum irrigation settings, leading to the possibility of overestimating the irrigation effects. The underlying assumption of the irrigation parameterization of an infinite water availability for irrigation, adds to the possible overestimation. REMO2020-iMOVE has an open water balance and therefore, no water limitations. Observational values, physical thresholds or, in the best case, a closed water balance as in hydrological models, would contribute to the estimation of realistic magnitudes of irrigation effects.

Furthermore, the new parameterization consists of only one irrigation method. As different irrigation methods affect various components and processes in the climate system, different irrigation methods require different parameterizations (Leng et al., 2017, Valmassoi et al., 2020*a*). For instance, for modeling sprinkler irrigation, interception has to be taken into account, as well as the infiltration process, affecting the evapotranspiration.

Another limitation of this study is the strong dependence of the LAI on temperature. The modeled, slower developing LAI in the irrigated simulations compared to the not irrigated simulation is not a realistic behaviour and should therefore be updated. Observational studies suggest the opposite behavior (Patanè, 2011), indicating the need for improvements in the REMO2020-iMOVE's representation of vegetation dynamics. Furthermore, the increase of the warm bias after the harvest event (Section 3.1, (Pietikäinen et al., 2025)) is another motivation for the improvement of the crop phenology.

The irrigation effects presented in this thesis result from one-year studies with REMO2020-iMOVE. For reducing the uncertainties of the magnitude of irrigation effects and investigating the effects and feedbacks on climate timescales, longer, at least 30 year long, simulations would be required. The longer timescale can capture different climate states and weather patterns, and give robust infor-

mation how irrigation affect the model bias. In addition, for analyzing irrigation effects a multi-model ensemble of RCMs following the example of the CORDEX initiative would be desirable, as including multiple models with different model configurations and different irrigation parameterizations can decrease the uncertainty. In general, it has to be stated that irrigation is a complex human-decision process, including dynamic socioeconomic and political factors (McDermid et al., 2023). Ignoring the human component always oversimplifies this process.

5 Conclusion and Outlook

5.1 Core outcomes and findings

RQ1: How can irrigation be represented in a regional climate model for high-resolution studies?

For the representation of irrigation, a new subgrid parameterization was developed for the RCM system REMO2020-iMOVE. The full coupling of soil, atmosphere and vegetation processes at high resolution, and linking the parameterization directly to the vegetation module, enables the development of effects and feedbacks between these compartments of the regional climate system. iMOVE has the advantage to represent interactions between soil moisture and vegetational parameters and processes, such as canopy conductance and photosynthesis intensity and their effect on e.g. the LAI, which consequently affect surface and atmospheric processes. The newly developed irrigation parameterization is represented on a separate irrigated fraction in a model grid cell, based on the GMIA by Siebert et al. (2013). It allows not only for exclusive irrigation of the dedicated grid cell fraction and the selected PFT, it also enables the investigation of irrigation effects on distinct land surface and vegetation parameters, which are not overlayed by other processes. Additionally, the subgrid-scale approach is a well-established method in climate modeling to capture potential non-linear interactions. Furthermore, the new subgrid fraction, as well as the incorporation of iMOVE, increase the heterogeneity of the land surface as well as of the soil, and is particularly an advantage for small-scale irrigated areas such as in Europe. The combination of both features result in a more realistic representation of the interaction between soil, vegetation and atmospheric processes.

The parameterization increases soil moisture directly. As REMO2020-iMOVE represents the soil hydrology uniformly in just one layer, a large amount of irrigation water is required, making physical thresholds a suitable approach. Irrigation is triggered by a soil moisture threshold and continues until a soil moisture target is reached. These values are user-defined and can be adjusted in the namelist of the model run. The parameterization consists of three water application schemes, which differ in their function of applying water within a specific time. While the first scheme, prescribes the irrigation water amount and the irrigation time, the

second scheme is linked to a soil moisture target during an open irrigation time. The third scheme applies irrigation with a time-dependent relaxation approach until the soil moisture target is reached. While the first two schemes apply irrigation linearly, the third scheme uses a non-linear approach. However, the differences among the irrigation effect of the three water application schemes are negligible when a similar water amount or a similar soil moisture target is used.

RQ2: What are the effects and feedbacks of irrigation on soil-vegetation-atmosphere interaction, and can they influence climate extreme events?
Irrigation increases the soil moisture, which results in an altered surface energy balance with an increased latent heat flux and a decreased sensible heat flux. While the latent heat flux becomes the dominating heat flux of the surface energy balance, the sensible heat flux changes its direction and becomes negative in the afternoon during irrigation hours, indicating a warmer lower atmosphere compared to the irrigated land surface. The altered surface energy balance leads to a decreased surface temperature as well as to decreased soil temperatures. The cooling signal propagates in the five soil temperature layers with a time delay, increasing with depth. The cooling signal at the surface is caused by the increased evapotranspiration, which results from an increased evaporation from bare soil along with enhanced transpiration from vegetation. The altered surface energy balance and the increased evapotranspiration transport the irrigation signal to the near-surface atmosphere through diffusion causing an increase of the 2 m relative humidity and decrease of the 2 m mean temperature. While there is agreement in the model results at both resolutions that the 2 m maximum temperature is reduced, the effects of irrigation on the 2 m minimum temperature range from a temperature reduction to a temperature increase. The ability of irrigation to reduce the diurnal maximum temperature, showed that the intensity of a heatwave in August 2017 could be reduced through delayed irrigation effects. Even after irrigation stopped, the high soil moisture caused a daytime cooling effect on the atmosphere. The cooling effect of irrigation feed back with meteorological patterns such as the regional and local wind field. In the case study of the Po Valley in summer 2017, the sea breeze is reduced due to irrigation, caused by the reduced temperature gradient between land and

sea. The cooling further decreases also the TKE as well as the PBL, leading to effects in convective conditions, which affect in turn the precipitation. The irrigation effects on precipitation are resolution dependent (RQ3). The increased soil moisture through irrigation affect vegetational processes directly and indirectly. One key process is the photosynthesis, which is driven by the stomatal conductance. In REMO2020-iMOVE, the concept is applied to canopies and is therefore called canopy conductance. The canopy conductance is determined by the soil moisture - the higher the soil moisture, the higher is the canopy conductance. This enhances photosynthesis, allowing more carbon to be absorbed from the atmosphere. As a result, gross primary production increases, leading to a consequent increase of NPP and LAI growth, , which reaches a higher peak in summer months due to irrigation. These effects influence consequently evapotranspiration as well as the vegetation ratio. The coupled model setup enables the reaction of vegetation to atmospheric processes as well. Temperature is an important variable, which drives vegetational processes such as the LAI growth. With the decrease of the 2 m mean temperature due to irrigation, the LAI develops slower. Additionally, the growing season, defined by a temperature sum, is extended by irrigation. However, it has to be noted, that these two effects are rather model-dependent effects, and might need improvement in the model.

RQ3: What is the role of resolution in modeling irrigation effects up to convection-permitting scale using a coupled regional climate model system?
Modeling irrigation effects up to convection-permitting scale implies a careful selection of the RCM version. While at 0.11° horizontal resolution the hydrostatic assumption, balancing the pressure gradient force and the gravitational force, is valid, convection-permitting scales require the non-hydrostatic dynamical core, which enables the resolution of the vertical velocity. These differences make the convection-permitting scale of particular interest and cause effects and feedbacks in the simulation results. Increasing the resolution from 0.11° horizontal resolution to 0.0275° resolves land surface features with more details and an increased heterogeneity, affecting the topography, the PFT distribution and the distribution of the irrigated fraction. The higher resolution results in more grid cells with a higher irrigated fraction, causing more localized and more pronounced irriga-

tion effects in the atmosphere, such as for the 2 m maximum temperature, which shows a high correlation of the irrigated fraction and the irrigation effect. In coupled RCM system, the vegetational processes develop very similarly at both resolutions, however, they react to differences in atmospheric conditions. A stronger resolution effect can be observed for precipitation. At convection-permitting resolution the diurnal cycle of precipitation aligns well with observational values. The irrigation effect on precipitation shows a different sign for the two resolution. While at 0.11° horizontal resolution, precipitation is increasing at the border of the Alps, the irrigation effect on precipitation at convection-permitting resolution shows rather small-scale changes with mixed responses, which sum up to a precipitation reduction above the Po Valley. These differences can be explained with the different development of CIN at both resolution and which shows more localized and mixed patterns at 0.0275° horizontal resolution.

5.2 Advancements and added values

This research contributes with a newly developed parameterization to the understanding of irrigation effects on the local and regional climate system. The parameterization is developed for the coupled RCM system REMO2020-iMOVE and incorporates the interaction of soil, vegetation and atmospheric processes. This model setup represents a step toward more complex and realistic regional climate model systems, and includes a human activity and land use practice. Irrigation studies are suitable test cases for complex regional climate modeling systems, as irrigation directly and indirectly influences atmospheric, vegetation, and soil processes. The interactive coupling showed, for instance, the improved plant growth conditions caused by irrigation represented with a higher LAI peak, but in the same time, the reaction of the plant growth to cooling effect in the atmosphere induced by irrigation.
Applying the interactively coupled model setup at convection-permitting resolution adds another characteristic to this study and contributes to the understanding which irrigation effects are resolution dependent, such as convection, while others show a higher consistency, for instance vegetation processes. Furthermore, the irrigation parameterization is implemented as a subgrid-scale parameteriza-

tion with a separate irrigated fraction. Until now, to the knowledge of the author, there is only one more irrigation study with one RCM, which follows the subgrid-scale approach and a separate irrigated fraction and therefore, is capable in capturing distinct irrigation effects as well as potential non-linear processes.

5.3 Implications for climate services

With this work, the RCM system REMO2020-iMOVE is extended by the human activity and land use practice irrigation. Human activities interfere with the natural conditions of our climate system and should be considered to be represented in climate modeling studies. In particular with the advances in increasing the resolution, the integration of small-scale processes of land such as irrigation in Europe becomes more important and contributes to the improvement of representing land in the regional climate system. This work used a coupled modeling setup of soil, vegetation and atmospheric processes, exploring the improvements of such a setup in combination with the new irrigation parameterization. Realistic, comprehensive and well understood processes are crucial for modeling studies, as they generate climate data and, therefore, provide the foundation for climate service products. Including irrigation in RCM studies can decrease the temperature bias in heavily managed areas , and thereby, improve the model results.
Furthermore, irrigation can be understood as climate adaptation measure with mitigation potential. This study quantified its potential cooling effect, contributing to the analysis of its mitigation potential, e.g. during a heatwave. Finally, the effects of irrigation may be of particular interest to society, as it is a human activity that can be actively influenced.

5.4 Future research directions

Irrigation is an important topic, which should be included in regional climate modeling studies. In particular facing climate change, the risk of water scarcity is a rising issue (Shukla et al., 2019). Therefore, parameterizations which do not only show the irrigation process, but include irrigation's characteristics and limitations in the real world such as water availability are desirable. In addition

to the dynamic water resources, the transient changes of irrigated areas should be accounted for in future RCM studies, following the example of IRRMIP at the global scale (Yao et al., 2025). A dataset tailored to RCMs including transient irrigated fractions was recently developed by Hoffmann et al. (2023). Furthermore, a coordinated, multi-model ensemble could create comparable experiments, which contribute to the assessment of advantages and disadvantages of irrigation parameterizations and lower the uncertainties in modeling irrigation effects.
In the last years, combined frameworks of observational and modeling approaches analyze the inter-connected processes of irrigation for example GRAINEX (Rappin et al., 2021) or LIAISE (Boone et al., 2025) and improve the available data on irrigation observations. Furthermore, advances in remote sensing create improved, high-resolution irrigation data maps such as Dari et al. (2023).

References

Abel, D. K.-J. (2023), Weiterentwicklung der Bodenhydrologie des regionalen Klimamodells REMO, doctoralthesis, Universität Würzburg.

Agenzia Interregionale per il fiume Po (AIPo) (2025), 'English presentation - agenzia interregionale per il fiume po'. Accessed: 2025-02-06. URL: https://www.agenziapo.it/content/english-presentation

Arakawa, A. and Lamb, V. R. (1977), Computational design of the basic dynamical processes of the ucla general circulation model, *in* J. CHANG, ed., 'General Circulation Models of the Atmosphere', Vol. 17 of *Methods in Computational Physics: Advances in Research and Applications*, Elsevier, pp. 173–265. URL: https://www.sciencedirect.com/science/article/pii/B9780124608177500094

Asselin, R. (1972), 'Frequency filter for time integrations', *Monthly Weather Review* 100(6), 487 – 490.

Avanzi, F., Munerol, F., Milelli, M. et al. (2024), 'Winter snow deficit was a harbinger of summer 2022 socio-hydrologic drought in the po basin, italy', *Communications Earth & Environment* 5, 64. URL: https://doi.org/10.1038/s43247-024-01222-z

Ban, N., Caillaud, C., Coppola, E. et al. (2021), 'The first multi-model ensemble of regional climate simulations at kilometer-scale resolution, part i: evaluation of precipitation', *Climate Dynamics* 57, 275–302. URL: https://doi.org/10.1007/s00382-021-05708-w

Bartholomé, E. and and, A. S. B. (2005), 'Glc2000: a new approach to global land cover mapping from earth observation data', *International Journal of Remote Sensing* 26(9), 1959–1977. URL: https://doi.org/10.1080/01431160412331291297

Bonan, G., Levis, S., Kergoat, L. and Oleson, K. (2002), 'Landscapes as patches of plant functional types: An integrating concept for climate and ecosystem models', *Global Biogeochemical Cycles* 16.

Boone, A., Bellvert, J., Best, M., Brooke, J. K., Canut-Rocafort, G., Cuxart, J., Hartogensis, O., Moigne, P. L., Miró, J. R., Polcher, J., Price, J., Seguí, P. Q., Bech, J., Bezombes, Y., Branch, O., Cristóbal, J., Dassas, K., Fanise, P., Gibert, F., Goulas, Y., Groh, J., Hanus, J., Hmimina, G., Jarlan, L., Kim, E., Dantec, V. L., Page, M. L., Lohou, F., Lothon, M., Mangan, M. R., Martí, B., Martínez-Villagrasa, D., McGregor, J., Kerr-Munslow, A., Ouaadi, N., Philibert, A., Quiros-Vargas, J., Rascher, U., Siegmann, B., Udina, M., Vial, A., Wrenger, B., Wulfmeyer, V. and Zribi, M. (2025), 'The land surface interactions with the atmosphere over the iberian semi-arid environment (liaise) field campaign', *Journal of the European Meteorological Society* 2, 100007. URL: https://www.sciencedirect.com/science/article/pii/S2950630125000018

Boyko, O., Reggiani, P. and Todini, E. (2022), 'Post-processing climate projections of precipitation for the po river basin: will italy's north become water-constrained?', *Hydrology Research* 53(11), 1414–1427. URL: https://doi.org/10.2166/nh.2022.063

Bozzola, M. and Swanson, T. (2014), 'Policy implications of climate variability on agriculture: Water management in the po river basin, italy', *Environmental Science & Policy* 43, 26–38. Mountain water governance: policy implications from the EU "ACQWA" Project. URL: https://www.sciencedirect.com/science/article/pii/S146290111300289X

Branch, O., Warrach-Sagi, K., Wulfmeyer, V. and Cohen, S. (2014), 'Simulation of semi-arid biomass plantations and irrigation using the wrf-noah model: a comparison with observations from israel', *Hydrology and Earth System Sciences* 18(5), 1761–1783. URL: https://hess.copernicus.org/articles/18/1761/2014/

Brouwer, C. and Heibloem, M. (1986), Irrigation water management: Irrigation water needs. training manual no. 3, Technical report, FAO Land and Water Development Division.

Brouwer, C., Prins, K., Kay, M. and Heibloem, M. (1988), Irrigation water management: Irrigation methods. training manual no 5, Technical report, FAO Land and Water Development Division, Rome, Italy.

Brovkin, V. (2002), 'Climate-vegetation interaction', *Journal de physique IV* 12, 57–72.

Chen, X. and Jeong, S.-J. (2018), 'Irrigation enhances local warming with greater nocturnal warming effects than daytime cooling effects', *Environmental Research Letters* 13.

Chou, C., Ryu, D., Lo, M.-H., Wey, H.-W. and Malano, H. (2018), 'Irrigation-induced land-atmosphere feedbacks and their impacts on indian summer monsoon', *Journal of Climate* 31, 8785–8801. URL: https://doi.org/10.1175/JCLI-D-17-0762.1

Copernicus Climate Change Service (2022), 'European state of the climate 2017', https://climate.copernicus.eu/CopernicusESC.

Coppola, E., Sobolowski, S., Pichelli, E. et al. (2020), 'A first-of-its-kind multi-model convection permitting ensemble for investigating convective phenomena over europe and the mediterranean', *Climate Dynamics* 55, 3–34.

Cotera, R. V., Egerer, S., Nam, C., Lierhammer, L., Moors, L. and Costa, M. M. (2024), 'Resilient agriculture: water management for climate change adaptation in lower saxony', *Journal of Water and Climate Change* 15(3), 1034–1053. URL: https://doi.org/10.2166/wcc.2024.455

Dari, J., Brocca, L., Modanesi, S., Massari, C., Tarpanelli, A., Barbetta, S., Quast, R., Vreugdenhil, M., Freeman, V., Barella-Ortiz, A., Quintana-Seguí, P., Bretreger, D. and Volden, E. (2023), 'Regional data sets of high-resolution (1 and 6 km) irrigation estimates from space', *Earth System Science Data* 15(4), 1555–1575. URL: https://essd.copernicus.org/articles/15/1555/2023/

De Bruin, H., Hartogensis, O., Allen, R. et al. (2004), 'Regional advection perturbations in an irrigated desert (rapid) experiment', *Theoretical and Applied Climatology* 80, 143–152. URL: https://doi.org/10.1007/s00704-004-0096-x

de Noblet-Ducoudré, N., Boisier, J.-P., Pitman, A., Bonan, G. B., Brovkin, V., Cruz, F., Delire, C., Gayler, V., van den Hurk, B. J. J. M., Lawrence, P. J., van der Molen, M. K., Müller, C., Reick, C. H., Strengers, B. J. and

Voldoire, A. (2012), 'Determining robust impacts of land-use-induced land cover changes on surface climate over north america and eurasia: Results from the first set of lucid experiments', *Journal of Climate* 25(9), 3261 – 3281. URL: https://journals.ametsoc.org/view/journals/clim/25/9/jcli-d-11-00338.1.xml

de Vrese, P. and Hagemann, S. (2018), 'Uncertainties in modelling the climate impact of irrigation', *Climate Dynamics* 51, 2023–2038. URL: https://doi.org/10.1007/s00382-017-3996-z

de Vrese, P., Hagemann, S. and Claussen, M. (2016), 'Asian irrigation, african rain: Remote impacts of irrigation', *Geophysical Research Letters* 43(8), 3737–3745. URL: https://agupubs.onlinelibrary.wiley.com/doi/abs/10.1002/2016GL068146

Dümenil, L. and Todini, E. (1992), Chapter 9 - a rainfall–runoff scheme for use in the hamburg climate model, *in* J. P. O'Kane, ed., 'Advances in Theoretical Hydrology', European Geophysical Society Series on Hydrological Sciences, Elsevier, Amsterdam, pp. 129–157. URL: https://www.sciencedirect.com/science/article/pii/B9780444898319500168

ESA (2017), Land Cover CCI Product User Guide Version 2, Technical report, European Space Agency. URL: http://maps.elie.ucl.ac.be/CCI/viewer/download/ESACCI-LC-Ph2-PUGv2_2.0.pdf

Farquhar, G. D., Caemmerer, S. and Berry, J. A. (1980), 'A biochemical model of photosynthesis in leaves of c3 species', *Planta* 149, 78–90.

Giorgi, F. (2019), 'Thirty years of regional climate modeling: Where are we and where are we going next?', *Journal of Geophysical Research: Atmospheres* 124, 5696–5723.

Giorgi, F. and Avissar, R. (1997), 'Representation of heterogeneity effects in earth system modeling: Experience from land surface modeling', *Reviews of Geophysics* 35(4), 413–437. URL: https://agupubs.onlinelibrary.wiley.com/doi/abs/10.1029/97RG01754

Goettel, H. (2009), 'Einfluss der nichthydrostatischen modellierung und der niederschlagsverdriftung auf die ergebnisse regionaler klimamodellierung', *Reports on Earth System Science* p. 125.

Hagemann, S., Botzet, M., Dümenil, L. and Machenhauer, B. (1999), 'MPI Report No. 289 - Derivation of global GCM boundary conditions from 1 km land use satellite date'.

Hoffmann, P., Reinhart, V., Rechid, D., de Noblet-Ducoudré, N., Davin, E. L., Asmus, C., Bechtel, B., Böhner, J., Katragkou, E. and Luyssaert, S. (2023), 'High-resolution land use and land cover dataset for regional climate modelling: historical and future changes in europe', *Earth System Science Data* 15(8), 3819–3852. URL: https://essd.copernicus.org/articles/15/3819/2023/

Hohenegger, C., Brockhaus, P., Bretherton, C. S. and Schär, C. (2009), 'The soil moisture–precipitation feedback in simulations with explicit and parameterized convection', *Journal of Climate* 22(19), 5003 – 5020. URL: https://journals.ametsoc.org/view/journals/clim/22/19/2009jcli2604.1.xml

Holdridge, L. R. (1967), *Life Zone Ecology*, Tropical Science Center, San José, Costa Rica.

Holton, J. R. and Hakim, G. J. (2013), *An introduction to dynamic meteorology*, Vol. 88, 5 edn, Academic Press.

Huber, D. B., Mechem, D. B. and Brunsell, N. A. (2014), 'The effects of great plains irrigation on the surface energy balance, regional circulation, and precipitation', *Climate* 2(2), 103–128. URL: https://www.mdpi.com/2225-1154/2/2/103

IPCC (2019), 'Climate change and land: an ipcc special report on climate change, desertification, land degradation, sustainable land management, food security, and greenhouse gas fluxes in terrestrial ecosystems'. In press. URL: https://www.ipcc.ch/srccl/

Jacob, D. and Podzun, R. (1997), 'Sensitivity studies with the regional climate model remo', *Meteorology and Atmospheric Physics* 63, 119–129.

Jacob, D., Teichmann, C., Sobolowski, S. et al. (2020), 'Regional climate downscaling over europe: perspectives from the euro-cordex community', *Regional Environmental Change* 20, 51. URL: https://doi.org/10.1007/s10113-020-01606-9

Joint Research Centre. European Commission (2018), 'Fact sheet: Po river basin'. Accessed: 2025-02-05. URL: https://water.jrc.ec.europa.eu/pdf/po-fs.pdf

Kang, S. and Eltahir, E. (2018), 'North china plain threatened by deadly heatwaves due to climate change and irrigation', *Nature Communications* 9, 2894. URL: https://doi.org/10.1038/s41467-018-05252-y

Kendon, E. J., Prein, A. F., Senior, C. A. and Stirling, A. (2021), 'Challenges and outlook for convection-permitting climate modelling'.

Knorr, W. (1997), Satellitengestützte Fernerkundung und Modellierung des globalen CO_2-Austauschs der Landvegetation, Examensarbeit, Max Planck Institute for Meteorology, Hamburg. Also published as: Satellite remote sensing and modelling of the global CO_2 exchange of land vegetation: A synthesis study.

Kotlarski, S. (2007), 'A subgrid glacier parameterisation for use in regional climate modelling', *Reports on Earth System Science* 42.

Kueppers, L. M., Snyder, M. A. and Sloan, L. C. (2007), 'Irrigation cooling effect: Regional climate forcing by land-use change', *Geophysical Research Letters* 34(3). URL: https://agupubs.onlinelibrary.wiley.com/doi/abs/10.1029/2006GL028679

Leng, G., Leung, L. and Huang, M. (2017), 'Significant impacts of irrigation water sources and methods on modeling irrigation effects in the ACME Land Model', *Journal of Advances in Modeling Earth Systems* 9.

Li, H., Lo, M.-H., Ryu, D., Peel, M. and Zhang, Y. (2022), 'Possible increase of air temperature by irrigation', *Geophysical Research Letters* 49(20), e2022GL100427. e2022GL100427 2022GL100427. URL: https://agupubs.onlinelibrary.wiley.com/doi/abs/10.1029/2022GL100427

Liu, H., Meng, Z., Zhu, Y. and Huang, Y. (2023), 'Convection initiation associated with a boundary layer convergence line over a real-world sharp vegetation-contrast area', *Monthly Weather Review* 151, 1189–1212.

Luyssaert, S., Jammet, M., Stoy, P., Estel, S., Pongratz, J., Ceschia, E., Churkina, G., Don, A., Erb, K.-H., Ferlicoq, M., Gielen, B., Grünwald, T., Houghton, R., Klumpp, K., Knohl, A., Kolb, T., Kuemmerle, T., Laurila, T., Lohila, A. and Dolman, H. A. (2014), 'Land management and land-cover change have impacts of similar magnitude on surface temperature', *Nature Climate Change* 4, 389–393.

Majewski, D. (1991), 'The europa-modell of the deutscher wetterdienst'.

Manabe, S. (1969), 'Climate and the ocean circulation: I. the atmospheric circulation and the hydrology of the earth's surface', *Monthly Weather Review* 97(11), 739 – 774. URL: https://journals.ametsoc.org/view/journals/mwre/97/11/1520-0493_1969_097_0739_catoc_2_3_co_2.xml

Marcella, M. P. and Eltahir, E. A. B. (2014), 'Introducing an irrigation scheme to a regional climate model: A case study over west africa', *Journal of Climate* 27(15), 5708 – 5723. URL: https://journals.ametsoc.org/view/journals/clim/27/15/jcli-d-13-00116.1.xml

Marchetti, M. (2002), 'Environmental changes in the central po plain (northern italy) due to fluvial modifications and anthropogenic activities', *Geomorphology* 44(3), 361–373. Geomorphology on Large Rivers. URL: https://www.sciencedirect.com/science/article/pii/S0169555X01001830

Martínez-Mena, M., Carrillo-López, E., Boix-Fayos, C., Almagro, M., García Franco, N., Díaz-Pereira, E., Montoya, I. and de Vente, J. (2020), 'Long-term effectiveness of sustainable land management practices to control runoff, soil erosion, and nutrient loss and the role of rainfall intensity in mediterranean rainfed agroecosystems', *CATENA* 187, 104352. URL: https://www.sciencedirect.com/science/article/pii/S0341816219304941

Massari, C., Modanesi, S., Dari, J., Gruber, A., De Lannoy, G. J. M., Girotto, M., Quintana-Seguí, P., Le Page, M., Jarlan, L., Zribi, M., Ouaadi, N., Vreugdenhil, M., Zappa, L., Dorigo, W., Wagner, W., Brombacher, J., Pelgrum, H., Jaquot, P., Freeman, V., Volden, E., Fernandez Prieto, D., Tarpanelli, A., Barbetta, S. and Brocca, L. (2021), 'A review of irrigation information retrievals from space and their utility for users', *Remote Sensing* 13(20). URL: https://www.mdpi.com/2072-4292/13/20/4112

Matte, D., Laprise, R. and Thériault, J. M. (2016), 'Comparison between high-resolution climate simulations using single- and double-nesting approaches within the big-brother experimental protocol', *Climate Dynamics* 47, 3613–3626. URL: https://doi.org/10.1007/s00382-016-3031-9

Matte, D., Laprise, R., Thériault, J. M. et al. (2017), 'Spatial spin-up of fine scales in a regional climate model simulation driven by low-resolution boundary conditions', *Climate Dynamics* 49, 563–574. URL: https://doi.org/10.1007/s00382-016-3358-2

McDermid, S., Nocco, M., Lawston-Parker, P., Keune, J., Pokhrel, Y., Jain, M., Jägermeyr, J., Brocca, L., Massari, C., Jones, A. D., Vahmani, P., Thiery, W., Yao, Y., Bell, A., Chen, L., Dorigo, W., Hanasaki, N., Jasechko, S., Lo, M.-H., Mahmood, R., Mishra, V., Mueller, N. D., Niyogi, D., Rabin, S. S., Sloat, L., Wada, Y., Zappa, L., Chen, F., Cook, B. I., Kim, H., Lombardozzi, D., Polcher, J., Ryu, D., Santanello, J., Satoh, Y., Seneviratne, S., Singh, D. and Yokohata, T. (2023), 'Irrigation in the earth system', *Nature Reviews Earth & Environment* 4(7), 435–453. URL: https://doi.org/10.1038/s43017-023-00438-5

Montanari, A., Nguyen, H., Rubinetti, S., Ceola, S., Galelli, S., Rubino, A. and Zanchettin, D. (2023), 'Why the 2022 po river drought is the worst in the past two centuries', *Science Advances* 9(32), eadg8304. URL: https://www.science.org/doi/abs/10.1126/sciadv.adg8304

Monteleone, B. and Borzí, I. (2024), 'Drought in the po valley: Identification, impacts and strategies to manage the events', *Water* 16(8). URL: https://www.mdpi.com/2073-4441/16/8/1187

Nordeng, T. E. (1994), 'Extended versions of the convective parametrization scheme at ecmwf and their impact on the mean and transient activity of the model in the tropics. technical memorandum 206.'. URL: https://www.ecmwf.int/en/elibrary/75843-extended-versions-convective-parametrization-scheme-ecmwf-and-their-impact-mean

Oke, T. (1988), *Boundary Layer Climates*, 2nd edn, Routledge, London.

Oleson, K., Lawrence, D., Bonan, G., Flanner, M., Kluzek, E., Lawrence, P., Levis, S., Swenson, S., Thornton, P., Dai, A., Decker, M., Dickinson, R., Feddema, J., Heald, C., Hoffman, F., Lamarque, J.-F., Mahowald, N., Niu, G.-Y., Qian, T. and Zeng, X. (2010), Technical description of version 4.0 of the community land model (clm), Technical report, NCAR.

Ozdogan, M. and Gutman, G. (2008), 'A new methodology to map irrigated areas using multi-temporal modis and ancillary data: An application example in the continental us', *Remote Sensing of Environment* 112(9), 3520–3537. URL: https://www.sciencedirect.com/science/article/pii/S0034425708001338

Ozdogan, M., Rodell, M., Beaudoing, H. K. and Toll, D. L. (2010), 'Simulating the effects of irrigation over the united states in a land surface model based on satellite-derived agricultural data', *Journal of Hydrometeorology* 11(1), 171 – 184. URL: https://journals.ametsoc.org/view/journals/hydr/11/1/2009jhm1116_1.xml

Patanè, C. (2011), 'Leaf area index, leaf transpiration and stomatal conductance as affected by soil water deficit and vpd in processing tomato in semi arid mediterranean climate', *Journal of Agronomy and Crop Science* 197(3), 165–176. URL: https://onlinelibrary.wiley.com/doi/abs/10.1111/j.1439-037X.2010.00454.x

Pfeifer, S. (2006), 'Modeling cold cloud processes with the regional climate model remo', *Reports on Earth System Science* . URL: https://pure.mpg.de/rest/items/item_994658_3/component/file_994657/content

Pietikäinen, J. P., Markkanen, T., Sieck, K., Jacob, D., Korhonen, J., Räisänen, P., Gao, Y., Ahola, J., Korhonen, H., Laaksonen, A. and Kaurola, J. (2018),

'The regional climate model remo (v2015) coupled with the 1-d freshwater lake model flake (v1): Fenno-scandinavian climate and lakes', *Geoscientific Model Development* 11, 1321–1342.

Pietikäinen, J.-P., O'Donnell, D., Teichmann, C., Karstens, U., Pfeifer, S., Kazil, J., Podzun, R., Fiedler, S., Kokkola, H., Birmili, W., O'Dowd, C., Baltensperger, U., Weingartner, E., Gehrig, R., Spindler, G., Kulmala, M., Feichter, J., Jacob, D. and Laaksonen, A. (2012), 'The regional aerosol-climate model remo-ham', *Geosci. Model Development Discussions* 5, 737–779. URL: https://gmd.copernicus.org/preprints/5/737/2012/gmdd-5-737-2012.pdf

Pietikäinen, J.-P., Sieck, K., Buntemeyer, L., Frisius, T., Nam, C., Hoffmann, P., Pop, C., Rechid, D. and Jacob, D. (2025), 'Remo2020: a modernized modular regional climate model', *EGUsphere* . [preprint]. URL: https://doi.org/10.5194/egusphere-2025-1586

Pongratz, J., Dolman, H., Don, A., Erb, K.-H., Fuchs, R., Herold, M., Jones, C., Kuemmerle, T., Luyssaert, S., Meyfroidt, P. and Naudts, K. (2018), 'Models meet data: Challenges and opportunities in implementing land management in earth system models', *Global Change Biology* 24(4), 1470–1487. URL: https://doi.org/10.1111/gcb.13988

Potes, M., Salgado, R., Costa, M. J., Morais, M., Bortoli, D., Kostadinov, I. and Mammarella, I. (2017), 'Lake–atmosphere interactions at alqueva reservoir: a case study in the summer of 2014', *Tellus A: Dynamic Meteorology and Oceanography* .

Poulter, B., MacBean, N., Hartley, A., Khlystova, I., Arino, O., Betts, R., Bontemps, S., Boettcher, M., Brockmann, C., Defourny, P., Hagemann, S., Herold, M., Kirches, G., Lamarche, C., Lederer, D., Ottlé, C., Peters, M. and Peylin, P. (2015), 'Plant functional type classification for earth system models: results from the european space agency's land cover climate change initiative', *Geoscientific Model Development* 8(7), 2315–2328. URL: https://gmd.copernicus.org/articles/8/2315/2015/

Prein, A. F., Langhans, W., Fosser, G., Ferrone, A., Ban, N., Goergen, K., Keller, M., Tölle, M., Gutjahr, O., Feser, F., Brisson, E., Kollet, S., Schmidli, J., Lipzig, N. P. V. and Leung, R. (2015), 'A review on regional convection-permitting climate modeling: Demonstrations, prospects, and challenges', *Reviews of Geophysics* 53, 323–361.

Puma, M. J. and Cook, B. I. (2010), 'Effects of irrigation on global climate during the 20th century', *Journal of Geophysical Research: Atmospheres* 115(D16). URL: https://agupubs.onlinelibrary.wiley.com/doi/abs/10.1029/2010JD014122

Qian, Y., Huang, M., Yang, B. and Berg, L. K. (2013), 'A modeling study of irrigation effects on surface fluxes and land–air–cloud interactions in the southern great plains', *Journal of Hydrometeorology* 14(3), 700 – 721. URL: https://journals.ametsoc.org/view/journals/hydr/14/3/jhm-d-12-0134_1.xml

Qian, Y., Yang, Z., Feng, Z. and et al. (2020), 'Neglecting irrigation contributes to the simulated summertime warm-and-dry bias in the central united states', *npj Climate and Atmospheric Science* 3, 31. URL: https://doi.org/10.1038/s41612-020-00135-w

Rappin, E., Mahmood, R., Nair, U., Pielke, R. A., Brown, W., Oncley, S., Wurman, J., Kosiba, K., Kaulfus, A., Phillips, C., Lachenmeier, E., Santanello, J., Kim, E. and Lawston-Parker, P. (2021), 'The great plains irrigation experiment (grainex)', *Bulletin of the American Meteorological Society* 102(9), E1756 – E1785. URL: https://journals.ametsoc.org/view/journals/bams/102/9/BAMS-D-20-0041.1.xml

Rechid, D., Davin, E., de Noblet-Ducoudré, N. and Katragkou, E. (2017), CORDEX Flagship Pilot Study "LUCAS - Land Use & Climate Across Scales" - a new initiative on coordinated regional land use change and climate experiments for Europe, *in* 'EGU General Assembly Conference Abstracts', EGU General Assembly Conference Abstracts, p. 13172.

Rechid, D. and Jacob, D. (2006), 'Influence of monthly varying vegetation on the simulated climate in europe', *Meteorologische Zeitschrift* 15, 99–116.

Rechid, D., Raddatz, T. J. and Jacob, D. (2009), 'Parameterization of snow-free land surface albedo as a function of vegetation phenology based on modis data and applied in climate modelling', *Theoretical and Applied Climatology* 95, 245–255.

Reick, C. H., Raddatz, T., Brovkin, V. and Gayler, V. (2013), 'Representation of natural and anthropogenic land cover change in mpi-esm', *Journal of Advances in Modeling Earth Systems* 5(3), 459–482. URL: https://agupubs.onlinelibrary.wiley.com/doi/abs/10.1002/jame.20022

Reinhart, V., Hoffmann, P., Rechid, D., Böhner, J. and Bechtel, B. (2022), 'High-resolution land use and land cover dataset for regional climate modelling: a plant functional type map for europe 2015', *Earth System Science Data* 14(4), 1735–1794. URL: https://essd.copernicus.org/articles/14/1735/2022/

Roeckner, E., Arpe, K., Bengtsson, L., Christoph, M., Claussen, M., Dümenil, L., Esch, M., Giorgetta, M., Schlese, U. and Schulzweida, U. (1996), 'The atmospheric gernal circulation model echam-4: Model description and simulation of present day climate'.

Saeed, F., Hagemann, S. and Jacob, D. (2009), 'Impact of irrigation on the south asian summer monsoon', *Geophysical Research Letters* 36(20). URL: https://agupubs.onlinelibrary.wiley.com/doi/abs/10.1029/2009GL040625

Sangelantoni, L., Sobolowski, S. P., Soares, P. M. M., Goergen, K., Cardoso, R. M., Adinolfi, M., Dobler, A., Katragkou, E., Scoccimarro, E., Ferretti, R., Tölle, M. and Feldmann, H. (2025), 'Heatwave future changes from an ensemble of km-scale regional climate simulations within cordex-fps convection', *Geophysical Research Letters* 52(2), e2024GL111147. URL: https://agupubs.onlinelibrary.wiley.com/doi/abs/10.1029/2024GL111147

Semmler, T. (2002), 'Der Wasser- und Energiehaushalt der arktischen Atmosphäre', *Examensarbeit - Max-Planck-Institut fur Meteorologie* pp. 101–106.

Sha, Z., Bai, Y., Li, R. et al. (2022), 'The global carbon sink potential of terrestrial vegetation can be increased substantially by optimal land management',

Communications Earth & Environment 3, 8. URL: https://doi.org/10.1038/s43247-021-00333-1

Shukla, P., Skea, J., Slade, R., van Diemen, R., Haughey, E., Malley, J., Pathak, M. and Pereira, J. P. (2019), *Technical Summary*, Intergovernmental Panel on Climate Change (IPCC). In press. URL: https://www.ipcc.ch/srccl/

Siebert, S. and Doell, P. (2010), 'Quantifying blue and green virtual water contents in global crop production as well as potential production losses without irrigation', *Journal of Hydrology* 384, 198–217.

Siebert, S., Henrich, V., Frenken, K. and Burke, J. (2013), 'Update of the digital global map of irrigation areas to version 5.'.

Singh, D., McDermid, S. P., Cook, B. I., Puma, M. J., Nazarenko, L. and Kelley, M. (2018), 'Distinct influences of land cover and land management on seasonal climate', *Journal of Geophysical Research: Atmospheres* 123(21), 12,017–12,039. URL: https://agupubs.onlinelibrary.wiley.com/doi/abs/10.1029/2018JD028874

Smith, P., Calvin, K., Nkem, J., Campbell, D., Cherubini, F., Grassi, G., Korotkov, V., Le Hoang, A., Lwasa, S., McElwee, P., Nkonya, E., Saigusa, N., Soussana, J.-F., Taboada, M. A., Manning, F. C., Nampanzira, D., Arias-Navarro, C., Vizzarri, M., House, J., Roe, S., Cowie, A., Rounsevell, M. and Arneth, A. (2020), 'Which practices co-deliver food security, climate change mitigation and adaptation, and combat land degradation and desertification?', *Global Change Biology* 26(3), 1532–1575. URL: https://onlinelibrary.wiley.com/doi/abs/10.1111/gcb.14878

Stevens, B., Fiedler, S., Kinne, S., Peters, K., Rast, S., Müsse, J., Smith, S. J. and Mauritsen, T. (2017), 'Macv2-sp: a parameterization of anthropogenic aerosol optical properties and an associated twomey effect for use in cmip6', *Geoscientific Model Development* 10(1), 433–452. URL: https://gmd.copernicus.org/articles/10/433/2017/

Teichmann, C. (2010), 'Climate and air pollution modelling in south america with focus on megacities', *Reports on Earth System Science* 76. URL: https://pure.mpg.de/rest/items/item_993870_4/component/file_993869/content

Thiery, W., Davin, E. L., Lawrence, D. M., Hirsch, A. L., Hauser, M. and Seneviratne, S. I. (2017), 'Present-day irrigation mitigates heat extremes', *Journal of Geophysical Research: Atmospheres* 122(3), 1403–1422. URL: https://agupubs.onlinelibrary.wiley.com/doi/abs/10.1002/2016JD025740

Tiedtke, M. (1989), 'A comprehensive mass flux scheme for cmulus parameterization in large-scale models', *Monthly Weather Review* pp. 1779–1800.

Tuinenburg, O. A., Hutjes, R. W. A., Stacke, T., Wiltshire, A. and Lucas-Picher, P. (2014), 'Effects of irrigation in india on the atmospheric water budget', *Journal of Hydrometeorology* 15(3), 1028 – 1050.

Uddin, J., Hancock, N., Smith, R. and Foley, J. (2013), 'Measurement of evapotranspiration during sprinkler irrigation using a precision energy budget (bowen ratio, eddy covariance) methodology', *Agricultural Water Management* 116, 89–100. URL: https://www.sciencedirect.com/science/article/pii/S0378377412002557

Udina, M., Peinó, E., Polls, F., Mercader, J., Guerrero, I., Valmassoi, A., Paci, A. and Bech, J. (2024), 'Irrigation impact on boundary layer and precipitation characteristics in weather research and forecasting model simulations during liaise-2021', *Quarterly Journal of the Royal Meteorological Society* 150(763), 3251–3273. URL: https://rmets.onlinelibrary.wiley.com/doi/abs/10.1002/qj.4756

Valmassoi, A., Dudhia, J., Di Sabatino, S. and Pilla, F. (2020*a*), 'Evaluation of three new surface irrigation parameterizations in the wrf-arw v3.8.1 model: the po valley (italy) case study', *Geoscientific Model Development Discussions* pp. 1–33.

Valmassoi, A., Dudhia, J., Di Sabatino, S. and Pilla, F. (2020*b*), 'Regional climate impacts of irrigation in northern italy using a high resolution model', *Atmosphere* 11(1). URL: https://www.mdpi.com/2073-4433/11/1/72

Valmassoi, A. and Keller, J. D. (2022), 'A review on irrigation parameterizations in earth system models', *Frontiers in Water* 4. URL: https://www.frontiersin.org/journals/water/articles/10.3389/frwa.2022.906664

Wang, Y., Yang, B., Yang, Z., Feng, Z., Qiu, B., Dai, G., Qian, Y. and Zhang, Y. (2024), 'Responses of summer mesoscale convective systems to irrigation over the north china plain based on convection-permitting model simulations', *Environmental Research Communications* 6(9), 091012. URL: https://dx.doi.org/10.1088/2515-7620/ad78ba

Wilhelm, C., Rechid, D. and Jacob, D. (2014), 'Interactive coupling of regional atmosphere with biosphere in the new generation regional climate system model remo-imove', *Geoscientific Model Development* 7, 1093–1114.

Wilkinson, M., Dumontier, M., Aalbersberg, I. J. et al. (2016), 'The fair guiding principles for scientific data management and stewardship', *Scientific Data* 3, 160018. URL: https://doi.org/10.1038/sdata.2016.18

Wu, L., Feng, J. and Miao, W. (2018), 'Simulating the impacts of irrigation and dynamic vegetation over the north china plain on regional climate', *Journal of Geophysical Research: Atmospheres* 123(15), 8017–8034. URL: https://agupubs.onlinelibrary.wiley.com/doi/abs/10.1029/2017JD027784

Wu, L., Feng, J., Qin, F. and Qiu, Y. (2022), 'Regional climate effects of irrigation over central asia using weather research and forecasting model', *Journal of Geophysical Research: Atmospheres* 127(12), e2021JD036210. e2021JD036210 2021JD036210. URL: https://agupubs.onlinelibrary.wiley.com/doi/abs/10.1029/2021JD036210

Wullschleger, S. D., Epstein, H. E., Box, E. O., Euskirchen, E. S., Goswami, S., Iversen, C. M., Kattge, J., Norby, R. J., van Bodegom, P. M. and Xu, X. (2014), 'Plant functional types in earth system models: past experiences and future directions for application of dynamic vegetation models in high-latitude ecosystems', *Annals of Botany* 114(1), 1–16. URL: https://doi.org/10.1093/aob/mcu077

Yang, B., Zhang, Y., Qian, Y., Tang, J. and Liu, D. (2016), 'Climatic effects of irrigation over the huang-huai-hai plain in china simulated by the weather research and forecasting model', *Journal of Geophysical Research: Atmospheres* 121(5), 2246–2264. URL: https://agupubs.onlinelibrary.wiley.com/doi/abs/10.1002/2015JD023736

Yang, Z., Qian, Y., Liu, Y., Berg, L. K., Hu, H., Dominguez, F., Yang, B., Feng, Z., Gustafson Jr, W. I., Huang, M. and Tang, Q. (2019), 'Irrigation impact on water and energy cycle during dry years over the united states using convection-permitting wrf and a dynamical recycling model', *Journal of Geophysical Research: Atmospheres* 124(21), 11220–11241. URL: https://agupubs.onlinelibrary.wiley.com/doi/abs/10.1029/2019JD030524

Yao, Y., Ducharne, A., Cook, B. I. et al. (2025), 'Impacts of irrigation expansion on moist-heat stress based on irrmip results', *Nature Communications* 16, 1045. URL: https://doi.org/10.1038/s41467-025-56356-1

Yuan, T., Tai, A. P., Mao, J., Tam, O. H., Li, R. K., Wu, J. and Li, S. (2023), 'Effects of different irrigation methods on regional climate in north china plain: A modeling study', *Agricultural and Forest Meteorology* 342, 109728. URL: https://www.sciencedirect.com/science/article/pii/S0168192323004185

Zhang, Z., He, C., Chen, F., Miguez-Macho, G., Liu, C. and Rasmussen, R. (2025), 'Us corn belt enhances regional precipitation recycling', *Proceedings of the National Academy of Sciences* 122(1), e2402656121. URL: https://www.pnas.org/doi/abs/10.1073/pnas.2402656121

Zobler, L. (1986), 'A world soil file for global climate modeling', *NASA Technical Memorandum* 87802. NASA Goddard Institute for Space Studies. New York, New York, U.S.A.

Zucaro, R. (2014), Atlas of italian irrigation systems, Technical report, Istituto Nazionale di Economia Agraria (INEA). URL: https://sigrian.crea.gov.it/wp-content/uploads/2019/11/Atlas_Italian_irrigation_2014_INEA.pdf

Appendices

A Original publications

A.1 Publication I

Geosci. Model Dev., 16, 7311–7337, 2023
https://doi.org/10.5194/gmd-16-7311-2023

Geoscientific Model Development
Open Access
EGU

Modeling and evaluating the effects of irrigation on land–atmosphere interaction in southwestern Europe with the regional climate model REMO2020–iMOVE using a newly developed parameterization

Christina Asmus[1], **Peter Hoffmann**[1], **Joni-Pekka Pietikäinen**[1], **Jürgen Böhner**[2], **and Diana Rechid**[1]

[1]Climate Service Center Germany (GERICS), Helmholtz-Zentrum Hereon, Hamburg, Germany
[2]Center for Earth System Research and Sustainability (CEN), Universität Hamburg, Hamburg, Germany

Correspondence: Christina Asmus (christina.asmus@hereon.de)

Received: 3 May 2023 – Discussion started: 14 July 2023
Revised: 20 October 2023 – Accepted: 22 October 2023 – Published: 19 December 2023

Abstract. Irrigation is a crucial land use practice to adapt agriculture to unsuitable climate and soil conditions. Aiming to improve the growth of plants, irrigation modifies the soil condition, which causes atmospheric effects and feedbacks through land–atmosphere interaction. These effects can be quantified with numerical climate models, as has been done in various studies. It could be shown that irrigation effects, such as air temperature reduction and humidity increase, are well understood and should not be neglected on local and regional scales. However, there is a lack of studies including the role of vegetation in the altered land–atmosphere interaction. With the increasing resolution of numerical climate models, these detailed processes have a chance to be better resolved and studied. This study aims to analyze the effects of irrigation on land–atmosphere interaction, including the effects and feedbacks of vegetation. We developed a new parameterization for irrigation, implemented it into the REgional climate MOdel (REMO2020), and coupled it with the interactive MOsaic-based VEgetation module (iMOVE). Following this new approach of a separate irrigated fraction, the parameterization is suitable as a subgrid parameterization for high-resolution studies and resolves irrigation effects on land, atmosphere, and vegetation. Further, the parameterization is designed with three different water application schemes in order to analyze different parameterization approaches and their influence on the representation of irrigation effects. We apply the irrigation parameterization for southwestern Europe including the Mediterranean region at a 0.11° horizontal resolution for hot extremes. The simulation results are evaluated in terms of the consistency of physical processes. We found direct effects of irrigation, like a changed surface energy balance with increased latent and decreased sensible heat fluxes, and a surface temperature reduction of more than −4 K as a mean during the growing season. Further, vegetation reacts to irrigation with direct effects, such as reduced water stress, but also with feedbacks, such as a delayed growing season caused by the reduction of the near-surface temperature. Furthermore, the results were compared to observational data, showing a significant bias reduction in the 2 m mean temperature when using the irrigation parameterization.

1 Introduction

Land use and land use practices are anthropogenic forcings that were shown to influence regional climate. They can be defined as the modification of the land surface through anthropogenic changes in land cover types or land use practices that alter the land surface within one land cover type (Luyssaert et al., 2014). Through land–atmosphere interactions, changes in the land conditions can affect the climate and cause feedback mechanisms, especially in the near-surface atmosphere levels (Jia et al., 2019). Luyssaert et al. (2014) pointed out that under specific circumstances the effects of land use practices reach the same magnitude as land use and land cover change effects and should therefore not be ne-

glected in climate studies. We find different land use practices in agriculture such as tillage, fertilization, and irrigation. Irrigation is the land use practice that has the strongest impact on the climate (Kueppers et al., 2007; Lobell et al., 2009; Sacks et al., 2009). Further, irrigation is a common land use practice in agriculture to adapt to unsuitable climatic conditions. Using numerical models, irrigation effects are studied on different scales, with different parameterizations, and for different regions. An overview can be found in Valmassoi and Keller (2022), who collected different irrigation modeling studies and identified the different aspects of irrigation parameterizations as sources of uncertainties for irrigation effects on the climate.

Global-scale irrigation studies show different developments of irrigation effects in different regions in the world (Thiery et al., 2017, 2020; Sacks et al., 2009; Lobell et al., 2009; Puma and Cook, 2010; de Vrese and Hagemann, 2018). All studies found near-surface and surface temperature reduction. Compared to observational data, using irrigation in the model of Lobell et al. (2009) could eliminate the warm and dry bias of CLM. de Vrese and Hagemann (2018) showed that irrigation has remote effects more than 100 km of distance from the irrigated area. Further, multiple studies showed that irrigation effects are more pronounced on local and regional scales (Sacks et al., 2009; Kueppers et al., 2007; Valmassoi et al., 2020c). In particular, high-resolution studies on a regional scale require an accurate representation of the land surface and soil processes to represent local and regional climatic patterns (Hagemann et al., 1999). For example, Saeed et al. (2009) showed the irrigation effects on the summer monsoon in India, which is weaker due to a smaller land–sea–temperature gradient. Also, Tuinenburg et al. (2014) studied irrigation effects in India and found a shift in the precipitation pattern through the additional moisture in the atmosphere. Valmassoi et al. (2020a) studied irrigation effects in the Po Valley on a convection-permitting scale and found an increase in precipitation in irrigated areas. Like Thiery et al. (2020) on a global scale, Kueppers et al. (2007) pointed out the potential of irrigation to mask the warming effects of greenhouse gases on a regional scale for a study in California. Further, Kueppers et al. (2007) showed that irrigation effects follow a seasonality. During the growing season, the effects are most pronounced, and for dry periods the effects are stronger than for wet periods. Thiery et al. (2020) and Jia et al. (2019) point out that the near-surface temperature reduction through irrigation decreases the probability of hot extremes. With these characteristics, irrigation becomes a potential adaptation measure to climate extremes, not only for water stress that plants experience during droughts, but in addition, it can be implemented to reduce the intensity of heat waves.

The simulated effects of irrigation on the land–atmosphere interaction depend, on one hand, on the amount of irrigation, as pointed out by Valmassoi et al. (2020c), and on the other hand on the design of the parameterization itself. The irrigation amount is driven by the soil hydrology of the model. Multiple models represent the soil hydrology using a layered scheme and prescribe observed irrigation amounts (Valmassoi et al., 2020c; Puma and Cook, 2010; Ozdogan et al., 2010; Yao et al., 2022). For models using a bucket scheme (Boucher et al., 2004; de Vrese and Hagemann, 2018), observed irrigation values might not fit due to the deep bucket. Therefore, the irrigation parameterizations are designed with thresholds based on specific model-internal physical values, e.g., values of the maximum water-holding capacity of soil, field capacity, leaf area index (LAI), or photosynthesis rates, to determine the irrigation amount or the irrigation start and end. However, using such a model-internal physical threshold rather than a prescribed irrigation amount often leads to an overestimation of the effects (Kueppers et al., 2007). Therefore, Thiery et al. (2017) added a water limit for the available irrigation amount to reach realistic values, and Leng et al. (2017) added a water source and closed the hydrological cycle. For representing irrigation in a climate model, it is recommended to have a separate soil column for irrigation (Lobell et al., 2009; Ozdogan et al., 2010; Thiery et al., 2017) and represent irrigated areas on a subgrid scale. Another aspect of representing irrigation in a climate model is the irrigation method. Irrigation methods differ in their water application. Mostly, irrigation is represented as an increase in soil moisture, neglecting canopy interactions (Sacks et al., 2009; Lobell et al., 2009; Ozdogan et al., 2010; Thiery et al., 2017; de Vrese and Hagemann, 2018). Newer studies consider canopy effects which are caused by, e.g., sprinkler irrigation (Valmassoi et al., 2020c; Leng et al., 2015; Yao et al., 2022). However, on a regional scale, the differences in the irrigation effects between different irrigation methods remain small and can be neglected (Valmassoi et al., 2020c).

For most methods, irrigation affects the land surface, altering the exchange processes through land–atmosphere interaction. At high resolution, a more detailed representation of the land surface and its processes is possible. An important driver of these land processes, such as the soil, the land surface, and the atmosphere, is vegetation, which is also affected by irrigation. However, there is a lack of high-resolution climate studies which include the irrigation effects on vegetation and its feedback on the atmosphere, soil, and surface. This study aims to represent irrigation effects in the model system REMO2020–iMOVE which represents land, atmosphere, and vegetation processes interactively. Whereas Saeed et al. (2009) analyzed large-scale irrigation effects with REMO2009, this study aims to provide a detailed representation of irrigation aspects and conducts high-resolution experiments. Thus, we implement a new irrigated fraction and represent irrigation on a subgrid scale. Our model region is southwestern Europe with a focus on one of the most intensely irrigated areas in Europe, the Po Valley. After we describe the model and the data that we used for this study in Sect. 2, we introduce our new irrigation parameterization (Sect. 3). In Sect. 4 we apply the new

irrigation parameterization and evaluate it with the consistency of physical processes as well as with the comparison of observational data. We point out some limitations of our parameterization in Sect. 5 and give concluding remarks in Sect. 6.

2 Model and data

2.1 The model REMO2020–iMOVE

For this study, the regional climate model REMO2020 was used. REMO is developed as a hydrostatic atmospheric circulation model based on the primitive equations of atmospheric motion at the Max Planck Institute for Meteorology, Hamburg, Germany (Jacob, 1997, 2001). It combines parts of the Europa Model (EM) of the German Weather Service (Majewski, 1991) and the physical parameterizations of ECHAM4 (Roeckner et al., 1996). With time, REMO was further developed and received additional features such as dynamic vegetation cover (Rechid and Jacob, 2006), glaciers (Kotlarski, 2007), lakes (Pietikäinen et al., 2018), a non-hydrostatic extension to the hydrostatic core (Goettel, 2009), and an interactive mosaic-based vegetation module (iMOVE) (Wilhelm et al., 2014). For this study, in particular, the land surface parameterizations are of interest.

The surface of one model grid box in REMO2020 is represented with the tile approach in which the subgrid fractions land, water (representing sea and lakes), and sea ice are introduced (Semmler, 2002). Using the lake module FLake (Pietikäinen et al., 2018), a separate lake subgrid fraction is added. In total, the fractions sum up to 100 % of the surface of a model grid box. Whereas the land fraction is constant, the sea ice fraction can vary, thereby changing the water fraction. For each fraction turbulent surface fluxes and radiation fluxes are calculated and averaged at the lowest atmospheric level using weighted means with respect to the fraction area of the model grid cell. Using the bulk transfer relations with transfer coefficients from the Monin–Obukhov similarity theory with a higher-order closure scheme, the turbulent fluxes of momentum and heat are calculated (Kotlarski, 2007). The exchange processes between the atmosphere and surface are determined by the vegetation coverage. Since the vegetation physiology depends strongly on seasonal cycles, the variations are included for the vegetation fraction, the LAI, and the background albedo (Rechid and Jacob, 2006). To improve the vegetation representation and its effects on the atmosphere, the iMOVE modules of REMO2009–iMOVE (Wilhelm et al., 2014) are implemented into REMO2020. Multiple elements of iMOVE are based on the dynamic land surface scheme JSBACH (Raddatz et al., 2007; Wilhelm et al., 2014). It represents the land cover with tiles of plant functional types (PFTs) using the Holdridge ecosystem classification scheme (Wilhelm et al., 2014). For this experiment, the definition and distribution of PFTs are based on the land cover maps of the European Space Agency Climate Change Initiative (ESA-CCI) (Reinhart et al., 2022; Hoffmann et al., 2023). The PFTs interact dynamically with the atmosphere and the soil, leading to varying phenology. Here, soil moisture and air temperature are important driving factors (Wilhelm et al., 2014). Furthermore, in REMO2020–iMOVE soil moisture determines the soil albedo following the findings of Peterson et al. (1979) and model adjustments of Wilhelm et al. (2014). As a result, the soil albedo is represented with a negative exponential relationship with the soil moisture.

The heat budget of the soil is represented with a five-layer scheme. The heat transfer is calculated with diffusion equations for five discrete layers. For solving the equations, it is assumed that the heat flux is zero at the lowest boundary. The heat transfer between the layers is mainly driven by the heat conductivity and heat capacity of the soil type, which vary with soil moisture. The soil hydrology consists of three water storage reservoirs: soil, skin reservoir (vegetation), and snow, for which budget equations are solved. The reservoirs are altered by precipitation, interception, dew, evapotranspiration, snowmelt, runoff, infiltration, and drainage (Kotlarski, 2007). Precipitation is split by the improved Arno scheme (Dümenil and Todini, 1992) into surface runoff and infiltration considering subgrid-scale heterogeneous field capacities of the land surface within one grid cell (Hagemann, 2002). The field capacity in REMO is at the level of the maximum water-holding capacity (wsmx), which is based on the global dataset of land surface parameters (LSPs) by Hagemann et al. (1999). Once the soil moisture reaches wsmx, runoff occurs. Infiltration fills up the soil moisture reservoir, which is represented as a simple bucket scheme with subsurface drainage. The drainage is led by the ratio of the soil moisture and wsmx. Drainage occurs for soil moisture larger than 5 % of wsmx. Between 5 % and 90 % of wsmx, drainage is slow. If the soil moisture is larger than 90 % of wsmx, the drainage is fast (Kotlarski, 2007).

Water can leave the soil moisture reservoir through evapotranspiration depending on vegetation characteristics and atmospheric conditions. For bare soil, evaporation takes place from the upper 10 cm. Subsurface water leaves the soil moisture reservoir only through transpiration by vegetation or drainage. At the surface or soil, there are no lateral flows of water within REMO2020 (Wilhelm et al., 2014).

2.2 Irrigation dataset

For an estimation of the spatial distribution of irrigated areas, the Global Map of Irrigated Areas Version 5 (GMIA5) by Siebert et al. (2013a) is used. The GMIA5 describes the area equipped for irrigation as well as the area actually irrigated on a resolution of 5 arcmin (0.083333 decimal degrees). It was developed at the Johann Wolfgang Goethe University, Frankfurt (Main), Germany, by Doell and Siebert (1999). Through cooperation with the Rheinische Friedrich-

Wilhelms-Universität, Bonn, Germany, and the Land and Water Division of the FAO, GMIA is constantly improved and updated. The dataset is mainly based on AQUASTAT, the FAO's information system on water and agriculture. The data are collected from national and subnational water resources and irrigation plans, statistics, yearbooks, and FAO technical reports. This information is combined with geospatial information on the position and extent of the irrigated area. The statistical data refer to the years 2000 to 2008, with the reference year depending on the country. The quality of GMIA5 was assessed by the density of subnational irrigation statistics used and by the density of the available geospatial records on the position and extent of irrigated areas (Siebert et al., 2013b).

For our study, we chose the data on the "area equipped for irrigation" of the GMIA5 due to better quality (Siebert et al., 2013b) as well as due to our study's purpose of showing maximal possible irrigation effects.

2.3 Observation data for evaluation

The Italian Institute for Environmental Protection and Research (ISPRA) established a database for meteorological observation data for Italy named SCIA (Italian: Sistema nazionale per la raccolta, l'elaborazione e la diffusione di dati Climatologici di Interesse Ambiental). SCIA works as a framework of the national environmental information system and combines data from national and regional networks, agro-meteorological stations (UCEA-RAN), hydro-meteorological stations, and tide gauge networks. The data are updated once per year and undergo a quality check. Climate indicators are available for different timescales such as means of 10 d, months, or years (Desiato et al., 2011) and are freely available on the SCIA website (http://www.scia.isprambiente.it, last access: 8 December 2023). For this study, the monthly means of the daily mean, maximum, and minimum 2 m temperature for the year 2017 are used.

3 Development of the irrigation parameterization

3.1 Implementation of a new irrigated land subfraction and a new PFT into REMO2020–iMOVE

In REMO2020–iMOVE, soil processes are defined for land fractions (Kotlarski, 2007). Irrigation influences soil and surface directly and is a new local process to implement into REMO2020–iMOVE. Since it affects the land fraction, we implement a new irrigated land fraction based on the "area equipped for irrigation" from the GMIA5 (Sect. 2.2). Before using it in REMO–iMOVE, GMIA5 has to be adapted to the desired resolution and geographic projection. The new irrigated land fraction in REMO2020–iMOVE is a new land fraction that can be understood as a subfraction of the land fraction (Fig. 1). All soil, surface, and vegetation processes

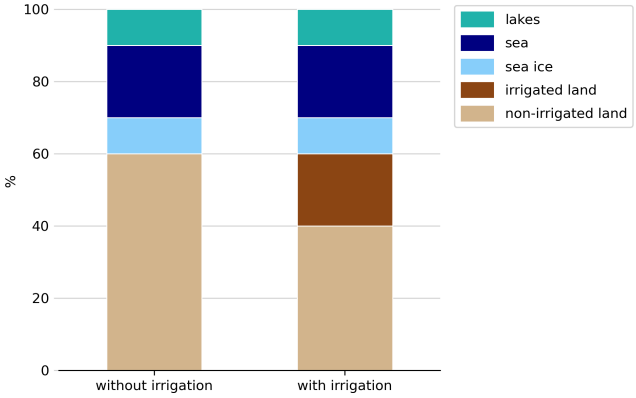

Figure 1. Fractions of one example model grid cell in REMO2020–iMOVE + FLake with and without irrigation.

are calculated for both land fractions, except for irrigation, which is applied exclusively to the irrigated land fraction.

As land cover, we implement a new PFT named "irrigated cropland" on the irrigated land fraction. The properties of irrigated cropland are based on the properties of the "cropland" PFT of the non-irrigated land fraction. REMO2020–iMOVE is able to distinguish between the photosynthesis path of cropland PFTs (C_3 or C_4); however, it does not distinguish between different crop types. In our case irrigated cropland is the only irrigated PFT and therefore the only PFT on the irrigated land fraction. With the separation into an irrigated and non-irrigated land fraction and the new PFT, we ensure that the irrigation process is only applied to areas that are truly irrigated. Having a separate irrigated land fraction gives a detailed representation of the heterogeneity of the surface and irrigated areas, which is an advantage for high-resolution and small-scale irrigation studies such as on the European continent where irrigated areas are rather scattered.

The implementation of the new irrigated land fraction is done during the model initialization. The irrigation module, which accounts for a check of irrigation requirements and water application, is called every time step exclusively for the irrigated land fraction. These irrigation processes are carried out after the hydrological processes of the soil from the previous time step ($t-1$). In this way, the irrigation processes are applied to the soil hydrology inherited from $t-1$. After the irrigation processes, the vegetation processes start, which are strongly influenced by the moisture content in the soil and in the atmosphere of the same time step (t) (Fig. A1).

3.2 Irrigation module and its different water application schemes

We implemented the new irrigation module into REMO2020–iMOVE, which can be turned on and off. The irrigation module determines where, when, and how irrigation will be applied. Irrigation is exclusively applied to the irrigated fraction (Sect. 3.1), which defines the area

equipped for irrigation from Siebert et al. (2013a) (Sect. 2.2). Using an adjustable threshold (irrthr) on the soil moisture, the irrigation module determines the grid cells with irrigation requirements and creates a daily irrigation mask at 7:00 LT as the starting time for irrigation in our parameterization following Valmassoi et al. (2020c). This determination is carried out during the growing season because only then do plants require irrigation. The growing season depends on the location and a growing degree threshold (Wilhelm et al., 2014). Upon fulfilling the requirements for irrigation (Fig. 2), the water application starts. For parameterizing channel irrigation, the water is added directly to the soil and increases the soil moisture. Here, we assume an infinite water supply. The water application and the irrigation amount strongly depend on the soil hydrology parameterization of the climate model, as well as on the intention of being close to reality. Therefore, we implemented three different water application schemes, which can be used for different purposes (Table 1).

The "prescribed irrigation" scheme applies a prescribed amount of water within a prescribed time. The prescribed water amount will be equally distributed over each time step during the irrigation time. The water amount can be based on observed irrigation values, but also extreme situations: a limited water supply or a huge water supply can be simulated. However, having a simple soil hydrology parameterization, such as the bucket scheme in REMO2020–iMOVE, suitable values for the prescribed water amount might differ from observed irrigation amount values, leading to a necessary adjustment to reach realistic soil moisture conditions in the model. The prescribed water amount is a universal value, which will be added to the irrigated fraction in all model grid cells that fulfill the irrigation requirements (Fig. 2). Further, the water amount in the model does not depend on the crop type, since REMO–iMOVE does not distinguish between different crop types.

The "flexible time irrigation (flextime)" is based on a prescribed soil moisture target and open irrigation time. For each grid cell, the water amount is calculated that is necessary to reach the soil moisture target. Again, the water amount is equally distributed over each time step within the prescribed time. Once the soil moisture target is reached, the water application stops regardless of the irrigation time. For this approach, a soil moisture target has to be chosen in relation to wsmx of the soil.

The "adaptive irrigation" is also based on a prescribed soil moisture target and a prescribed, limited irrigation time. Again, for each grid cell, the water amount is calculated that is necessary to reach the soil moisture target. The water amount added every time step follows a relaxation approach (Eq. 1) which simulates the increase in soil moisture during the time steps of irrigation and simultaneously considers the changes in soil moisture not related to irrigation. Further, our relaxation approach takes into account the number of irrigation time steps remaining. Using this approach the

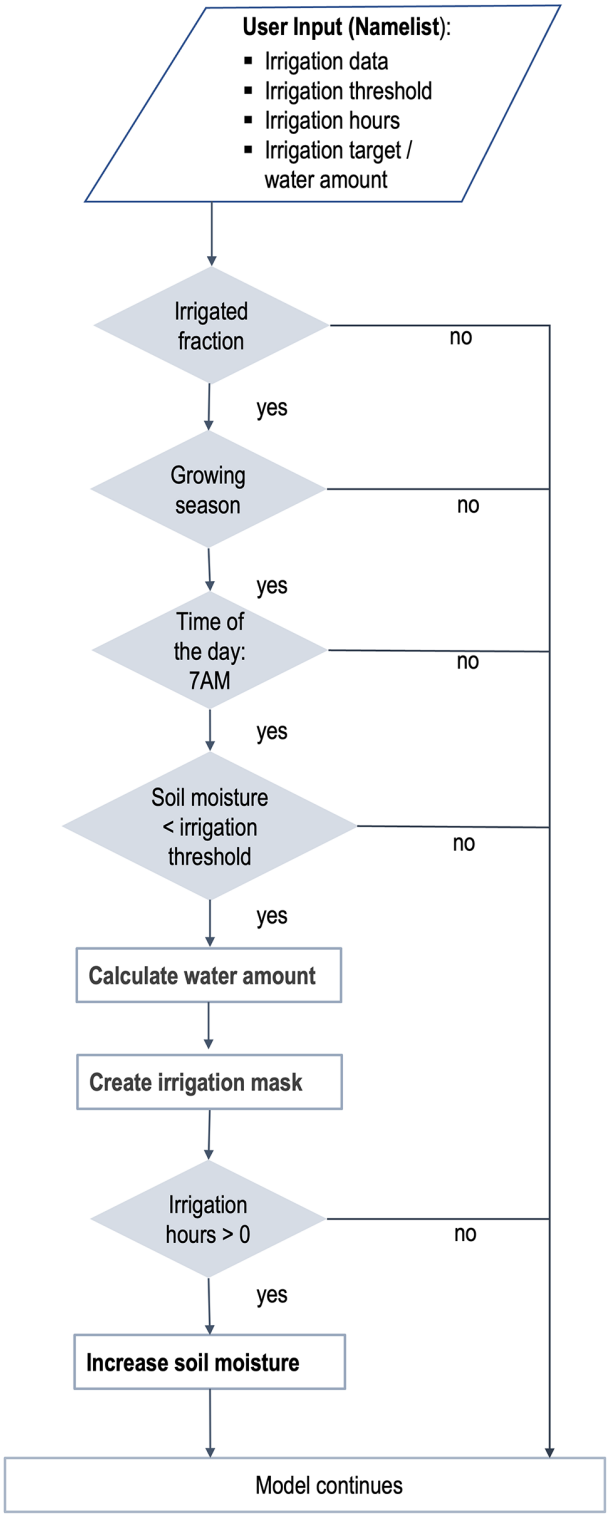

Figure 2. Irrigation process flow in REMO2020–iMOVE.

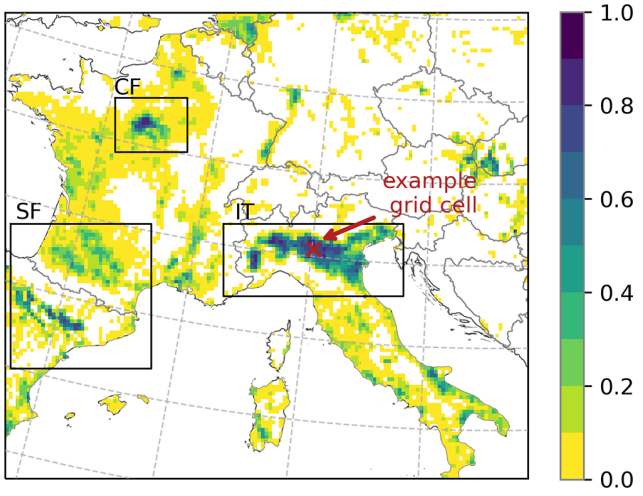

Figure 3. Model domain grid cells with the fraction of irrigated areas interpolated from area equipped for irrigation in Siebert et al. (2013a) and the analysis regions in Italy (IT), northern Spain and southern France (SF), and central France (CF). The example grid cell of Sect. 4.2 is pointed out.

soil moisture increases until the irrigation target is exactly reached during the prescribed irrigation time:

$$\mathrm{ws}_{t+1} = \mathrm{ws}_t + \frac{\mathrm{irrtar} \times \mathrm{wsmx} - \mathrm{ws}_t}{\mathrm{nirr}_t}, \quad (1)$$

where ws is soil moisture, irrtar is irrigation target, wsmx is maximum water-holding capacity, nirr is the number of remaining irrigation time steps, and t is the time step.

4 Results and evaluation of the parameterization

4.1 Experiment setup

We employ REMO2020–iMOVE for our model domain covering southwestern (SW) Europe and the Mediterranean region, including some of the most intensely irrigated areas such as the Po Valley and the Ebro Basin (Fig. 3). In 2017, SW Europe experienced exceptionally high temperatures, starting in June and reaching a heat wave in early August (Sect. 4.3). This is the period we chose for our simulation because, first, irrigation is most important for agriculture during hot periods, and second, the effects of irrigation are most pronounced (Kueppers et al., 2007).

We conduct three 1-month simulations to test the different water application schemes (T1–T3, Table 2) for June 2017. Based on these short tests, we decide on one water application scheme to conduct a 1-year simulation (S1) and analyze the effects of irrigation in the course of the year 2017. Simulation S0 is our baseline experiment and does not apply irrigation. All our simulations use a rotated grid with the rotated North Pole at 39.25° N, 162° W and have a horizontal resolution of 0.11°. We use ERA5 on 50 vertical levels as boundary data and set the time step to 60 s. S0 and S1 start from 1 January 2017. We initialized S0 and S1 with ERA5 (Table 2), except for the soil conditions. Since soil conditions have a long spin-up time in regional climate models (RCMs), we initialize the soil variables with a previous long-term (> 10 years) REMO simulation to get the soil variables in an equilibrium state. This method is also known as a "warm start" (Pietikäinen et al., 2018). The test simulations are started as a restart from our baseline experiment S0 from 1 June 2017. Table 2 summarizes the settings for the different test simulations T1 to T3, as well as for the 1-year simulations S0 and S1.

T1, T2, and T3 test the water application schemes prescribed, flexible time (flextime), and adaptive to estimate their effect on the development of irrigation effects. For all three test simulations, the irrigation threshold for the soil moisture is set to 0.75 of wsmx. For the model, this threshold is important because, from 0.75 of wsmx, the vegetation processes have optimal conditions to develop.

T1 uses a prescribed irrigation amount of 150 mm d^{-1} which is evenly distributed over the irrigation time in all grid cells with irrigation requirements. We selected 150 mm d^{-1} as the irrigation amount from experience using the bucket scheme as soil hydrology (Sect. 3.2). Following Bjorneberg (2013) and Zucaro (2014) channel irrigation is performed for up to 24 h depending on the channel width and length; we chose 10 h irrigation time for our experiment. With the irrigation start time at 7:00 LT (Sect. 3.2), irrigation is applied during daytime in our experiment. T2 tests the water application scheme with flexible time. This water application scheme is driven by the difference between the soil moisture at irrigation start at 7:00 LT and the irrigation target. We set the irrigation target to the maximum water-holding capacity. T3 tests the adaptive water application scheme. As in T2, the irrigation target is set to the maximum. The irrigation time is set to 10 h as in T1. Since the test simulations are started as restarts from S0, the irrigation module detects grid cells with irrigation requirements from 1 June 2017.

After testing the irrigation parameterization with its different water application schemes, our experiment aims to investigate irrigation effects on multiple variables and processes in the model system REMO2020–iMOVE and to check their physical consistency over the course of 1 year. We quantify the irrigation effect by the difference between one simulation with the irrigation parameterization turned on (S1) and our baseline simulation with the irrigation parameterization turned off (S0). In S1 the irrigation process starts with the growing season of crops in the model domain. It only turns off once the crops are harvested. In the course of the year, we analyze delayed irrigation effects and how they affect hot extremes. S1 applies the adaptive water application scheme with the irrigation threshold and the irrigation target at wsmx, leading to the maximum irrigation effects.

Table 1. Properties of the different water application schemes in REMO2020–iMOVE.

	Prescribed irrigation	Flexible time irrigation (flextime)	Adaptive irrigation
Namelist variables	– irrigation time – irrigation amount	– approx. irrigation time – soil moisture target	– irrigation time – soil moisture target
Irrigation amount (irrw)	prescribed in namelist	$\text{irrw} = \Delta\text{ws}$ $= \text{irrtar} \times \text{wsmx} - \text{ws}_t$	$\text{irrw} = \Delta\text{ws}_t$ $= \text{irrtar} \times \text{wsmx} - \text{ws}_t$
Irrigation stop	limited to irrigation amount	reaching soil moisture target	reaching soil moisture target after irrigation time
Water application	evenly distributed over each time step during irrigation time	evenly distributed over each time step during irrigation time	adaptive distributed over each time step during irrigation time

Table 2. Simulation setup for the different water application scheme tests and the 1-year simulation.

Simulation	Simulation period (in 2017)	Boundary data	Initial condition (in 2017)	Water application scheme	irrthr (as a fraction of wsmx) [–]	irrtar (as a fraction of wsmx) [–]	Irrigation duration [h]	Preset irrigation water [mm]
T1	1–30 June	ERA5	restart from S0	prescribed	0.75	–	10	150
T2	1–30 June	ERA5	restart from S0	flextime	0.75	1.0	–	–
T3	1–30 June	ERA5	restart from S0	adaptive	0.75	1.0	10	–
S0	1 January–30 December	ERA5	ERA5*	not irrigated	–	–	–	–
S1	1 January–30 December	ERA5	ERA5*	adaptive	1.0	1.0	10	–

* With soil conditions in equilibrium state from previous REMO simulation.

4.2 Testing the different water application schemes

Figure 4 shows the irrigation process with the different water application schemes for one representative irrigated grid cell in the Po Valley (63, 85) (Fig. 3) for the first irrigation day, 1 June 2017. We use a single grid cell to analyze the development of soil moisture in detail without any averaging. The soil moisture is at 0.47 of wsmx, leading to irrigation from 7:00 LT. For the prescribed water application scheme (T1) the soil moisture increases linearly until the irrigation time is finished, in this case at 17:00 LT (Fig. 4a). During the irrigation time, the same water amount is added for every time step. In the example grid cell, it is $15\,\text{mm}\,\text{h}^{-1}$ (Fig. 4b). At the end of irrigation, soil moisture reaches 0.87 of wsmx and stays close to this level until the end of the day (Fig. 4a).

For the simulation using the flextime water application scheme (T2) the soil moisture increases linearly until the irrigation target is reached after 301 min (Fig. 4a). As in T1, the same water amount is added to the soil moisture for each time step. However, the amount of added water is driven by the difference between the soil moisture at 7:00 LT and the irrigation target, leading to a higher added water amount per time step than in T1 ($40\,\text{mm}\,\text{h}^{-1}$, Fig. 4b).

The adaptive water application scheme causes a nonlinear increase in the soil moisture, converging to the irrigation target and reaching it in the last time step of the irrigation time (Fig. 4a), which is set to 10 h. The water application adjusts itself in each time step depending on the difference between the actual soil moisture and the irrigation target as well as on the remaining time steps with irrigation (Eq. 1). Thus, for the first irrigation time steps, when the difference is the greatest, the water amount added is the greatest at $38\,\text{mm}\,\text{h}^{-1}$. It decreases with the following irrigation time steps (Fig. 4b).

Comparing the irrigation amount used in June (Fig. 5), the water amount added in T2 and T3 is very similar (max. 380 mm per month), which is also shown in the distribution of the irrigation water amount in Fig. 5d. The irrigation water amount added by the prescribed scheme in T1, in particular, in grid cells in the Po Valley, the Ebro Basin, and southern Italy is larger than in T2 and T3. The prescribed scheme also reaches the highest irrigation water value (max. 450 mm per month, Fig. 5d). The reason for these differences is that the prescribed water application scheme stops the irrigation in one day once the prescribed irrigation amount is finished within the prescribed irrigation time, regardless of the saturation of soil moisture. This leads to multiple irrigation requirements in June once the soil moisture drops below the irrigation threshold, turning on irrigation. Using the flexible time (T2) and the adaptive water application scheme (T3), in most grid cells only one irrigation event is necessary in June, whereas using the prescribed irrigation scheme (T1) required up to three irrigation events always adding the same prescribed irrigation amount (Fig. A2).

The overall effects of the three water application schemes as monthly mean values are similar (Figs. A3, A4). Therefore, we select only one scheme to further analyze the effects of irrigation on the regional climate. The water application scheme selected is the adaptive water application scheme, since it has multiple advantages. First, it smoothly reaches the irrigation target and takes into account the actual soil

moisture of each grid cell and the remaining irrigation time steps. Second, the relaxation method is a common method in climate modeling. And third, the adaptive water application scheme is the user-friendliest scheme of the three schemes because it does not require experience values of the irrigation amount depending on the soil hydrology of the climate model.

4.3 Simulated meteorological conditions during spring and summer 2017 with REMO2020–iMOVE

SW Europe and the Mediterranean region experienced dry and warm weather during spring and summer in 2017. According to E-OBS data, spring (MAM) was 1.7 °C warmer than the reference period 1981–2010. During summer (JJA) several heat waves occurred in SW Europe, as well as in the Balkans (Copernicus Climate Change Service, 2023). One of the first heat waves hit SW Europe in June (Sánchez-Benítez et al., 2018), in particular Spain and France. Another heat wave developed at the beginning of August 2017 in southern Europe, this time in particular in Spain, France, Italy, and the Balkans (Kew et al., 2019), causing several wildfires (Copernicus Climate Change Service, 2023).

The warm and dry meteorological conditions in spring as well as the hot conditions in summer are represented in the REMO2020–iMOVE simulation in the southern part of the model domain (Figs. 6, 7). Within spring and summer, the months of April, May, and June (AMJ) are of particular interest because irrigation is linked to the growing season and these months will be fully irrigated. Therefore, we analyze the meteorological conditions during AMJ (Fig. 6a–c) as well as for the heat wave in August (Fig. 6d–f) to investigate delayed irrigation effects in the model without active irrigation. The mean 2 m temperature distribution for AMJ follows a north–south pattern as well as the topography. The highest values of up to 25 °C occur in the river valleys of the Po, the Ebro, and the Garonne and Adour (Fig. 6a). In these valleys, the soil moisture is the lowest in the model domain (Fig. 6b); most precipitation, which could fill up the soil moisture, falls in the Alps, Pyrenees, Central Massif, and Dinaric Alps (Fig. 6c). Figure 6d–f show the simulated mean conditions during the heat wave from 3–5 August 2017. The highest temperatures of up to 40 °C are reached in Italy as well as in the Balkans (Fig. 6d). In the northern part of the model domain, the heat wave was not present. Figure 7 shows the evolution of the meteorological conditions from April until August in the three analysis regions, IT (Italy), CF (central France), and SF (Spain–southern France) (Fig. 3). Within the course of the year and the beginning of summer (June), the soil moisture drops in all three analysis regions. Since the soil properties differ, the soil moisture differs in the analysis regions, with higher values in CF and the lowest values in IT. Due to low precipitation rates, in particular in IT and SF, the soil moisture cannot be filled up in the analysis regions. The evolution of temperature in the analysis regions shows hot summer periods (Fig. 7d–f). Whereas IT experienced the most extreme heat wave at the beginning of August, CF experienced its highest temperatures at the end of August. The heat wave in IT lasted for 3 d in accordance with E-OBS data (Copernicus Climate Change Service, 2023). As a regional mean the daily 2 m maximum temperature reaches up to 35 °C and the daily 2 m minimum temperature up to 25 °C.

4.4 Process analysis of irrigation effects

To understand the effects of the irrigation parameterization, we analyze the results of the extreme scenario, in which the irrigation threshold and the irrigation target are wsmx of the soil; this is the maximum possible value of irrigation effects. This setting causes everyday irrigation during the growing season, resulting in soil moisture close to wsmx in the irrigated grid cells.

4.4.1 Effects on soil and surface fluxes

The irrigation effects are analyzed in terms of their spatial distribution as well as their occurrences in the diurnal and annual cycles. The soil moisture is directly increased by the parameterization, which is shown in Fig. 8a as a mean of the irrigated months April, May, and June (AMJ). Depending on the local wsmx of the soil and the actual soil moisture, the irrigation requirements in each grid cell differ from each other. Figure 8a shows a north–south gradient of the irrigation requirement with the highest values of up to 600 mm in the south like in the Ebro Basin in Spain and the Balearic Islands as well as in Italy in Sardinia, Puglia, Lazio, and the Po Valley. In the northern irrigated areas such as in France, the irrigation requirement is on average 200 mm for AMJ in the model.

Irrigation effects appear in the diurnal cycle of the soil moisture (Fig. 8b). The irrigation start time is at 7:00 LT, which increases the soil moisture, slowly at first, then faster as we get closer to the end of the irrigation end time. At 17:00 LT, the maximum irrigation effect is reached for soil moisture with an increase of 202 mm as a spatial average of irrigated areas in the model domain during AMJ.

In the annual cycle, the irrigation effects start to occur from March and increase until July (Fig. 8c). In July, the irrigation effects of the soil moisture reach +300 mm as a monthly average of all irrigated areas in the model domain. In most areas of the model domain, the growing season stops in July. Therefore, the irrigation effects decrease from August until the end of the year. Nevertheless, the soil moisture remains at a higher level than in the simulation without irrigation due to irrigation in the months before.

The effects of irrigation occur in different layers of the soil temperature as well as in the surface temperature (Fig. 8d–f). In general, irrigation reduces the surface temperature (Fig. 8d). The spatial distribution of that cooling follows the

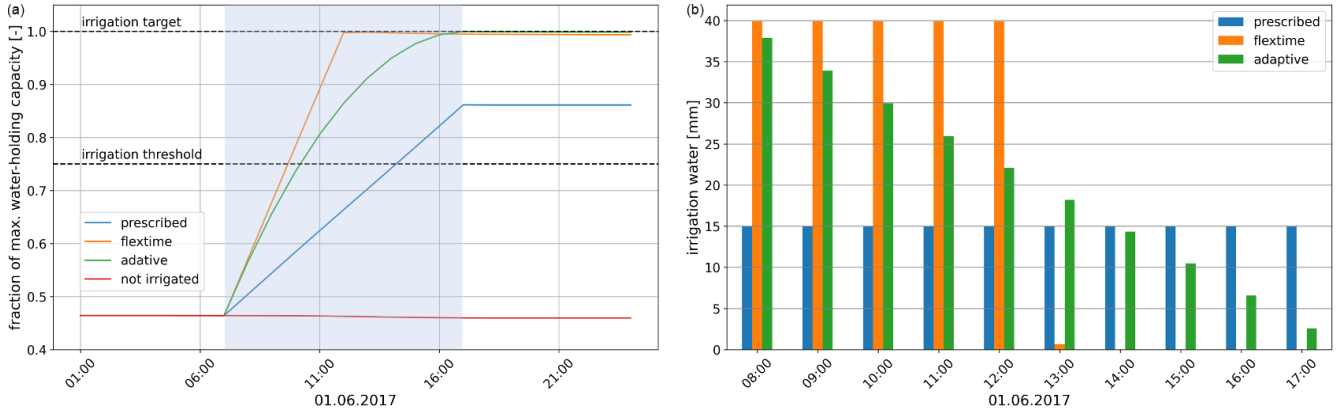

Figure 4. Irrigation process on the first irrigation day (1 June 2017) using the different water application schemes in one representative example grid cell (63, 85). Settings: irrigation threshold at 0.75 of wsmx, irrigation target at wsmx, irrigation time of 10 h. The blue shaded region is irrigation time. **(a)** Soil moisture as a fraction of wsmx and **(b)** irrigation water used.

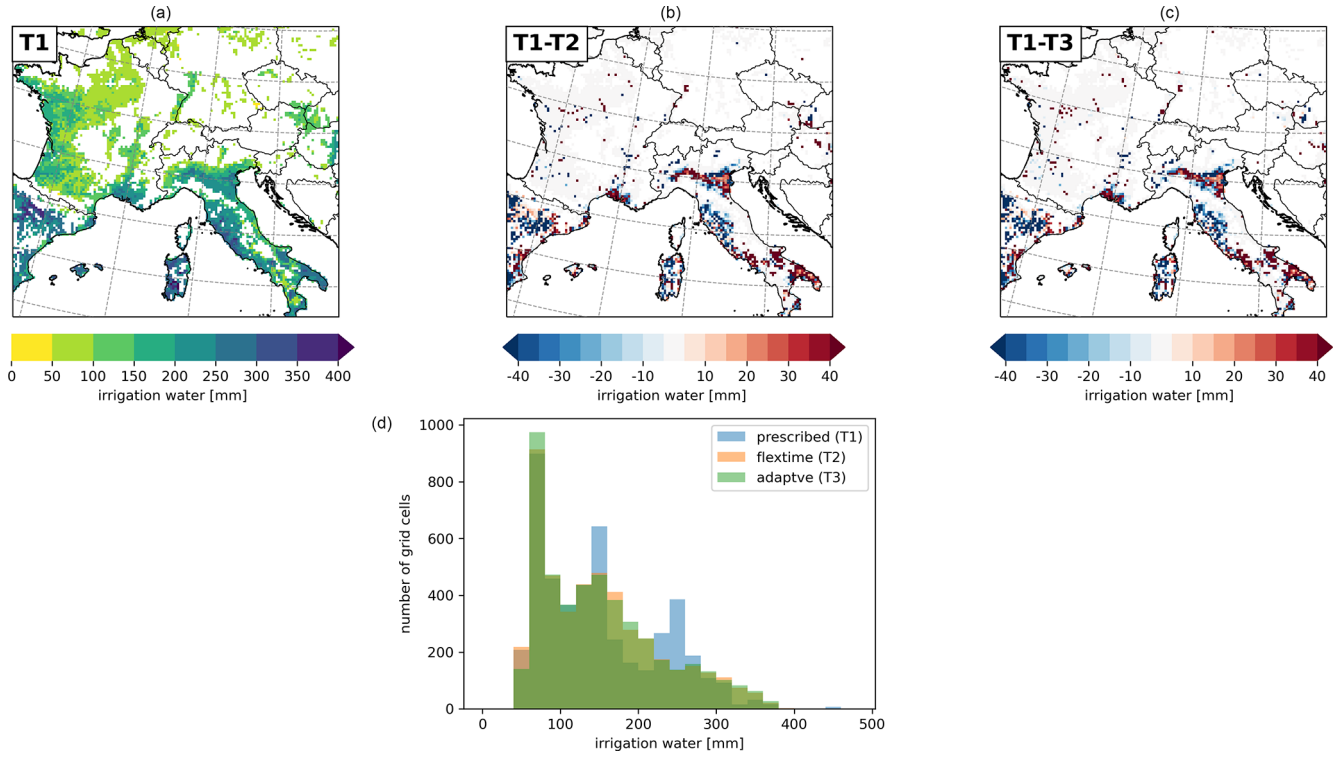

Figure 5. Irrigation water used for the different water application schemes in June 2017: **(a)** prescribed (T1), **(b)** as the difference between prescribed (T1) and flextime (T2), **(c)** as the difference between the prescribed (T1) and adaptive scheme (T3), and **(d)** the distribution of irrigation water in irrigated grid cells.

changes in the surface fluxes (Fig. 9). The strongest cooling effect in the soil occurs in the Ebro Basin and in the southern Po Valley with −4 K as a mean value in AMJ. The cooling at the surface propagates to the deeper layers of the soil, which is shown in the diurnal and annual cycle of the soil temperatures at different depths (Fig. 8e–f). The upper three layers up to a depth of 1.232 m are influenced by the surface processes. In Fig. 8e, the effects on the upper soil temperature from 0.0 to 0.065 m follow the solar radiation, reaching maximum cooling by irrigation at 13:00 LT with −3.2 K. The temperature of the second soil layer has a time-shifted reaction and reaches its maximum cooling by irrigation at 18:00 LT with −1.9 K. The levels from 0.319 m depth no longer show a diurnal cycle; however, they show a cooling between −0.05 and −1.4 K.

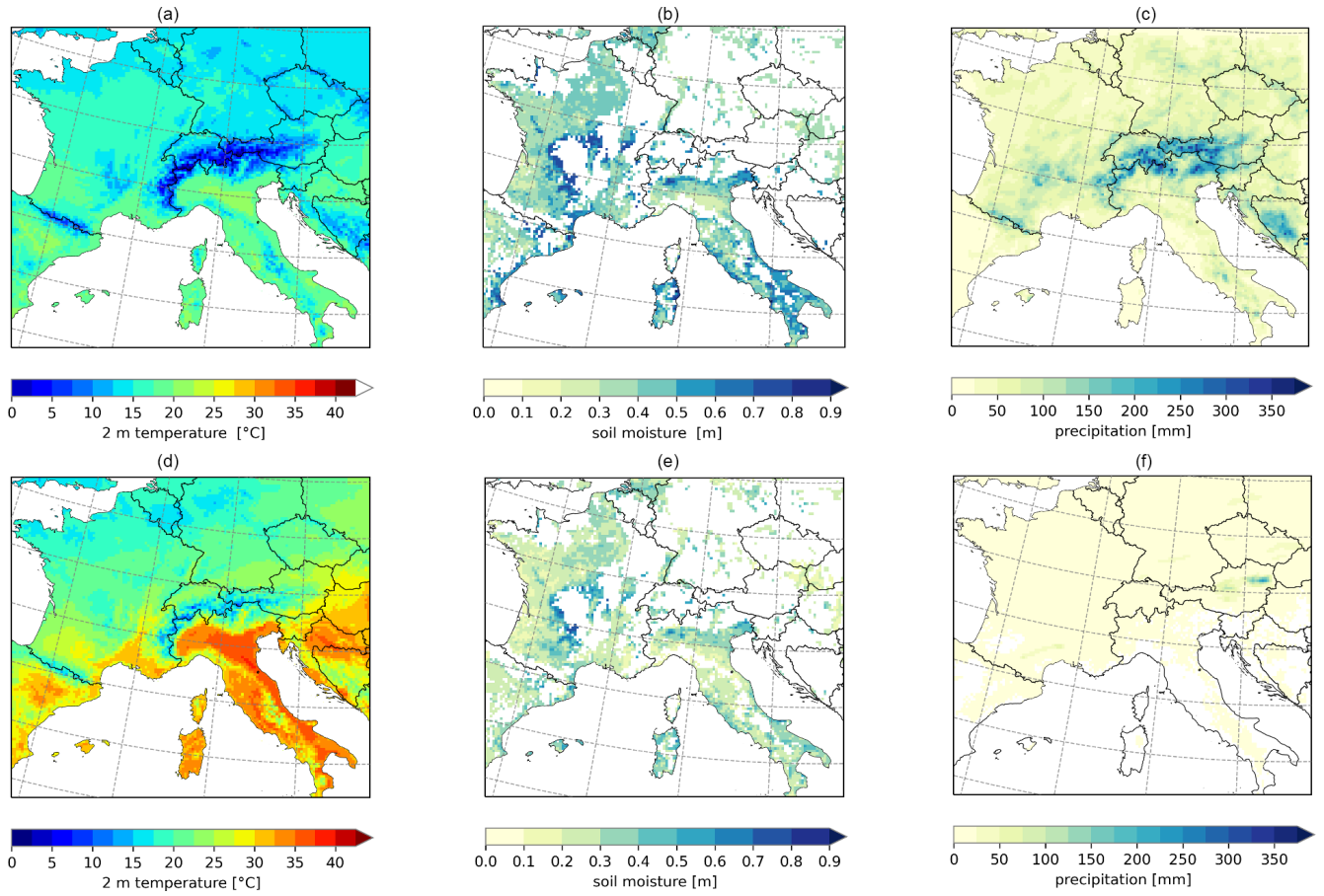

Figure 6. Simulated mean meteorological condition with REMO2020–iMOVE for **(a)** 2 m temperature during AMJ, **(b)** soil moisture during AMJ, **(c)** monthly mean of summed precipitation for AMJ, **(d)** 2 m temperature during a heat wave (3–5 August 2017), **(g)** mean soil moisture during a heat wave (3–5 August 2017), and **(f)** mean of summed precipitation during a heat wave (3–5 August 2017).

Since soil reacts inertly, the irrigation effects on the soil temperature throughout the year 2017 are analyzed with monthly mean values (Fig. 8f). The same order of the magnitude of the cooling effect is shown for the different temperature layers as it is in the diurnal cycle (Fig. 8e). The upper four layers react immediately to irrigation and show a cooling from March where the upper layer at the surface reaches a cooling of up to -1.5 K and the fourth layer at 1.232 m depth reaches a cooling of -0.05 K. The two upper layers reach their maximum cooling effect in April, whereas the third layer reaches its maximum cooling effect in July, the fourth layer in August, and the fifth layer in December. This time shift shows the inertial reaction of the soil temperature. The cooling of the three upper soil layers develops in spring (from March) and summer months until the harvest in July begins in wide areas of the model domain. From August the cooling effect is reduced in the upper three layers.

In general, the cooling in the soil temperature is mainly explained by two processes. First, surface processes like the enhanced latent heat flux and evaporation cool the surface temperature. This cooling slowly propagates in deeper levels. Secondly, the cooling is caused by the soil-moisture-dependent heat capacity and thermal conductivity, which increase with higher soil moisture (Eggert, 2011). This leads to faster signal transmissions and thus to faster cooling rates.

In the irrigated months AMJ, irrigation leads to an increase in evapotranspiration with the maximum in the Ebro Basin, Sardinia, and Lazio with an evapotranspiration increase of up to $+150$ mm (Fig. 8g). The magnitude of the increase depends on the local meteorological condition, the soil moisture, and the state of vegetation. Furthermore, in REMO2020–iMOVE, evapotranspiration is composed of evaporation from bare soil, transpiration from vegetation, and evaporation from the skin reservoir. In the diurnal cycle (Fig. 8h), the evapotranspiration increase reaches its maximum at 13:00 LT, the hour with the highest solar radiation in the model domain. During AMJ the increase in the evaporation of bare soil drives the changes in evapotranspiration. Evaporation from the skin reservoir shows negligible effects, as it is only affected by the LAI and the occurrence of precipitation or dew. Transpiration from vegetation shows a reduction through irrigation in comparison to the

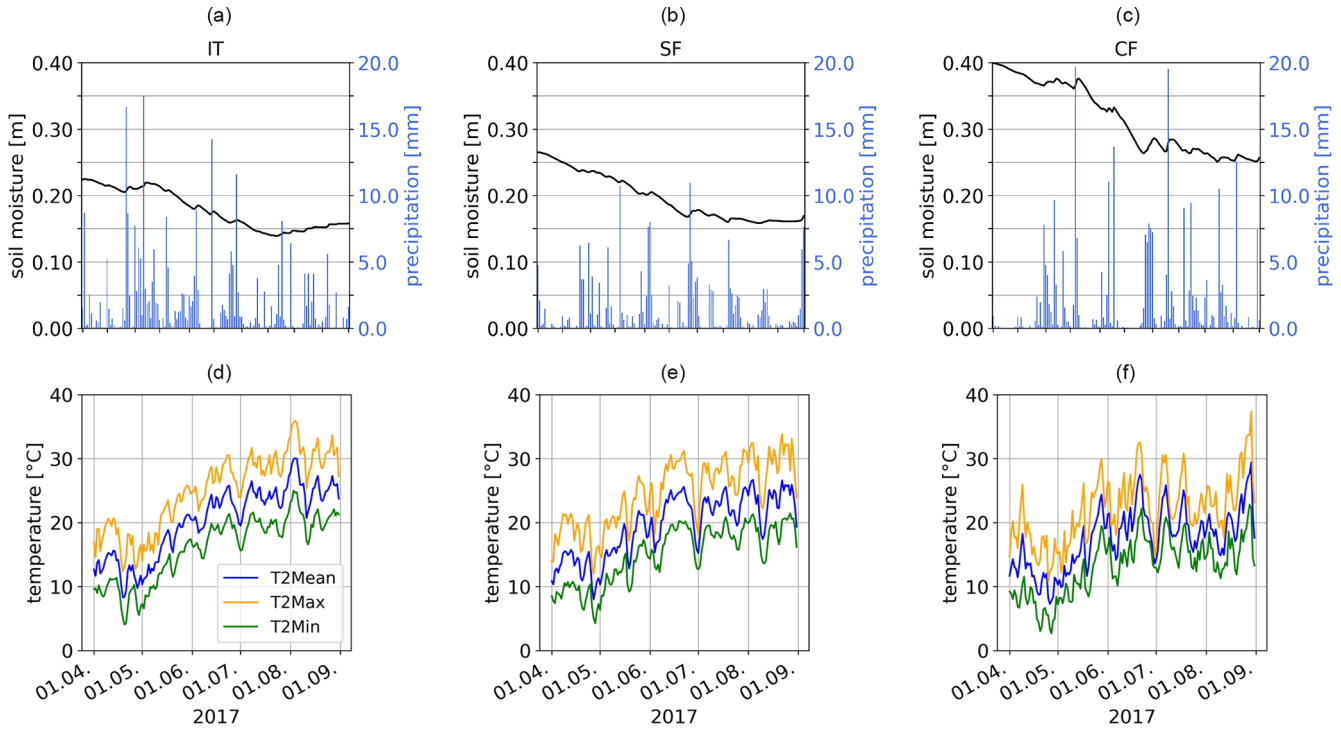

Figure 7. Meteorological conditions as spatial means of the analysis regions IT, SF, and CF in 2017 for AMJJA for **(a–c)** soil moisture and precipitation, as well as **(d–f)** 2 m temperatures.

non-irrigated simulation from 9:00 LT to 16:00 LT in AMJ. Figure 8i shows the annual cycle of the effects on the different evaporative fractions. The transpiration from vegetation is reduced with irrigation for March, April, and May before it shows an increase from June to September of up to +14 mm per month. The reduction in spring is explained by the slower development of the LAI (Fig. 14a–b) in the irrigated simulation due to lower air temperatures (Fig. 11), which lead to reduced transpiration. In different seasons of the year, different evaporative fractions are the driver of evapotranspiration (Fig. 8i). Bare soil evaporation increases with irrigation and is the main driver of irrigation effects in evapotranspiration until July with the highest increase of +28 mm per month in April. Once the LAI reaches its maximum in July (Fig. 14a), it becomes the driver of evapotranspiration. After the crops are harvested, there is only evaporation from bare soil and from the skin reservoir.

Irrigation affects the surface energy budget by changing the energy fluxes (Fig. 9). The latent heat flux increases by up to $+150\,\mathrm{W\,m^{-2}}$ and the sensible heat flux decreases by up to $-120\,\mathrm{W\,m^{-2}}$ in the Ebro Basin, Sardinia, and Lazio during April, May, and June. These changes lead to a shift in and a reduction of the Bowen ratio by up to −1 (Fig. 9a–c), which shows that the energy transfer between the surface and the atmosphere is driven by evaporative fluxes rather than sensible heat fluxes.

Irrigation effects on the surface energy balance in the irrigation hotspot regions show a diurnal cycle and are most pronounced during noon (Fig. 10). In SF, we see the strongest effects. There, irrigation increases the latent heat flux by up to $+200\,\mathrm{W\,m^{-2}}$, whereas it reduces the sensible heat flux by up to $-185\,\mathrm{W\,m^{-2}}$ during AMJ. The net radiation is slightly reduced in all three analysis regions, which can be explained by a combination of lower surface temperature (Fig. 8d), reduced surface albedo due to higher soil moisture, and increased humidity in the atmosphere with altered cloud cover. The ground heat flux is calculated as a residuum in the surface balance. During the irrigation hours, it decreases in all three analysis regions and causes less heat storage in the ground.

4.4.2 Effects on the atmosphere

The effects of irrigation propagate to the atmosphere through land–atmosphere interactions, in particular through fluxes. The effects occur mostly in grid cells with a high proportion of irrigated areas like in the Po Valley and the Ebro Basin (Fig. 11a and d). In both regions, the irrigation effects on the 2 m mean temperature (T2Mean) reach a reduction of up to −2 K averaged over AMJ. Figure 11b shows the diurnal cycle of T2Mean effects in the irrigated areas of the model domain. The whiskers and the outliers show the range of irrigation effects. Overall, T2Mean is reduced starting with the irrigation at 7:00 LT and reaches the highest reduction at

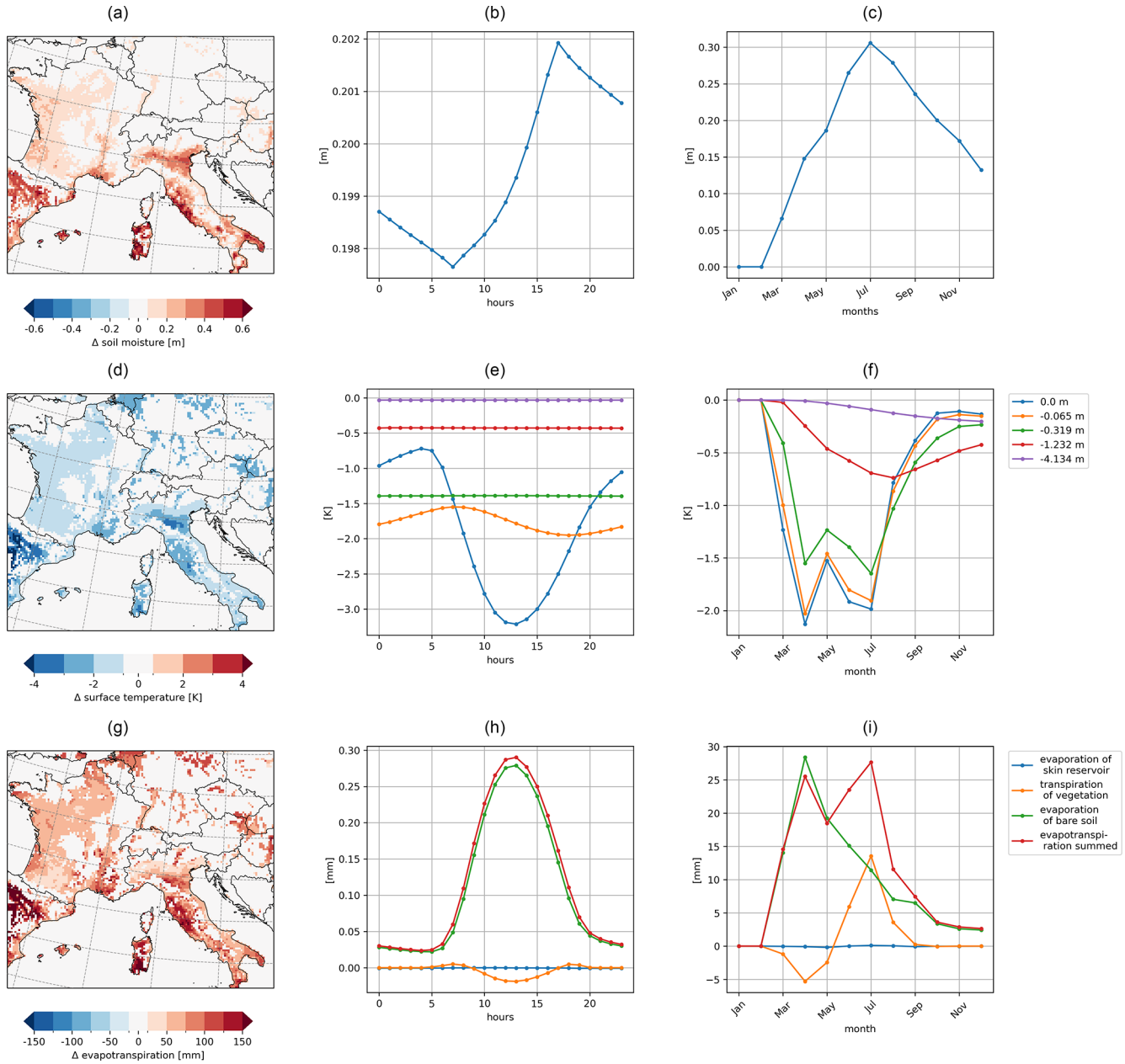

Figure 8. Irrigation effects based on the difference between the simulation with irrigation (S1) and the simulation without irrigation (S0) on soil and surface processes for the irrigated fraction **(a, d, g)** as a spatial distribution of mean values of AMJ, **(b, e, h)** as a diurnal cycle of mean values of irrigated areas in AMJ, and **(c, f, i)** as an annual cycle of mean values of irrigated areas for **(a–c)** soil moisture, **(d–f)** soil temperature at different depths, and **(g–i)** evapotranspiration fractions.

14:00 LT with about −3 K in irrigated areas. After that, the temperature reduction declines until the next irrigation starts at 7:00 LT the next day. We can find outliers showing a slight temperature increase, which is connected to grid cells with a low proportion of irrigated areas. Overall, the median shows a temperature reduction of −0.3 K in the irrigated areas of the model domain.

In Fig. 11c, the monthly mean of the irrigation effect on the 2 m daily maximum (T2Max), minimum (T2Min), and T2Mean is shown. T2Max shows the strongest irrigation effects, whereas T2Min shows the smallest. The effects develop within the first irrigation month in March and reduce the 2 m temperatures. In the course of the year, the effects increase until irrigation stops in August, which is the first not completely irrigated month. As a mean of the irrigated areas in the model domain, the highest temperature reduction for T2Max and T2Mean is reached in July with −0.68 and −0.39 K, respectively. In contrast, T2Min reaches its

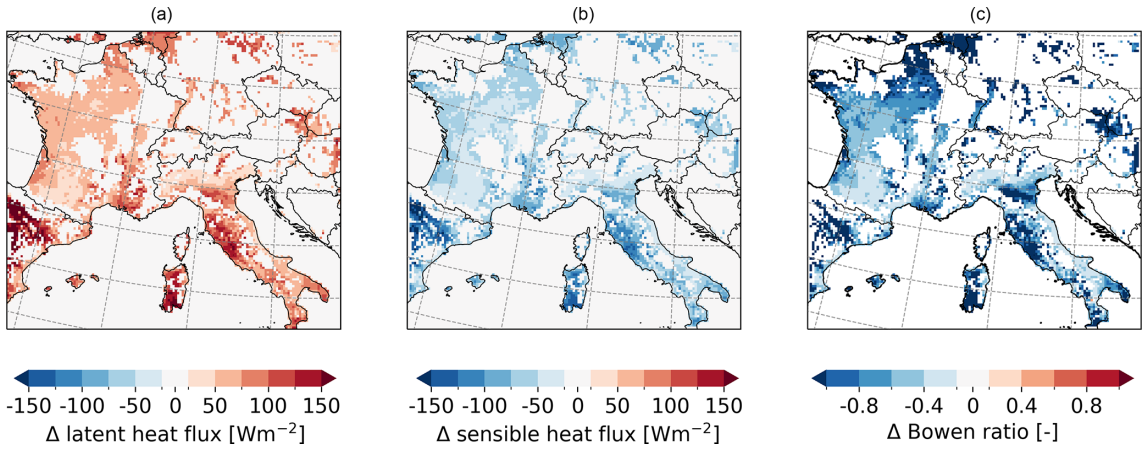

Figure 9. Irrigation effects based on the difference between the simulation with irrigation (S1) and the simulation without irrigation (S0) on surface fluxes as a spatial distribution of means for AMJ for **(a)** latent heat flux, **(b)** sensible heat flux, and **(c)** Bowen ratio shift.

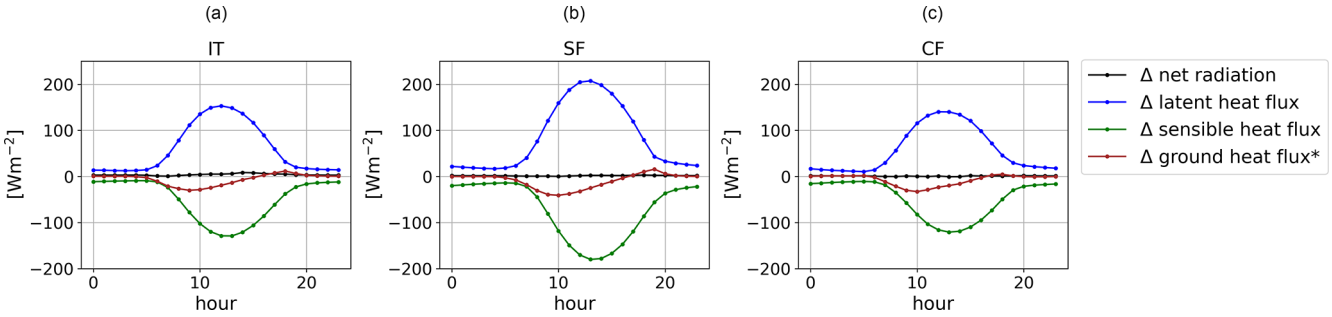

Figure 10. Irrigation effects based on the difference between the simulation with irrigation (S1) and the simulation without irrigation (S0) on the surface energy balance of the irrigated fraction as hourly mean values of AMJ in the analysis regions **(a)** IT, **(b)** SF, and **(c)** CF.

strongest temperature reduction in April with −0.21 K. With the end of irrigation the temperature reduction declines from August for the 2 m temperatures. T2Min reaches a temperature increase in the simulations with irrigation from September to November, which can be explained by the higher humidity in the atmosphere and its higher heat absorption as the driving effect. During the growing season, this effect is masked by the evaporative cooling from vegetation and soil. In May, the temperature reduction declines due to the smaller irrigation requirement.

The increases in the latent heat flux (Fig. 9b) and the evaporation (Fig. 8g–i) lead to an increase in the 2 m relative humidity (Fig. 11d–f). As for the 2 m temperature, the irrigation effects are particularly pronounced in grid cells with a high proportion of the irrigated fraction, as in the Po Valley and the Ebro Basin. The 2 m relative humidity increases in these grid cells by up to +20 % as a mean for AMJ. Areas with smaller irrigated fractions reach a 2 m relative humidity increase of +8 %. This wide range of effects also occurs in the diurnal cycle, where the strongest irrigation effects develop in the evening hours after the irrigation stops (Fig. 11e) and the air temperature starts to decrease. Then, the relative humidity increases by up to +23 % in single grid cells. However, the median for the irrigation effect on 2 m relative humidity is at +3 %. In the annual cycle, the irrigation effect on 2 m relative humidity starts with irrigation in March. March and April, as the first irrigated months, reach the highest 2 m relative humidity increase through irrigation because these are the months with the highest irrigation requirement. In the course of the year, the irrigation effects decline to a minimum in October with less than 1 % as a spatial mean of the irrigated areas (Fig. 11f).

For precipitation, the effects of irrigation are not as clear as for the 2 m temperatures and 2 m relative humidity (Fig. 12). In the spatial distribution, there is no clear pattern of the irrigation effects (Fig. 12a). There are areas along the Alps in which precipitation increased by +100 mm as a monthly mean value for AMJ. However, the pattern is very patchy. As monthly mean values for the whole model domain, the precipitation increases slightly during the irrigated months from March to July (Fig. 12b and c). After irrigation stops in July, precipitation shows a reduction in comparison to the non-irrigated simulation in August and September before it increases again from October to December. In our model setup, precipitation is represented with the shallow convection parameterization. To be able to analyze the physical processes

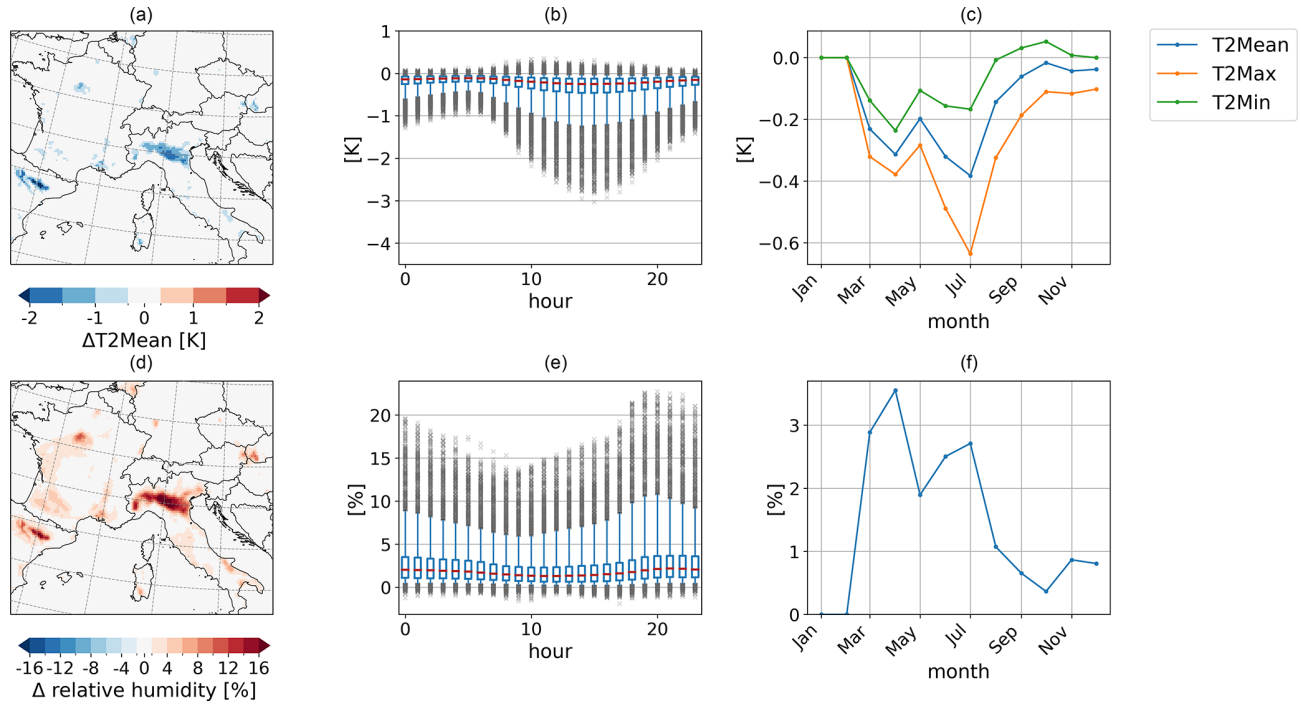

Figure 11. Irrigation effects based on the difference between the simulation with irrigation (S1) and the simulation without irrigation (S0) on the atmosphere above irrigated areas as **(a, d)** a spatial distribution of mean values of AMJ, **(b, e)** a mean diurnal cycle in AMJ (with the box spanning the 1st to the 3rd quartile, the red line showing the median, the whiskers showing the 5th and 95th percentile, and outliers as values outside these limits), and **(c, f)** an annual cycle of mean values for **(a–c)** 2 m temperatures and **(d–f)** 2 m relative humidity.

that affect precipitation, we would have to resolve convection.

4.4.3 Effects on the vegetation

For the vegetation modules of iMOVE, soil moisture is a crucial variable that drives multiple plant processes, such as the growing and shedding of leaves represented in the LAI. In addition, the LAI is driven by a growing degree threshold of temperature, simulating the growing season. Reaching the growing degree threshold, the LAI will decrease through harvest in the model. Due to the warm summer, the growing season ends in the southern parts of the model domain in the middle of July. As shown in Fig. 13a–c, the irrigation effects on the LAI depend on the month, in particular on the progressing growing season, and on the region. In April and May (Fig. 13a and b), the LAI decreases in wide parts of the model domain such as central France (Fig. 13b) by $-1\,\mathrm{m^2\,m^{-2}}$. This negative irrigation effect is caused by the 2 m temperature reduction (Fig. 11a–c), which is one of the drivers of LAI development leading to slower LAI growth in the first months of the growing season in the irrigated simulation (Fig. 14a and b). The more the growing season progresses and the vegetation approaches harvest, irrigation shows a positive effect on LAI. In June, the LAI increases with irrigation (Fig. 13c) in the Po Valley, the Ebro Basin, and Sardinia; these are areas that have experienced a warm summer and where the growing season is about to end. The LAI increases with irrigation because vegetation never experiences water stress. In June, the irrigation leads to smaller LAI in northern France as well as in parts of Germany. Again, the growing season has not yet progressed so far and the LAI develops slower with irrigation than without irrigation. The effects on the LAI mainly drive the effects on net primary production (NPP). In this study, NPP values refer to the carbon of fresh matter, following the description in Wilhelm et al. (2014). In April and May (Fig. 13d and e), the irrigation effects on NPP are very small because the growing season has not yet progressed far and vegetation just started to develop. From May onwards, irrigation increases NPP by $+800\,\mathrm{gC\,m^{-2}}$ per month in the Ebro Basin as well as in the Po Valley. Where the LAI decreases (Fig. 13b), the NPP also decreases slightly, as in central France. In June, the NPP increases through irrigation by up to $+1200\,\mathrm{gC\,m^{-2}}$ per month. As in the LAI, the influence of irrigation on NPP is greater as the growing season progresses. The LAI and the NPP reach their maximum in June in both simulations, with and without irrigation (Fig. 14a and c). The maximum irrigation effects of the LAI and NPP are reached shortly before the harvest in July (Fig. 14).

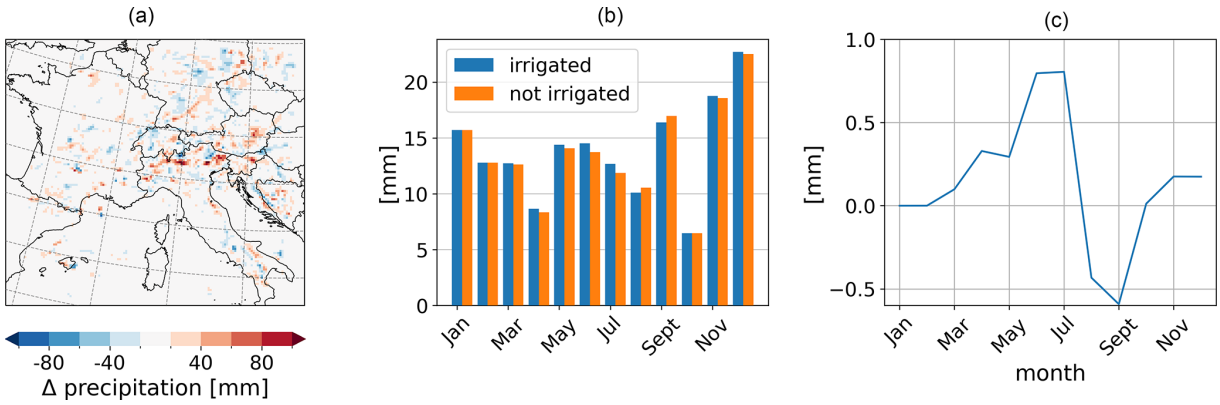

Figure 12. Irrigation effects based on the difference between the simulation with irrigation (S1) and the simulation without irrigation (S0) on summed precipitation above irrigation areas as **(a)** a spatial distribution of mean values of AMJ, **(b)** monthly mean values of the irrigated and not irrigated simulation, and **(c)** monthly mean effects.

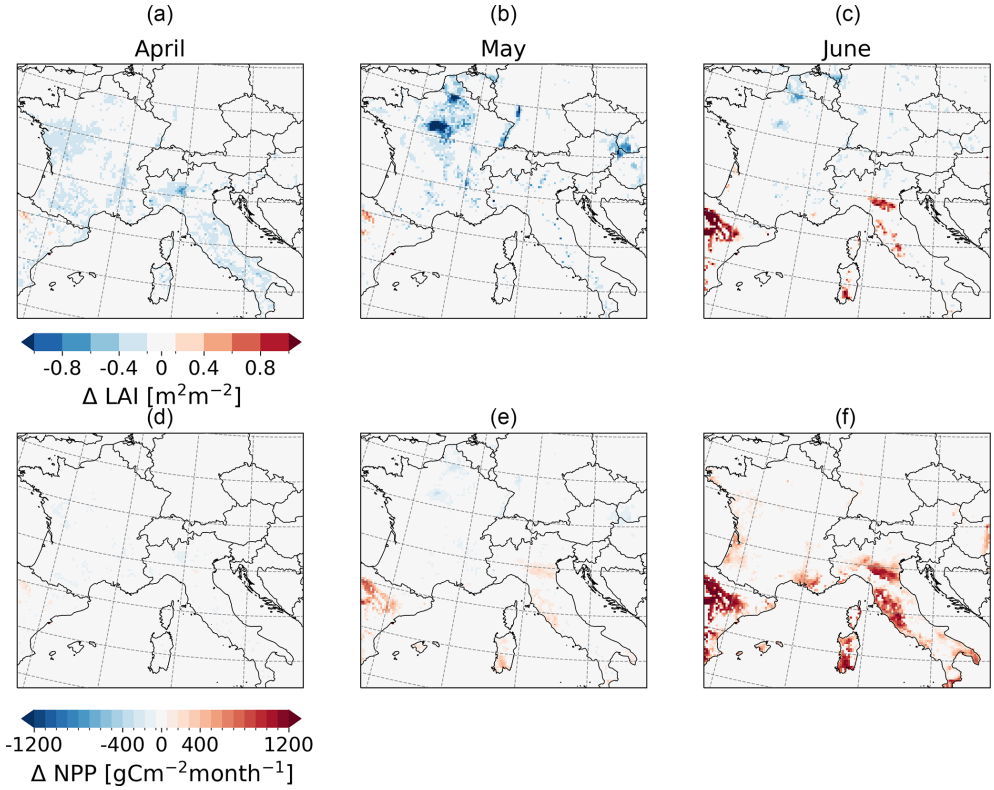

Figure 13. Irrigation effects based on the difference between the simulation with irrigation (S1) and the simulation without irrigation (S0) on vegetation as a spatial distribution of monthly mean values of the irrigated fraction of **(a–c)** LAI and **(d–f)** NPP of cropland in carbon of fresh matter.

4.4.4 Delayed effects during a heat wave

As described in Sect. 4.3, SW Europe, particularly Italy, experienced a heat wave in early August 2017. Therefore, we will focus on the region IT including the Po Valley with its high fraction of irrigated areas for this analysis (Fig. 3). Due to its temperature-reducing effect (Fig. 11a–c), irrigation is able to reduce the intensity of heat waves. In our experiment, irrigation is performed exclusively in the growing season. The growing season depends on the 2 m temperature. In 2017, the summer in IT was exceptionally warm and the growing season ended in July (Fig. 14a); thus, there was no irrigation during the August heat wave in IT (Fig. B1). Nevertheless, irrigation shows delayed effects. Even if there was

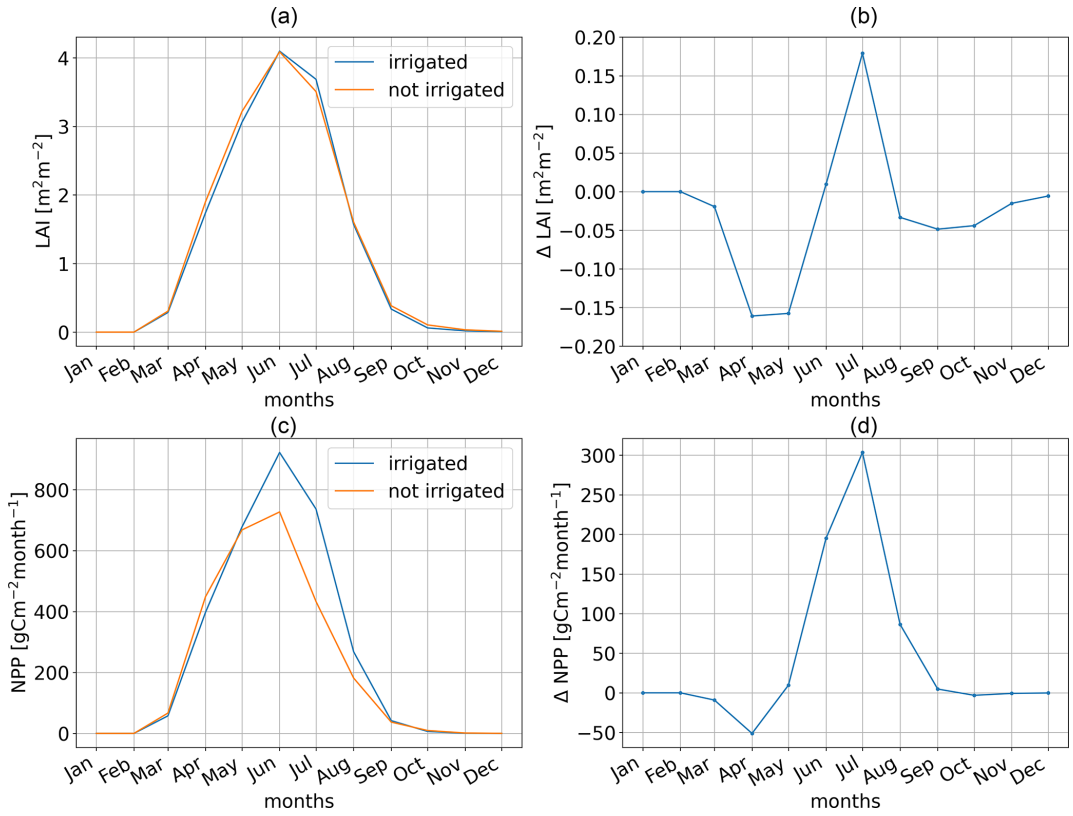

Figure 14. Development of **(a)** LAI and **(c)** NPP, as well as the irrigation effects based on the difference between the simulation with irrigation (S1) and the simulation without irrigation (S0) on **(b)** LAI and **(d)** NPP of the irrigated fraction.

no active irrigation, the 2 m temperature is reduced during the heat wave by previous irrigation. T2Mean is reduced by up to −4.5 K and T2Max is reduced by up to −6.6 K. As with active irrigation (in AMJ, Sect. 4.4.2c), the reduction of T2Min is smaller than for the maximum temperature and reaches −2.5 K in the northwestern part of IT (Fig. 15b and c). Figure 16a shows the 2 m temperature development during the week of the heat wave from 1 August until 7 August for IT. In both simulations the hottest days are 3 and 4 August; however, T2Max is reduced by −1.5 K in the irrigated simulation, reaching 35 °C instead of more than 36 °C. After the peak of the heat wave, the 2 m temperature drops from 5 August in both simulations. In the irrigated simulation, the relative soil moisture stays close to saturation at a high level of 0.91 of wsmx after irrigation stopped, whereas in the non-irrigated simulation, it stays at a low level of 0.45 of wsmx (Fig. 16b). In IT, precipitation (Fig. 16c) occurs on 2 and 3 August at very low rates, which can be neglected, and on 5, 6, and 7 August at higher rates up to 4.5 mm d^{-1} in the non-irrigated simulation and 2.5 mm d^{-1} in the irrigated simulation. However, these precipitation rates are very low and affect the soil moisture with a small increase from 0.45 of wsmx to 0.47 of wsmx in the non-irrigated simulation on 5 August. As in Sect. 4.4.2, the effect of irrigation on precipitation is unclear during the heat wave. In Fig. 16c, in the irrigated simulation precipitation increases on 5 August, decreases on 6 August, and stays the same on 7 August. A possible explanation for the precipitation increase might be the higher evapotranspiration rate and higher relative humidity (as shown in Sect. 4.4.2). However, the temperature changes through irrigation can also affect wind patterns so that the humidity is advected outside our analysis region IT. Further, the cooling effect of irrigation on the surface temperature and near-surface temperature leads to fewer convective processes, which might have developed in the non-irrigated simulation on 6 August. During the heat wave, transpiration of the remaining vegetation and evaporation of the soil are the drivers of evapotranspiration (Fig. 16d). However, in the irrigated simulation the evapotranspiration rate with up to 4 mm d^{-1} is almost double the evapotranspiration rate if irrigation is not turned on. This difference can be explained by the evaporation of bare soil. In the irrigated simulation the soil remained close to saturation (Fig. 16b) and can evaporate. In the non-irrigated simulation, the soil moisture is at a very low level and barely evaporates (Fig. 16d). After the precipitation events, the skin reservoir also evaporates on 6 and 7 August.

The delayed irrigation effects decrease the intensity of the heat wave and provide moisture in the soil to be evaporated, which can prevent the wilting of vegetation.

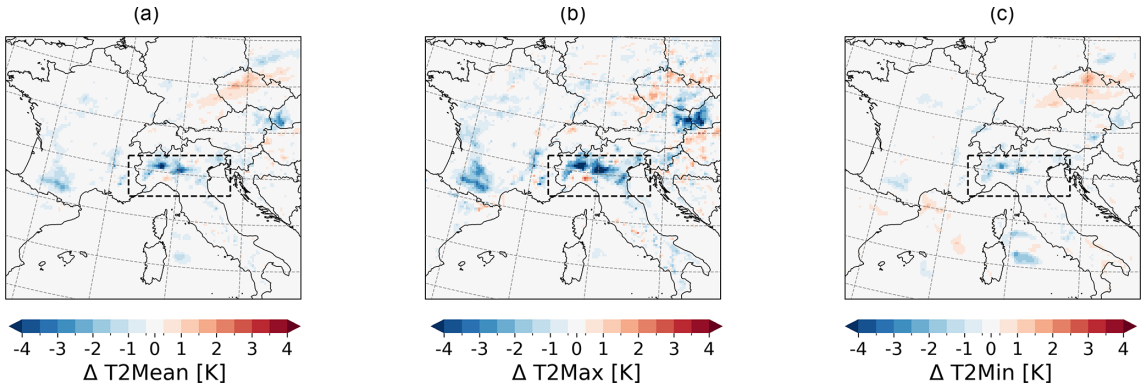

Figure 15. Delayed irrigation effects based on the difference between the simulation with irrigation (S1) and the simulation without irrigation (S0) on 2 m temperature during the heat wave from 1–7 August 2017 in IT: **(a)** T2Mean, **(b)** T2Max, and **(c)** T2Min.

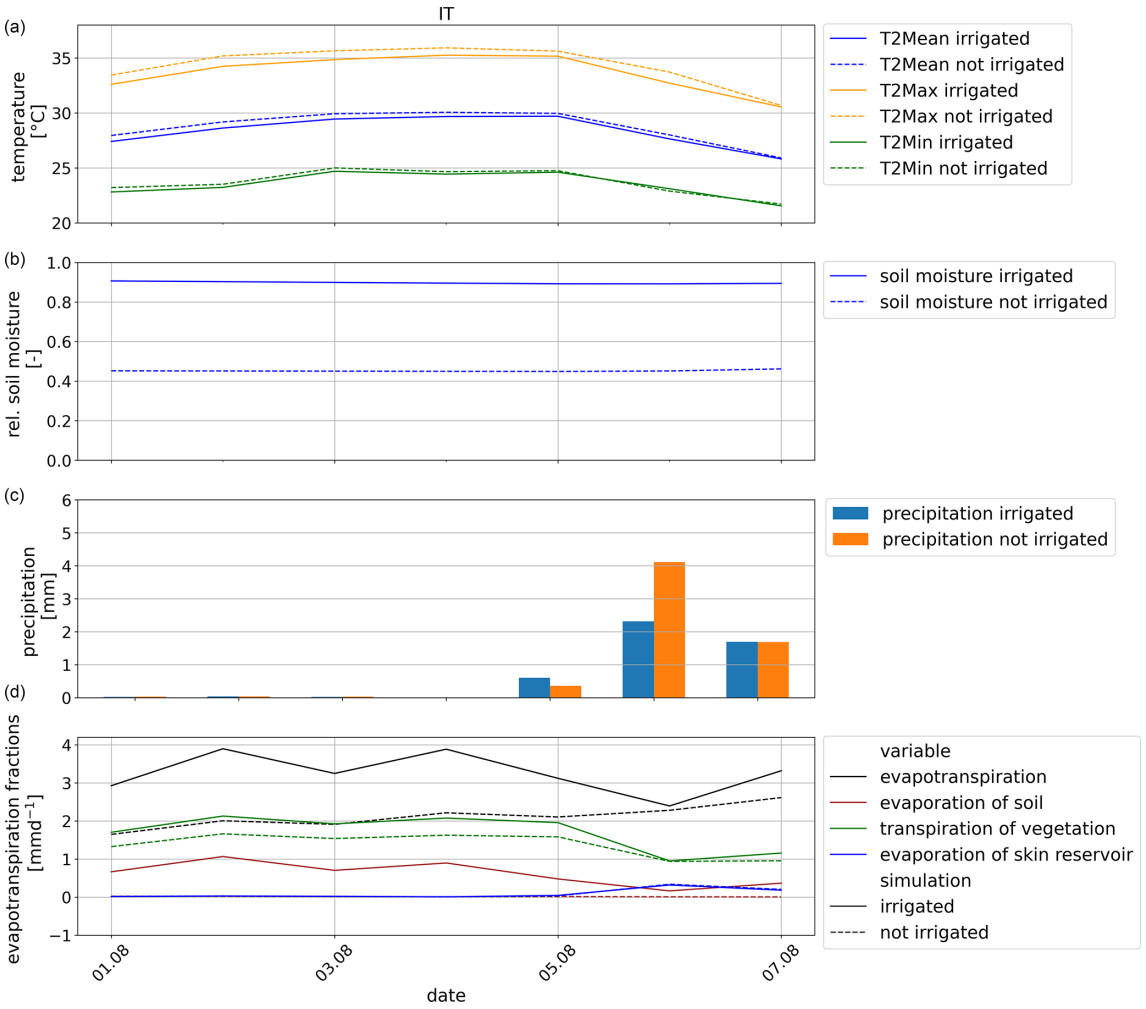

Figure 16. Development of delayed irrigation effects based on the difference between the simulation with irrigation (S1) and the simulation without irrigation (S0) during the heat wave in August (1–7 August 2017) in IT as **(a)** a spatial mean of 2 m temperatures, **(b)** a spatial mean of relative soil moisture, **(c)** a spatial sum of precipitation, and **(f)** a spatial mean of evapotranspiration.

4.5 Comparison with observational data

The results of the simulations are compared to observational data collected within SCIA (Sect. 2.3). For the comparison, we have focused exclusively on the Po Valley, represented in the analysis region IT (Fig. 3). In the Po Valley, we have the largest cluster of grid cells with a high proportion of irrigated fraction (Fig. 3) and therefore the most developed irrigation effects in the atmosphere. To compare the model results to the observational data, we filtered the SCIA data for April to August, as months with active irrigation, as well as months with delayed irrigation effects. Further, we filtered the SCIA data for the location in the IT region and the presence of an irrigated fraction. We selected the SCIA data with an irrigated fraction higher than 31 %, which is the mean of the irrigated fraction in that area, to reach a clear signal from the irrigation effects. The model data were then interpolated to the locations of the filtered observational data using inverse distance weighting with four known points. We calculated the bias for each station location and averaged it across all locations for each month. As the last step, the statistical significance of the bias distributions is evaluated with a Student's t test for two independent samples using a significance level (α) of 0.05. This process was performed for the results from the simulation with irrigation as well as for the results from the simulation without irrigation. The filtering results in a different number of suitable station data for each variable (Table 3, Fig. C1).

For this comparison, we focus on the near-surface temperature variables T2Mean, T2Max, and T2Min. In general, the irrigation parameterization reduces the 2 m temperatures. Without irrigation, REMO2020–iMOVE overestimates T2Mean from April to August in IT. Using the irrigation parameterization, the bias can be significantly reduced from April to July, in particular in May with a remaining bias of 0.04 K. However, July and especially August have the largest bias in the irrigated and non-irrigated simulation results. The delayed irrigation effects cause only a minor, nonsignificant bias reduction in August from 4.67 K in the non-irrigated simulation to 4.47 K in the irrigation simulation. The large biases in July (irrigated: 1.41 K, not irrigated: 3.36 K) and August are most probably connected to the early harvest and the drop in vegetation. Vegetation is an important contributor to the evapotranspiration of the surface, which has a cooling effect on the 2 m temperature (Fig. 8g–i). The early harvest and the early end of the growing season lead to an end of active irrigation.

For T2Mean, the irrigation parameterization caused significant bias reductions from April to July with high t values and p values of 0.0. For T2Max and T2Min, the results are not as clear as for T2Mean. REMO2020–iMOVE overestimates T2Max in April, June, July, and August. Using the irrigation parameterization leads to an underestimation of T2Max, except for August when the delayed cooling effect of irrigation reduces the large bias of 4.61 to 3.65 K. Again, August has the largest bias in both simulations and can be explained by the drop in vegetation. In general, T2Max is represented closer to observational values without irrigation.

The T2Min is overestimated with and without the irrigation parameterization by REMO2020–iMOVE. However, the irrigation parameterization significantly reduces the bias in April, June, and July. As for T2Mean and T2Max, August is the month with the largest bias in both simulations. However, the irrigation parameterization increases the bias even more from 5.47 to 5.89 K this time with its warming effect in August for T2Min (Fig. 11). The results for T2Min show lower t values and larger p values, pointing out the lower robustness of the bias distributions.

5 Discussion

We developed a new subgrid parameterization representing channel irrigation and implemented it in the regional climate model system REMO2020–iMOVE. An older version of the model, REMO2009, was previously tested with an irrigation parameterization by Saeed et al. (2009). The study analyzed large-scale irrigation effects over the Indian subcontinent at 0.5° horizontal resolution. In contrast to our study, the parameterization represented irrigation in the whole model grid cell, leading to possible overestimation of irrigation effects. However, it pointed out the importance of representing irrigation in climate models, in particular over large-scale, intensely irrigated areas such as the Indus Basin because irrigation decreases dry biases and affects the development of meteorological patterns such as the South Asian summer monsoon by adding water to the climate system (Saeed et al., 2009). In our experiment, we focus on higher-resolution simulations. The representation of irrigation on a subgrid scale is an improvement in the representation of irrigated areas and qualifies the parameterization for high-resolution studies in heterogeneous regions such as Europe. According to Im et al. (2010) and Giorgi and Avissar (1997), subgrid-scale representation of land cover and land use improves the representation of land–atmosphere interaction in climate models. In the new parameterization, irrigation is exclusively realized where it is required. Therefore, only the irrigated fraction is part of the irrigation process. The subgrid-scale approach is also used in, e.g., Lawrence et al. (2019) and Ozdogan et al. (2010). Our irrigation parameterization has different water application schemes that can be used to address different research questions. An influence of the different water application schemes on irrigation effects could not be found for similar settings. However, it has to be considered that the irrigation effects depend strongly on the irrigation amount, which in turn depends on the soil hydrology of the climate model. Due to the bucket scheme in REMO2020–iMOVE, suitable prescribed values of the irrigation amount differ from observed values because the water is added to the whole soil column. Therefore, model-specific values need to be chosen

Table 3. The 2 m temperature bias for the irrigated and non-irrigated simulation with t-test results. Bold values indicate statistical significance with $\alpha = 0.05$.

	T2Mean (51 stations)				T2Max (60 stations)				T2Min (53 stations)			
	irri	noirri	t value	p value	irri	noirri	t value	p value	irri	noirri	t value	p value
April	**0.20**	1.37	−7.43	0.0	−1.36	0.43	−10.6	0.0	**2.03**	2.55	−2.0	0.05
May	**0.04**	0.98	−5.02	0.0	−1.55	−0.03	−9.17	0.0	1.68	2.05	−1.41	0.16
June	**−0.11**	1.44	−7.3	0.0	−2.39	0.24	−12.09	0.0	**2.14**	2.7	−2.11	0.04
July	**1.41**	3.36	−10.21	0.0	**−0.34**	2.98	−16.61	0.0	**3.07**	3.99	−3.52	0.0
August	4.47	4.67	−1.3	0.2	**3.65**	4.62	−6.5	0.0	5.89	5.47	1.9	0.06

and the irrigation amount cannot be validated with observational values. However, to simulate irrigation effects, irrigation using physical thresholds as the irrigation start and target, as in the flextime and adaptive water application scheme, is more suitable and able to represent realistic soil conditions. For the future, for irrigation studies, we recommend the representation of the soil hydrology with a multiple-layer scheme as in WRF (Valmassoi et al., 2020c) and CLM (Lawrence et al., 2019; Ozdogan et al., 2010); it already exists and was developed for REMO2015 (Abel, 2023). A multiple-layer scheme will allow the usage of observed values for the irrigation amount and improves the representation of soil hydrology. Further, to represent an observed irrigation amount, irrigation water loss through, e.g., evaporation or leaks during water transport, has to be considered. Our irrigation parameterization adds the irrigation water directly to the soil moisture and therefore does not take into account irrigation efficiency.

For REMO2020–iMOVE and its bucket scheme, we selected the adaptive water application scheme as the default scheme because it does not require model-specific values and reaches the irrigation target in the prescribed time. To the authors' knowledge, a nonlinear approach, such as the adaptive scheme, has never been used for irrigation parameterization before but has proven to be suitable in this study.

The simulated effects of the irrigation parameterization on the surface energy balance are more pronounced in our study than in comparable studies (Valmassoi et al., 2020b; Lobell et al., 2009). This can be explained by the newly implemented fraction that has its own surface energy balance. In this study, we exclusively analyzed the values of the irrigated fraction and no grid cell averages of the soil and surface variables. Further, in our experiment, we used the maximum irrigation target and the maximum irrigation threshold to show the maximum possible effects. The effects on the atmosphere are in the same range as other studies (Valmassoi et al., 2020b; Lobell et al., 2009; Thiery et al., 2017). For example, Valmassoi et al. (2020b) found a monthly T2Max reduction of up to −3 K in the Po Valley, whereas we found a T2Max reduction of up to −4 K in single grid cells. The effect on vegetation, slowing down the development of the LAI, is model-specific and could not be verified with other studies. In contrast, studies found that with irrigation the LAI is larger than without (Patanè, 2011). Therefore, the interactive LAI representation in REMO2020–iMOVE might have to be improved. Further, the large positive bias in August in comparison to observational data can be attributed to the missing vegetation and the early harvest in July, which is represented as an LAI drop, causing a stop to vegetation processes. The missing evaporative cooling of the transpiration of vegetation leads to increasing 2 m temperatures. This effect was already observed by Wilhelm et al. (2014) and Rai et al. (2022). Nevertheless, the irrigation parameterization could significantly reduce the bias for T2Mean in 2017 in the Po Valley, particularly in months with active irrigation. For T2Max, the irrigation parameterization adds a cold bias, whereas, for T2Min, the irrigation parameterization reduces the warm bias. We can infer that the irrigation parameterization decreases the diurnal range of the 2 m temperature. However, as the warm bias in T2Min is also still high with irrigation, other processes in the model need to be considered as the source. The underestimation of T2Max can be traced back to our experiment design, which shows maximum irrigation effects. Therefore, it might overestimate irrigation effects. First, our irrigated fraction is based on the area equipped for irrigation that is not completely irrigated in reality. Second, in our experiments, we keep the soil moisture at very high levels (higher than 0.75 of wsmx) at which plants do not experience any water stress and the potential transpiration by plants is reached. And third, we irrigate in daytime hours, leading to strong effects on variables with a distinct diurnal cycle such as the surface fluxes, evapotranspiration, and T2Max. The effect of irrigation timing was analyzed by Valmassoi et al. (2020c), who showed a rather low impact of irrigation timing on the development of irrigation effects.

For our irrigation parameterization, we assumed unlimited water availability for all grid cells. However, for irrigation practice, this is not the case. First, the probability of heat waves and droughts in western and southern Europe increases with climate change (Kew et al., 2019) and there is likely not sufficient water available during these periods (IPCC, 2019). Second, during heat waves and droughts, governments have to ration water, as happened during the intense heat wave in 2022 in northern Italy (Balmer and Amante,

2022; Giuffrida, 2022). Having a limited water reservoir in REMO2020–iMOVE would be a step towards a more realistic irrigation amount.

Our parameterization increases the soil moisture directly and can therefore be understood as a representation of channel irrigation. Additionally, there are more irrigation methods, e.g., sprinkler or drip methods, which require canopy interactions and different parameterization approaches as Valmassoi et al. (2020c) and Yao et al. (2022) pointed out.

In our study irrigation effects on precipitation remain unclear and cannot reproduce the findings in observation studies showing a regional annual decrease in precipitation as found in Szilagyi and Franz (2020). However, irrigation effects on precipitation are indirect and influenced by many interconnected factors such as atmospheric stability, specific humidity, temperature, and wind patterns. These make a comparison difficult. To find clearer patterns of irrigation effects on precipitation, a longer experiment is necessary. Further, in our study, the convective precipitation is parameterized and the generating processes are not resolved. Therefore, we recommend using convection-permitting resolution for analyzing precipitation–irrigation feedback.

6 Conclusions

By implementing irrigation into the regional climate model system REMO2020–iMOVE, we include a widely used land use practice and an important aspect of anthropogenic forcing on the climate system, enabling the investigation of irrigation effects. Our newly developed parameterization is designed for high-resolution studies using a separate irrigated land fraction, ensuring that exclusively irrigated areas are irrigated in the model and irrigation effects can be realistically estimated. Further, our parameterization takes into account vegetation processes. With our model system REMO2020–iMOVE, we could show the irrigation effects and feedbacks regarding LAI development, which develops slower in the model but reaches higher maxima, and regarding the process of NPP, which increases with irrigation. Our parameterization is characterized by three water application schemes, which simulate irrigation with prescribed irrigation, with flexible time irrigation, and with adaptive irrigation. Even though the irrigation schemes differ in irrigation time, irrigation events, and water application per time step, the differences in the effects are small and can be neglected. However, the different irrigation schemes can be applied to different research questions in the future. Rather than the water application, the water amount is an important driver of irrigation effects. Therefore, simulations with a realistic irrigation amount together with a layer model are desirable for the future.

We applied our irrigation parameterization for dry and hot conditions in 2017 in SW Europe. Whereas the effects on soil and surface variables are more pronounced in our study using the fractional approach than in comparable studies, the effects on the atmosphere match the range of temperature reduction. For effects on small-scale precipitation, the resolution of our study is not high enough and we cannot resolve convective processes, leading to unclear irrigation effects. Therefore, studies with higher resolution, such as on a convection-permitting scale, and with a longer extent are necessary. For REMO2020–iMOVE the application of our irrigation parameterization significantly decreased the monthly warm bias of T2Mean during AMJ with active irrigation. But delayed irrigation effects also occur, influencing the summer season. Our study showed that irrigation effects such as temperature reduction and soil moisture increase are not only an adaptation measure during droughts or heat waves, but also that these irrigation effects have the potential to prevent or mitigate such climate extremes on a local scale.

Appendix A: Parameterization development

A1 Implementing irrigation into REMO2020–iMOVE

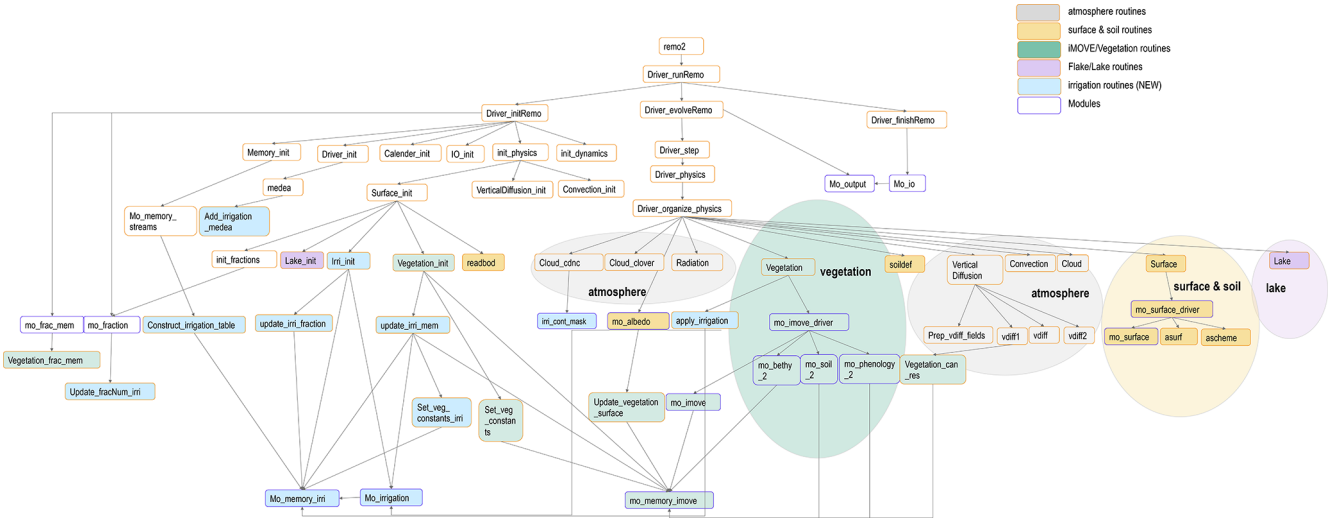

Figure A1. Remo2020–iMOVE + FLake call tree for the version with subgrid irrigation.

A2 Water application schemes

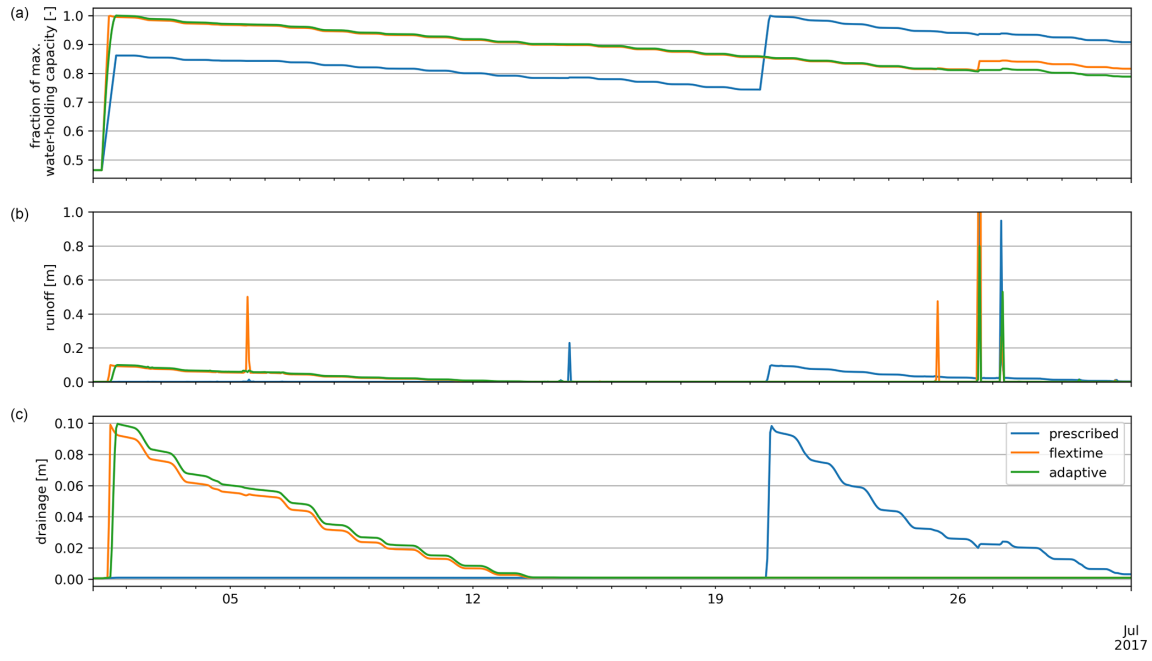

Figure A2. Results of different water application schemes (T1, T2, T3) for **(a)** relative soil moisture, **(b)** runoff, and **(c)** drainage.

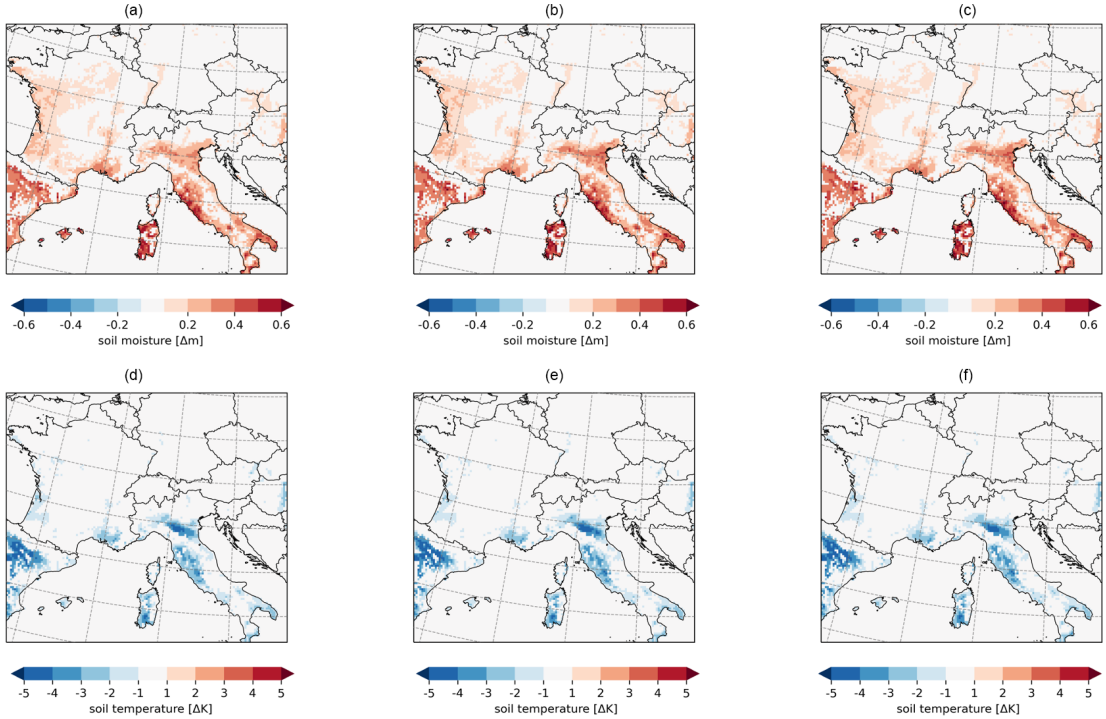

Figure A3. Spatial distribution of the mean effects of different water application schemes in June 2017 for **(a)**–**(c)** soil moisture and **(d)**–**(f)** surface temperature using the **(a, d)** prescribed, **(b, e)** flextime, and **(c, f)** adaptive scheme.

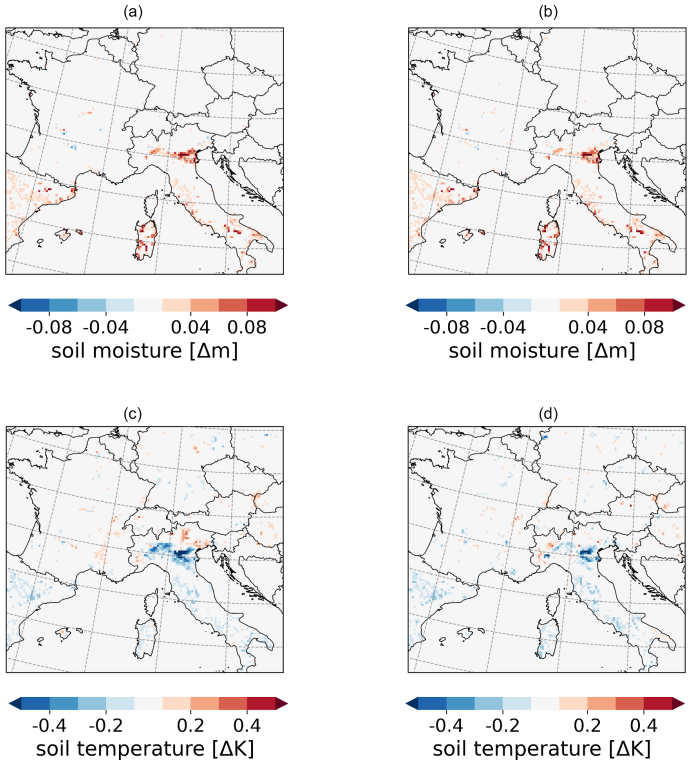

Figure A4. Differences between water application schemes in June 2017 for **(a–b)** soil moisture and **(c–d)** surface temperature between **(a–c)** the flextime and prescribed schemes and between **(b–d)** the adaptive and prescribed schemes.

Appendix B: Irrigation conditions during August

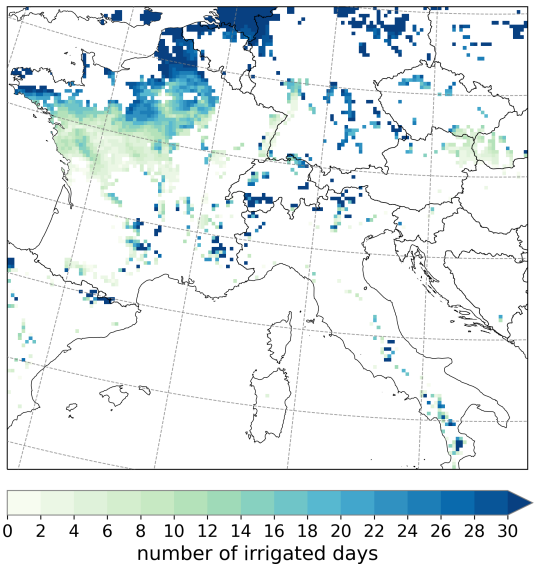

Figure B1. Number of irrigation days in August 2017.

Appendix C: Station location used for comparison with observational data

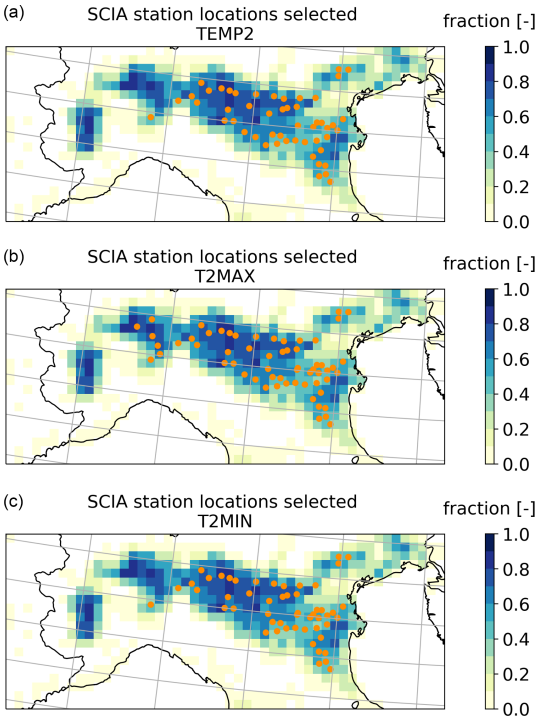

Figure C1. Station location for **(a)** T2Mean, **(b)** T2Max, and **(c)** T2Min.

Code and data availability. The model code of REMO2020–iMOVE with the new irrigation parameterization is available on request (contact@remo-rcm.de).

The scripts used to produce the results presented in this paper are archived on Zenodo (https://doi.org/10.5281/zenodo.7889384, Asmus and Buntemeyer, 2023), as are the simulation data together with the observational data from SCIA (https://doi.org/10.5281/zenodo.7867328, Asmus, 2023) after we received their permission. Originally, we downloaded the observation data from http://www.scia.isprambiente.it/ (last access: 8 December 2023) using the API http://193.206.192.214/servertsutm/serietemporali400.php (Desiato et al., 2011).

Author contributions. CA, PH, DR, and JB developed the experiments. CA developed the irrigation module. CA and JPP implemented the parameterization in the model code in close cooperation with PH. CA conducted the analysis including the visualizations under the supervision of DR and JB. CA prepared the initial paper. All authors reviewed the paper draft and contributed to the final paper.

Competing interests. The contact author has declared that none of the authors has any competing interests.

Disclaimer. Publisher's note: Copernicus Publications remains neutral with regard to jurisdictional claims made in the text, published maps, institutional affiliations, or any other geographical representation in this paper. While Copernicus Publications makes every effort to include appropriate place names, the final responsibility lies with the authors.

Acknowledgements. We are grateful for the support and help of the REMO developer team located at GERICS. We want to thank Lars Buntemeyer in particular for preparing the ERA5 data as model forcing and helping with the publication of the analysis code and data. We also thank Juliane El Zohbi for internally reviewing our paper draft. We are grateful to DKRZ for providing the high computing capacity, with which we performed our simulations. Further, we want to thank ISPRA for collecting and providing observation data publicly in the SCIA database and FAO for providing the GMIA V5 publicly.

Financial support. This work was financed within the framework of the Helmholtz Institute for Climate Service Science (HICSS), a cooperation between the Climate Service Center Germany (GERICS) and Universität Hamburg, Germany, and it was conducted as part of the LANDMATE (Modelling human LAND surface modifications and its feedbacks on local and regional cliMATE) project.

The article processing charges for this open-access publication were covered by the Helmholtz-Zentrum Hereon.

Review statement. This paper was edited by Hisashi Sato and reviewed by Hisashi Sato and one anonymous referee.

References

Abel, D. K.-J.: Weiterentwicklung der Bodenhydrologie des regionalen Klimamodells REMO, PhD thesis, Universität Würzburg, https://doi.org/10.25972/OPUS-31146, 2023.

Asmus, C.: Modeling and evaluating the effects of irrigation on land-atmosphere interaction in southwestern Europe with the regional climate model REMO2020-iMOVE using a newly developed parameterization, Zenodo [data set], https://doi.org/10.5281/zenodo.7867328, 2023.

Asmus, C. and Buntemeyer, L.: Modeling and evaluating the effects of irrigation on land-atmosphere interaction in southwestern Europe with the regional climate model REMO2020-iMOVE using a newly developed parameterization, Zenodo [code], https://doi.org/10.5281/zenodo.7889384, 2023.

Balmer, C. and Amante, A.: Analysis: Wasted water saps battle against Italy's worst drought in decades, Reuters, https://www.reuters.com/world/europe/wasted-water-saps-battle-against-italys-worst-drought-decades-2022-07-19/ (last access: 30 November 2023), 2022.

Bjorneberg, D.: IRRIGATION | Methods, in: Reference Module in Earth Systems and Environmental Sciences, Elsevier, ISBN 978-0-12-409548-9, https://doi.org/10.1016/B978-0-12-409548-9.05195-2, 2013.

Boucher, O., Myhre, G., and Myhre, A.: Direct human influence of irrigation on atmospheric water vapour and climate, Clim. Dynam., 22, 597–603, https://doi.org/10.1007/s00382-004-0402-4, 2004.

Copernicus Climate Change Service: European State of the Climate 2017, Climate in 2017 – Focus Region: Southwest Europe, Southwest Europe – dry conditions, https://climate.copernicus.eu/climate-2017-focus-region-southwest-europe, last access: 1 December 2023.

Desiato, F., Fioravanti, G., Fraschetti, P., Perconti, W., and Toreti, A.: Climate indicators for Italy: calculation and dissemination, Adv. Sci. Res., 6, 147–150, https://doi.org/10.5194/asr-6-147-2011, 2011 (data available at: http://193.206.192.214/servertsutm/serietemporali400.php, last access: 8 December 2023).

de Vrese, P. and Hagemann, S.: Uncertainties in modelling the climate impact of irrigation, Clim. Dynam., 51, 2023–2038, https://doi.org/10.1007/s00382-017-3996-z, 2018.

Doell, P. and Siebert, S.: A Digital Global Map of Irrgated Areas, Report A9901, Center for Environmental Systems Research, University of Kassel, Kurt Wolters Strasse 3, 34109 Kassel, Germany, https://doi.org/10.13140/2.1.2726.2080, 1999.

Dümenil, L. and Todini, E.: Chapter 9 – A rainfall–runoff scheme for use in the Hamburg climate model, in: Advances in Theoretical Hydrology, edited by: O'Kane, J. P., European Geophysical Society Series on Hydrological Sciences, Elsevier, Amsterdam, 129–157, https://doi.org/10.1016/B978-0-444-89831-9.50016-8, 1992.

Eggert, B.: Auswirkungen der Oberflächeneigenschaften in REMO auf die Simulation der unteren Atmosphäre, CSC Report,

8, https://epub.sub.uni-hamburg.de/epub/volltexte/2013/23967/pdf/csc_report8.pdf (last access: 30 November 2023), 2011.

Giorgi, F. and Avissar, R.: Representation of heterogeneity effects in Earth system modeling: Experience from land surface modeling, Rev. Geophys., 35, 413–437, https://doi.org/10.1029/97RG01754, 1997.

Giuffrida, A.: More than 100 towns in Italy's Po valley asked to ration water, The Guardian, https://www.theguardian.com/world/2022/jun/15/italy-drought-po-valley-ration-water (last access: 30 November 2023), 2022.

Goettel, H.: Einfluss der nichthydrostatischen Modellierung und der Niederschlagsverdriftung auf die Ergebnisse regionaler Klimamodellierung, PhD thesis, MPI für Meteorologie, Hamburg, https://doi.org/10.17617/2.994076, 2009.

Hagemann, S.: An Improved Land Surface Parameter Dataset for Global and Regional Climate Models, MPI Report 336, Max-Planck-Institut fuer Meteorologie, 21 pp., https://doi.org/10.17617/2.2344576, 2002.

Hagemann, S., Botzet, M., Dümenil, L., and Machenhauer, B.: Derivation of global GCM boundary conditions 10 from 1 km land use satellite date, MPI Report No. 289, Max-Planck-Institut fuer Meteorologie, 34 pp., https://pure.mpg.de/rest/items/item_1562156_5/component/file_1562155/content (last access: 30 November 2023), 1999.

Hoffmann, P., Reinhart, V., Rechid, D., de Noblet-Ducoudré, N., Davin, E. L., Asmus, C., Bechtel, B., Böhner, J., Katragkou, E., and Luyssaert, S.: High-resolution land use and land cover dataset for regional climate modelling: historical and future changes in Europe, Earth Syst. Sci. Data, 15, 3819–3852, https://doi.org/10.5194/essd-15-3819-2023, 2023.

Im, E.-S., Coppola, E., Giorgi, F., and Bi, X.: Validation of a High-Resolution Regional Climate Model for the Alpine Region and Effects of a Subgrid-Scale Topography and Land Use Representation, J. Climate, 23, 1854–1873, https://doi.org/10.1175/2009JCLI3262.1, 2010.

IPCC: Summary for Policymakers, in: Climate Change and Land: an IPCC special report on climate change, desertification, land degradation, sustainable land management, food security, and greenhouse gas fluxes in terrestrial ecosystems, edited by: Shukla, P. R., Skea, J., Calvo Buendia, E., Masson-Delmotte, V., Pörtner, H.-O., Roberts, D. C., Zhai, P., Slade, R., Connors, S., van Diemen, R., Ferrat, M., Haughey, E., Luz, S., Neogi, S., Pathak, M., Petzold, J., Portugal Pereira, J., Vyas, P., Huntley, E., Kissick, K., Belkacemi, M., and Malley, J., https://doi.org/10.1017/9781009157988.001, 2019.

Jacob, D.: A note to the simulation of the annual and inter-annual variability of the water budget over the Baltic Sea drainage basin, Meteorol. Atmos. Phys., 77, 61–73, https://doi.org/10.1007/s007030170017, 2001.

Jacob, D.and Podzun, R.: Sensitivity studies with the regional climate model REMO, Meteorol. Atmos. Phys., 63, 119–129, https://doi.org/10.1007/BF01025368, 1997.

Jia, G., Shevliakova, E., Artaxo, P., De Noblet-Ducoudré, N., Houghton, R., House, J., Kitajima, K., Lennard, C., Popp, A., Sirin, A., Sukumar, R., and Verchot, L.: Land–climate interactions, in: Climate Change and Land: an IPCC special report on climate change, desertification, land degradation, sustainable land management, food security, and greenhouse gas fluxes in terrestrial ecosystems, edited by: Shukla, P. R., Skea, J., Calvo Buendia, E., Masson-Delmotte, V., Pörtner, H.-O., Roberts, D., Zhai, P., Slade, R., Connors, S., van Diemen, R., Ferrat, M., Haughey, E., Luz, A., Neogi, S., Pathak, M., Petzold, J., Portugal Pereira, J., Vyas, P., Huntley, E., Kissick, K., Belkacemi, M., and Malley, J., book section Chapter 2, Intergovernmental Panel on Climate Change, https://www.ipcc.ch/site/assets/uploads/sites/4/2022/11/SRCCL_Chapter_2.pdf (last access: 30 November 2023), in press, 2019.

Kew, S. F., Philip, S. Y., van Oldenborgh, G. J., van der Schrier, G., Otto, F. E. L., and Vautard, R.: The Exceptional Summer Heat Wave in Southern Europe 2017, B. Am. Meteorol. Soc., 100, S49–S53, https://doi.org/10.1175/BAMS-D-18-0109.1, 2019.

Kotlarski, S.: A subgrid glacier parameterisation for use in regional climate modelling, PhD Thesis, University of Hamburg, Hamburg, https://doi.org/10.17617/2.994357, 2007.

Kueppers, L., Snyder, M., and Sloan, L.: Irrigation cooling effect: Regional climate forcing by land-use change, Geophys. Res. Lett., 34, L03703, https://doi.org/10.1029/2006GL028679, 2007.

Lawrence, D. M., Fisher, R. A., Koven, C. D., Oleson, K. W., Swenson, S. C., Bonan, G., Collier, N., Ghimire, B., van Kampenhout, L., Kennedy, D., Kluzek, E., Lawrence, P. J., Li, F., Li, H., Lombardozzi, D., Riley, W. J., Sacks, W. J., Shi, M., Vertenstein, M., Wieder, W. R., Xu, C., Ali, A. A., Badger, A. M., Bisht, G., van den Broeke, M., Brunke, M. A., Burns, S. P., Buzan, J., Clark, M., Craig, A., Dahlin, K., Drewniak, B., Fisher, J. B., Flanner, M., Fox, A. M., Gentine, P., Hoffman, F., Keppel-Aleks, G., Knox, R., Kumar, S., Lenaerts, J., Leung, L. R., Lipscomb, W. H., Lu, Y., Pandey, A., Pelletier, J. D., Perket, J., Randerson, J. T., Ricciuto, D. M., Sanderson, B. M., Slater, A., Subin, Z. M., Tang, J., Thomas, R. Q., Val Martin, M., and Zeng, X.: The Community Land Model Version 5: Description of New Features, Benchmarking, and Impact of Forcing Uncertainty, J. Adv. Model. Earth Sy., 11, 4245–4287, https://doi.org/10.1029/2018MS001583, 2019.

Leng, G., Huang, M., Tang, Q., and Leung, L. R.: A modeling study of irrigation effects on global surface water and groundwater resources under a changing climate, J. Adv. Model. Earth Sy., 7, 1285–1304, https://doi.org/10.1002/2015MS000437, 2015.

Leng, G., Leung, L. R., and Huang, M.: Significant impacts of irrigation water sources and methods on modeling irrigation effects in the ACME Land Model, J. Adv. Model. Earth Sy., 9, 1665–1683, https://doi.org/10.1002/2016MS000885, 2017.

Lobell, D., Govindasamy, B., Mirin, A., Phillips, T., Maxwell, R., and Rotman, D.: Regional Differences in the Influence of Irrigation on Climate, J. Climate, 22, 2248–2255, https://doi.org/10.1175/2008JCLI2703.1, 2009.

Luyssaert, S., Jammet, M., Stoy, P., Estel, S., Pongratz, J., Ceschia, E., Churkina, G., Don, A., Erb, K.-H., Ferlicoq, M., Gielen, B., Grünwald, T., Houghton, R., Klumpp, K., Knohl, A., Kolb, T., Kuemmerle, T., Laurila, T., Lohila, A., and Dolman, H. A.: Land management and land-cover change have impacts of similar magnitude on surface temperature, Nat. Clim. Change, 4, 389–393, https://doi.org/10.1038/nclimate2196, 2014.

Majewski, D.: The EUROPA-modell of the Deutscher Wetterdienst, in: Seminar on Numerical Methods in Atmospheric Models, 9–13 September 1991, vol. II, ECMWF, ECMWF, Shinfield Park, Reading, 147–193, https://www.ecmwf.int/node/10940 (last access: 1 December 2023), 1991.

Ozdogan, M., Rodell, M., Beaudoing, H. K., and Toll, D. L.: Simulating the Effects of Irrigation over the United States in a Land Surface Model Based on Satellite-Derived Agricultural Data, J. Hydrometeorol., 11, 171–184, https://doi.org/10.1175/2009JHM1116.1, 2010.

Patanè, C.: Leaf Area Index, Leaf Transpiration and Stomatal Conductance as Affected by Soil Water Deficit and VPD in Processing Tomato in Semi Arid Mediterranean Climate, J. Agron. Crop Sci., 197, 165–176, https://doi.org/10.1111/j.1439-037X.2010.00454.x, 2011.

Peterson, J. B., Robinson, B. F., and Beck, R. H.: Predictability of Change in Soil Reflectance on Wetting, LARS Symposia, Paper 279, http://docs.lib.purdue.edu/lars_symp/279 (last access: 1 December 2023), 1979.

Pietikäinen, J.-P., Markkanen, T., Sieck, K., Jacob, D., Korhonen, J., Räisänen, P., Gao, Y., Ahola, J., Korhonen, H., Laaksonen, A., and Kaurola, J.: The regional climate model REMO (v2015) coupled with the 1-D freshwater lake model FLake (v1): Fenno-Scandinavian climate and lakes, Geosci. Model Dev., 11, 1321–1342, https://doi.org/10.5194/gmd-11-1321-2018, 2018.

Puma, M. and Cook, B.: Effects of irrigation on global climate during the 20th century, J. Geophys. Res, 115, D16120, https://doi.org/10.1029/2010JD014122, 2010.

Raddatz, T. J., Reick, C. H., Knorr, W., Kattge, J., Roeckner, E., Schnur, R., Schnitzler, K.-G., Wetzel, P., and Jungclaus, J.: Will the tropical land biosphere dominate the climate–carbon cycle feedback during the twenty-first century?, Clim. Dynam., 29, 565–574, https://doi.org/10.1007/s00382-007-0247-8, 2007.

Rai, P., Ziegler, K., Abel, D., Pollinger, F., and Paeth, H.: Performance of a regional climate model with interactive vegetation (REMO-iMOVE) over Central Asia, Theor. Appl. Climatol., 150, 1385–1405, https://doi.org/10.1007/s00704-022-04233-y, 2022.

Rechid, D. and Jacob, D.: Influence of monthly varying vegetation on the simulated climate in Europe, Meteorol. Z., 15, 99–116, https://doi.org/10.1127/0941-2948/2006/0091, 2006.

Reinhart, V., Hoffmann, P., Rechid, D., Böhner, J., and Bechtel, B.: High-resolution land use and land cover dataset for regional climate modelling: a plant functional type map for Europe 2015, Earth Syst. Sci. Data, 14, 1735–1794, https://doi.org/10.5194/essd-14-1735-2022, 2022.

Roeckner, E., Arpe, K., Bengtsson, L., Christoph, M., Claussen, M., Dümenil, L., Esch, M., Giorgetta, M., Schlese, U., and Schulzweida, U.: The Atmospheric General Circulation Model ECHAM-4: Model Description and Simulation of Present Day, Climate MPI Report No. 218, Max-Planck-Institut für Meteorologie, Hamburg, Germany, ISSN 0937-1060, https://esdynamics.geo.uni-tuebingen.de/wiki/files/modelling/pdf/MPI-Report_218.pdf (last access: 1 December 2023), 1996.

Sacks, W. J., Cook, B. I., Buenning, N., Levis, S., and Helkowski, J. H.: Effects of global irrigation on the near-surface climate, Clim. Dynam., 33, 159–175, https://doi.org/10.1007/s00382-008-0445-z, 2009.

Saeed, F., Hagemann, S., and Jacob, D.: Impact of irrigation on the South Asian summer monsoon, Geophys. Res. Lett., 36, L20711, https://doi.org/10.1029/2009GL040625, 2009.

Sánchez-Benítez, A., García-Herrera, R., Barriopedro, D., Sousa, P. M., and Trigo, R. M.: June 2017: The Earliest European Summer Megaheatwave of Reanalysis Period, Geophys. Res. Lett., 45, 1955–1962, https://doi.org/10.1002/2018GL077253, 2018.

Semmler, T.: Der Wasser- und Energiehaushalt der arktischen Atmosphäre, PhD Thesis, Universität Hamburg, Hamburg, https://pure.mpg.de/rest/items/item_995430_6/component/file_995429/content (last access: 1 December 2023), 2002.

Siebert, S., Henrich, V., Frenken, K, and Burke, J.: Global Map of Irrigation Areas version 5, Rheinische Friedrich-Wilhelms-University, Bonn, Germany/Food and Agriculture Organization of the United Nations, Rome, Italy, https://www.fao.org/aquastat/en/geospatial-information/global-maps-irrigated-areas/latest-version (last access: 1 December 2023), 2013a.

Siebert, S., Henrich, V., Frenken, K., and Burke, J.: Update of the Digital Global Map of Irrigation Areas to Version 5; Food and Agriculture Organization of the United Nations (FAO), Rome, Italy, https://doi.org/10.13140/2.1.2660.6728, 2013b.

Szilagyi, J. and Franz, T. E.: Anthropogenic hydrometeorological changes at a regional scale: observed irrigation–precipitation feedback (1979–2015) in Nebraska, USA, Sustainable Water Resources Management, 6, 1, https://doi.org/10.1007/s40899-020-00368-w, 2020.

Thiery, W., Davin, E. L., Lawrence, D. M., Hirsch, A. L., Hauser, M., and Seneviratne, S. I.: Present-day irrigation mitigates heat extremes, J. Geophys. Res.-Atmos., 122, 1403–1422, https://doi.org/10.1002/2016JD025740, 2017.

Thiery, W., Visser, A., Fischer, E., Hauser, M., Hirsch, A., Lawrence, D., Lejeune, Q., Davin, E., and Seneviratne, S.: Warming of hot extremes alleviated by expanding irrigation, Nat. Commun., 11, 290, https://doi.org/10.1038/s41467-019-14075-4, 2020.

Tuinenburg, O. A., Hutjes, R. W. A., Stacke, T., Wiltshire, A., and Lucas-Picher, P.: Effects of Irrigation in India on the Atmospheric Water Budget, J. Hydrometeorol., 15, 1028–1050, https://doi.org/10.1175/JHM-D-13-078.1, 2014.

Valmassoi, A. and Keller, J.: A review on irrigation parameterizations in Earth system models, Frontiers in Water, 4, 906664, https://doi.org/10.3389/frwa.2022.906664, 2022.

Valmassoi, A., Dudhia, J., Di Sabatino, S., and Pilla, F.: Irrigation impact on precipitation during a heatwave event using WRF-ARW: The summer 2015 Po Valley case, Atmos. Res., 241, 104951, https://doi.org/10.1016/j.atmosres.2020.104951, 2020a.

Valmassoi, A., Dudhia, J., Di Sabatino, S., and Pilla, F.: Regional Climate Impacts of Irrigation in Northern Italy Using a High Resolution Model, Atmosphere, 11, 72, https://doi.org/10.3390/atmos11010072, 2020b.

Valmassoi, A., Dudhia, J., Di Sabatino, S., and Pilla, F.: Evaluation of three new surface irrigation parameterizations in the WRF-ARW v3.8.1 model: the Po Valley (Italy) case study, Geosci. Model Dev., 13, 3179–3201, https://doi.org/10.5194/gmd-13-3179-2020, 2020c.

Wilhelm, C., Rechid, D., and Jacob, D.: Interactive coupling of regional atmosphere with biosphere in the new generation regional climate system model REMO-iMOVE, Geosci. Model Dev., 7, 1093–1114, https://doi.org/10.5194/gmd-7-1093-2014, 2014.

Yao, Y., Vanderkelen, I., Lombardozzi, D., Swenson, S., Lawrence, D., Jägermeyr, J., Grant, L., and Thiery, W.: Implementation and Evaluation of Irrigation Techniques in the Community

Land Model, J. Adv. Model. Earth Sy., 14, e2022MS003074, https://doi.org/10.1029/2022MS003074, 2022.

Zucaro, R.: Atlas of Italian Irrigation systems, Tech. rep., Istituto Nazionale di Economia Agraria (INEA), https://sigrian.crea.gov.it/wp-content/uploads/2019/11/Atlas_Italian_irrigation_2014_INEA.pdf (last access: 1 December 2023), 2014.

A.2 Publication II

The role of horizontal resolution in modeling irrigation effects with a coupled regional climate model system up to convection-permitting scale

Christina Pop[1], Jürgen Böhner[2], Peter Hoffmann [1], Joni-Pekka Pietikäinen[1], and Diana Rechid[1]

[1]Climate Service Center Germany (GERICS), Helmholtz-Zentrum Hereon, Hamburg, Germany
[2]Center for Earth System Research and Sustainability (CEN), Universität Hamburg, Hamburg, Germany

Key Points:

- Finer resolved surface features influence modeled irrigation effects, resulting in more localized and distinct effects.
- Coupled model systems capture interactions between irrigation, vegetation, and the atmosphere, resolving feedback mechanisms.
- With explicitly resolved convection, irrigation effects on precipitation differ, showing a reduction over irrigated areas.

Corresponding author: Christina Pop, christina.pop@hereon.de

Abstract

Increasing the resolution of regional climate models up to convection-permitting scales enables explicitly resolved convection and finer resolved surface features. In this work, we use the benefits of the high resolution climate model and apply it to model irrigation effects and feedbacks on the local and regional climate, focusing on the interaction of irrigation with soil, surface, atmosphere, and vegetation processes. We employ the regional climate model REMO2020 interactively coupled to its vegetation module iMOVE and incorporate our newly developed irrigation parameterization. We conduct two simulations sets with and without the irrigation parameterization. In the first set, we employ the hydrostatic model version at 0.11° horizontal resolution for Southwestern Europe. For the second set, we repeat the experiment employing the non-hydrostatic model version at convection-permitting resolution of 0.0275° for Northern Italy. Our results indicate that improved vegetation conditions due irrigation, such as an increased canopy conductance, lead to effects in the atmosphere. For the atmosphere, we find more distinct and localized irrigation effects for the simulations at convection-permitting resolution with enhanced near-surface cooling of up to -2 K compared to the simulations at 0.11°. In the boundary layer, irrigation effects are highly influenced by turbulences, transporting the irrigation effect in higher levels. The largest differences in representing irrigation effects on the two resolutions were found in precipitation. While at 0.11° horizontal resolution, precipitation increases due to favorable convection conditions, explicitly resolving convection leads to rather mixed effects with a decrease of precipitation above irrigated areas, where the convection inhibition increased.

Plain Language Summary

This study investigates irrigation effects and feedbacks on the atmosphere at two different horizontal resolution using the regional climate model REMO. The model is interactively coupled to its vegetation module iMOVE and incorporates the newly developed irrigation parameterization of Asmus et al. (2023). Simulations are conducted covering Northern Italy at 0.11° and at 0.0275° horizontal resolution, latter one explicilty resolving convective processes. Irrigation affects vegetational processes such as the intensity of the canopy conductance, as well as surface fluxes and consequently, the boundary layer of the atmosphere. As the higher resolution resolves surface features with more details, the effects of irrigation in the lower atmosphere, such as temperature reduction in 2 m height, develop more distinct. Boundary layer processes, such as turbulences play an important role in the development of irrigation effects in the atmosphere. Irrigation on precipitation differ between these two resolutions. While at the high resolution with explicitly resolved convection, irrigation leads to a precipitation decrease above the irrigated areas due to convection inhibiting conditions, at the coarse resolution, precipitation increases due to irrigation. However, not above the irrigated areas, but particularly windward at a nearby mountain foot.

1 Introduction

With the advances in regional climate modeling and the growth in computing power, regional climate models (RCMs) achieve a horizontal resolution up to convection-permitting scales (< 4 km) and are able to simulate multiple decades. At such high resolutions, hydrostatic approximation for the dynamics in the RCM is no longer applicable due to the non-negligible acceleration of the vertical velocity, as was the case for coarser resolutions (Prein et al., 2015). The deep convection is computed with a non-hydrostatic dynamic core, eliminating the need for convection parameterizations, which added another source of uncertainty in RCMs (Ban et al., 2014; Fosser et al., 2014; Kendon et al., 2021; Lucas-Picher et al., 2021). The convection-permitting scale explicitly resolves the trigger mechanism of convective updrafts, as well as the upward transport and detrainment of mois-

ture and aerosols into the upper troposphere (Prein et al., 2015). Multiple studies showed that resolving these convective processes improves the precipitation representation in RCMs, such as the diurnal cycle as well as the precipitation intensity in regard of extreme precipitation (Prein et al., 2015; Ban et al., 2021; Cortés-Hernández et al., 2024; Lucas-Picher et al., 2021; Kendon et al., 2021; Knist et al., 2019).

In addition to the effect of resolving convective processes, a higher resolution improves the representation of land surface in terms of topography, land cover classes, and small-scale features such as lakes, rivers and coastlines (Kendon et al., 2021). This is important for areas with complex topography, where atmospheric processes are heavily influenced by elevation, because a higher resolution provides a more detailed representation of the terrain than coarser resolutions. For instance, Heim et al. (2020) analyzed the role of elevation in simulating moist convection in the Alps and found that convection was triggered more frequently at convection-permitting resolution. For flat areas, this means that the representation of land cover and small-scale features can be more precisely resolved. Jiménez-Esteve et al. (2018) and Tölle and Churiulin (2021) investigated the role of land cover and land use in convection-permitting modeling by using different land cover and land use datasets in RCMs and their effects in representing near-surface variables. Both studies revealed that adjusting the land cover, for instance by increasing the resolution or employing a more recent dataset, can improve the simulation results. In the study by Tölle and Churiulin (2021), which employs the RCM COSMO-CLM, the differences between the effects of the different land cover products are lower than the model bias compared to observations. The land-use change experiment employing the RCM WRF by Broucke and Lipzig (2017) showed that the effects of afforestation on surface fluxes are more consistent with observations at convection-permitting than at coarser resolutions. Land-atmosphere interaction with effects on upper levels of the atmosphere were studied by Hohenegger et al. (2009) and Leutwyler et al. (2021), who investigated the soil moisture-precipitation feedback and found an overestimation of the land-atmosphere coupling in convection-parameterized simulations.

The effect of soil moisture changes in combination with land use and irrigation processes has been investigated by multiple modeling studies at different scales. For instance, de Vrese et al. (2016); Thiery et al. (2020); Puma and Cook (2010), and Sacks et al. (2009) explored irrigation effects on global scale showing the regional differences of irrigation effects worldwide as well as remote effects of large-scale irrigation in e.g. India. At the regional level, irrigation effects have been studied by Boucher et al. (2004); Leng et al. (2015); Ozdogan et al. (2010); Saeed et al. (2009); Valmassoi et al. (2019); Asmus et al. (2023) and Udina et al. (2024). These studies showed that increasing the soil moisture modifies the biogeophysical and biochemical properties of the land surface, vegetation, and soil. This modification results in altered energy and water fluxes, influencing land-atmosphere interactions and causing various effects and feedbacks on the local and regional climate. While most of these studies are consistent with the direction of irrigation effects, the intensity and feedbacks with land, atmosphere, and vegetation remain, however, uncertain and depend strongly on the representation of irrigation in the model as well as on the spatio-temporal resolution of the experiment (Valmassoi & Keller, 2022). So far, only few studies investigate irrigation effects at convection-permitting scales. Liu et al. (2023) examined convection initiation in areas with highly heterogeneous land cover along the boundary between irrigated land and desert in Northern China focusing on the air parcels trajectory during convection. Wang et al. (2024) found a decrease of the warm-and-dry bias of the 2 m temperature and relative humidity over the North China Plain in summer in WRF simulations at convection-permitting scale using an irrigation scheme increasing the occurrence frequency, and intensity of mesoscale convective systems,driven by additional atmospheric moisture, despite the suppression of convection due to reduced surface heating. A similar result was further found by Qian et al. (2020), showing the reduction of the precipitation and the warm-and-dry-bias through an increase of mesoscale convective systems in the Contiguous United States. Zhang et al. (2025) employed the WRF model above the Great Plains in the US with groundwater, crop growth, and ir-

rigation processes, showing a reduced temperature and precipitation bias in convection-permitting simulations, resulting from an increase in precipitation recycling when irrigation is activated. For the Po Valley, Valmassoi et al. (2020b) showed an improved representation of precipitation in the Po Valley by applying irrigation in convection-permitting simulations with WRF. Udina et al. (2024) employed the irrigation parameterization of Valmassoi et al. (2019) and investigated boundary layer processes during the LIAISE campaign in the Ebro Basin, Spain Their study found contrasting effects of irrigation on precipitation when using convection-permitting simulations or employing the convection parameterization. Interactive vegetation processes and their feedback with the atmosphere are rarely included in studies at convection-permitting scale. One example is Vanden Broucke and Van Lipzig (2017), who investigated the effects of deforestation and showed a reduced bias in in the incoming shortwave radiation and the sensible heat flux when applying the experiment at convection-permitting scale. Halladay et al. (2024) analyzed different surface and atmosphere improvements, such as an increased moisture availability from groundwater or in canopies to reduce the warm and dry bias in convection-permitting simulations over Europe.

The present study aims to investigate the representation of irrigation effects on convection-parameterized and convection-permitting scales using the RCM REMO2020-iMOVE, considering the interactions between soil, atmosphere and vegetation. We employ the irrigation parameterization with the same settings as described in Asmus et al. (2023) and examine the effects of irrigation on the land-atmosphere interaction at both resolutions, as well as on variables known to be sensitive to convection-permitting scales such as precipitation. The Po Valley was chosen as model domain because it is one of the most intensely irrigated regions in Europe. Additionally, its proximity to the mountainous Alps region allows us to take advantage of the high resolution in the convection-permitting simulations. The remainder of the paper is organized as follows: Section 2 describes the model and data used; section 2. The differences of the simulations caused explicitly by the resolution are examined in section 3.1, and the associated irrigation effects in section 3.2. Section 4 examines our findings, and Section 5 wraps them up.

2 Materials and methods

2.1 REMO2020-iMOVE with irrigation module

In this work, we employ the REgional climate MOdel REMO2020 (Pietikäinen et al., n.d.). REMO, originally based on a hydrostatic core, received a non-hydrostatic extension enabling the resolution of convective processes (Goettel, 2009) (REMO-nh). Therefore, REMO is applicable in both hydrostatic and non-hydrostatic configurations. In the hydrostatic configuration, cumulus convection is parameterized using the Tiedtke scheme (Tiedtke, 1989) and its modifications by Nordeng (1994). Tiedtke (1989) uses the mass flux approach and considers shallow, penetrative, and mid-level convection. However, this approach uses highly simplified cloud microphysics and multiple assumptions (Tiedtke, 1989). For the non-hydrostatic configuration, which implies very high resolutions for REMO (< 4 km), the vertical velocity is explicitly resolved enabling the development of convection in the model (Goettel, 2009). REMO is interactively coupled to the lake module FLake (Pietikäinen et al., 2018), and to its mosaic-based vegetation module iMOVE (Wilhelm et al., 2014). iMOVE is based on the dynamic land surface model JSBACH (Jena Scheme for Biosphere Atmosphere Coupling in Hamburg) (Reick et al., 2021) and represents plants' phenology in interaction with soil and atmospheric processes for 16 plant functional types (PFT) (Wilhelm et al., 2014). The variables driving the coupling process are the canopy conductance, the albedo, and vegetation ratio of one grid cell. Together with a PFT-specific surface roughness length, the vegetation is able to react to the conditions of air temperature, radiation, humidity and CO_2 in the atmosphere, as well as to soil moisture. A more detailed description of the coupling processes important for this study can be found in the Appendix A. The first employment of REMO-iMOVE is described in Wilhelm et al.

(2014). The PFT distribution is based on the European Space Agency Climate Change Initiative Land Cover (ESA CCI LC) (ESA, 2017) and aggregated to the LAND surface modifications and its feedbacks on local and regional cliMATE PFTs (LANDMATE PFTs) (Reinhart et al., 2022)) considering the land use and land cover change in the year 2017 of the Land Use and Climate Across Scales Land Use Change (LUCAS LUC) dataset by Hoffmann et al. (2023). Furthermore, we use the irrigation parameterization developed by (Asmus et al., 2023). The irrigation parameterization uses the "area equipped for irrigation" from Siebert et al. (2013) on which basis it creates a separate, subgrid irrigated fraction of the model grid cell. Considering a subgrid irrigated fraction, represented with separate land surface and soil processes such as heat and moisture fluxes, enables the analysis of distinct irrigation effects on the atmosphere and enhances the subgrid heterogeneity of the land surface. This approach aids applying irrigation exclusively to the irrigated fraction of grid cells with soil moisture lower than the irrigation threshold. The irrigation parameterization consists of different water application schemes. The adaptive water application scheme used in this study increases the soil moisture within the irrigation duration until the irrigation target is reached. A detailed description of the irrigation process in REMO2020-iMOVE can be found in Asmus et al. (2023). At higher resolutions, grid cells tend to exhibit a larger fraction of a single land cover type. Therefore, to use the irrigation parameterization at high resolution, adjustments were required in the data preparation. We interpolated the irrigation map from GMIA to our model domain and integrated it in the PFT distribution. Here, we tested for not exhibiting the original cropland fraction nor the land fraction by including the irrigated fraction.

2.2 Experiment setup

The setup of all simulations is described in Table 1. Our simulations cover the summer of 2017, which was characterized by multiple heat waves during the summer months (JJA) in southern Europe (Copernicus Climate Change Service, 2022). We conduct two sets of simulations with and without irrigation parameterization (Table 1). For the first set, we employ REMO2020-iMOVE in its hydrostatic configuration at 0.11° over Southwestern Europe (S11_irri, S11_noirri, Figure 1a). The convection parameterizations are activated. In this case, ERA5 is used as forcing data on 49 pressure levels including balanced soil parameters from a previous REMO simulation. This procedure ("warm start") eliminates the spin-up time of the soil parameters (Pietikäinen et al., 2018). For the second set of simulations, we employ REMO2020-iMOVE in its non-hydrostatic configuration at 0.0275° (S0275_irri, S0275_noirri). The convection parameterizations are deactivated. Due to the high computational coast of non-hydrostatic simulations, we reduce our model domain covering the Po Valley and surrounding areas (D0275, Figure 1). The simulations at 0.0275° are nested in the simulations at 0.11° to prevent a large resolution jump on the borders. With this nesting method, our jump in resolution for S11 to S0275 is a factor of four. For the analysis region of the Po Valley, we follow Dominic et al. (2017) and consider the minimum spatial spin-up zone. As irrigation effect, we define the difference between the simulation with the irrigation parameterization activated (S11_irri, S0275_irri) and the simulation with the same settings but with the irrigation parameterization deactivated (S11_noirri, S0275_noirri). In the irrigated simulations we apply the irrigation parameterization with the "adaptive water application scheme" (Asmus et al., 2023). We use the same irrigation setup as in Asmus et al. (2023) and set the irrigation duration to ten hours and the irrigation target as well as the irrigation threshold to the maximal water-holding capacity, resulting in daily irrigation during the growing season. The irrigation process is integrated in the growing season (Asmus et al., 2023). As in JSBACH (Reick et al., 2021), the growing season in the northern hemisphere starts for cropland on 11th of March (10th of March in leap years) in REMO2020-iMOVE and ends in September.

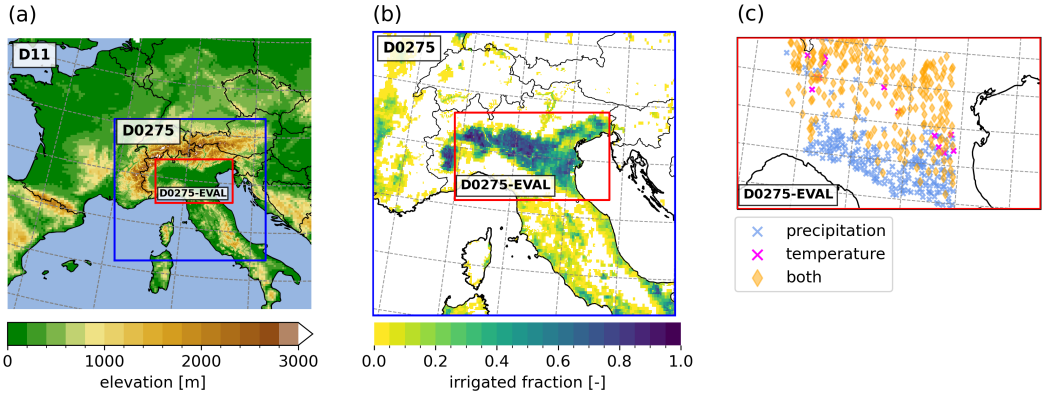

Figure 1. a) Orography in double nesting approach of model domains for simulations on 0.11° (D11), on 0.0275° (D0275), as well as the evaluation domain D0275-EVAL, b) interpolated irrigated fraction with data from GMIA (Siebert et al., 2013) in D0275 and station locations measuring precipitation, temperature or both in the evaluation domain D0275-EVAL.

Table 1. Simulation settings.*The soil variables were initialized with soil variables in equilibrium from a previous, long-term (> 10 years) REMO run, a procedure known as "warm start" (Pietikäinen et al., 2018).

name	model version	res.	domain with grid cells	sim. period	boundary data	initial condition	irrigation	convection setting
S11_irri	REMO 2020-iMOVE	0.11°	D11 145x129	01/01/-31/12/	ERA5	ERA5*	on	parameterized
S11_noirri	REMO 2020-iMOVE	0.11°	D11 145x129	01/01/-31/12/	ERA5	ERA5*	off	parameterized
S0275_irri	REMO 2020-nh-iMOVE	0.0275°	D0275 289x271	01/01/-31/12/	S11_noirri	S11_noirri	on	explicitly resolved
S0275_noirri	REMO 2020-nh-iMOVE	0.0275°	D0275 289x271	01/01/-31/12/	S11_noirri	S11_noirri	off	explicitly resolved

2.3 Observation data

In Italy, data from observational stations is collected by the Regional Agency for the Protection of the Environment (ARPA, Italian: Agenzia Regionale per la Protezione Ambientale) on the federal level. We use data, which is located in D0275_EVAL (Figure 1c), from the regions Emilia-Romagna (ARPA Emilia-Romagna, 2023), Lombardia (ARPA Lombardia, 2023a, 2023b), and Veneto (ARPAV Veneto, 2023) for the variables 2 m mean temperature and hourly precipitation. D0275_EVAL covers the Po Valley, which is characterized by clusters of high fractions of irrigated areas (Figure 1b). Since we are investigating local and regional irrigation effects, stations located in grid cells with-

out irrigated fractions are also included. After checking for continuous data during the irrigated period from March 2017 - July 2017 (MAMJJ), we include 728 stations (Figure 1c) in total. Most stations measure both 2 m mean temperature and precipitation data, although it should be noted that some stations record only one variable. Using inverse-distance interpolation, we interpolate the simulation data to the station locations to evaluate our model results.

3 Results

For analyzing the representation of the land surface at different resolutions, we focus on the D0275 domain to include the effect in mountainous areas such as the Alps. For comparing the representation of local irrigation effects, we focus on D0275-EVAL, as D0275-EVAL encompasses the largest continuous area of grid cells with irrigated fractions (Figure 1), and thereby increasing the likelihood of the emergence of distinct irrigation effects. D0275_EVAL is further the area, in which the stations are located for evaluating the 2 m hourly mean temperature and precipitation. In order to obtain a distinct signal of the irrigation effects in both resolutions, we extract specific grid cells with high irrigated fractions and the LAI in growing state, ensuring irrigation was applied. For this extraction, we firstly interpolate the grid of D11 to the grid of D0275, respectively D0275-EVAL by using nearest neighbor interpolation, resulting in the same number of grid cells in both domains. Secondly, we extract grid cells according to the irrigated fraction of D0275 in both simulations sets (D0275 and interpolated D11), ensuring comparable distributions by selecting identical grid cells.

3.1 Effects of higher resolution and explicitly resolved convection

3.1.1 Distributions

Representing the land surface at different resolutions affects among others, the distribution of elevation values and irrigated fractions (Figure 2a and b). The higher resolution of 0.0275° facilitates a more precise representation of mountainous terrain. In our experiments, the difference between the coarse (0.11°) horizontal resolution and the high resolution (0.0275°) of convection permitting scale is present particularly in the altitudes above 2600 m (Figure 2a). This resolution-dependent phenomenon is also evident in the distribution of irrigated fractions, with a greater number of grid cells at 0.0275° exhibiting irrigated fractions higher than 0.75 compared to those at 0.11° resolution, since the grid cells cover a smaller area at 0.0275° resolution (Figure 2b).
The different distribution of the hourly 2 m mean temperature and precipitation values are additionally to the higher resolution influenced by the explicitly resolved convection treatment in our high-resolution simulations at 0.0275°. The distributions include values from the simulations during the irrigated months MAMJJ. The 2 m temperature distribution shows an overall good fit with the observation data (Figure 2c) from the ARPA stations (section 2.3). However, the model overestimates the frequency of higher temperature values (> 35 °C), in particular in the simulations without irrigation and at 0.0275° resolution. When comparing the irrigated with the non-irrigated simulations, it becomes evident that regardless of the horizontal resolution, the temperature distributions of the irrigated simulations result in fewer values above 30 °C. The distribution of precipitation values is logarithmically decreasing with intensity (Figure 2d). Except for low-intensity values below 2.5 mmh^{-1} the precipitation values are underestimated by the model at both resolutions compared to the observation data. However, it should be noted that the observational data represents point measurements of precipitation, while the modeled data shows grid cells. This mismatch leads to the strong underestimation of hourly precipitation rates in all simulations. The precipitation in simulations at 0.0275° horizontal resolution results in higher hourly values exceeding 2.5 mmh^{-1} than in simulations at 0.11°,

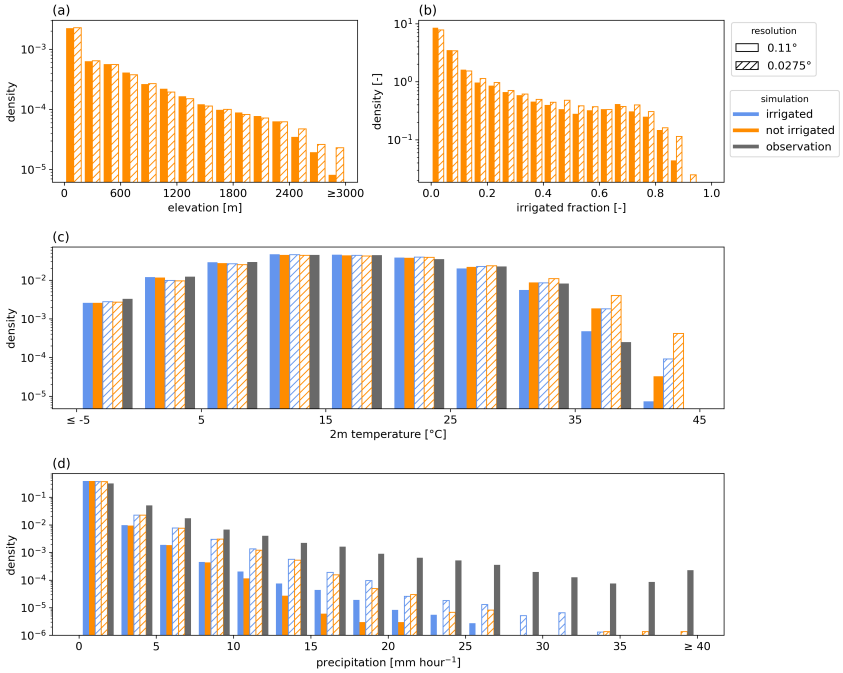

Figure 2. Normalized histograms of (a) elevation in D0275 and (b) irrigated fraction in D0275, and hourly values of (c) 2 m mean temperature in D0275-EVAL and (d) precipitation in D0275-EVAL for the simulation results and the observations at the station location. Significance was tested with Wilcoxon Sign-rank test for significant differences between irrigated and not irrigated distributions with respect to their resolution, as well as for 0.0275° resolution and 0.11° resolution with respect to the irrigation treatment. All tests found the differences between the distributions significant at a 5% significance level.

irrespective of the presence of irrigation. Consequently, precipitation at 0.0275° aligns more closely with observational data. In particular, heavy precipitation with values above 27.5 mmh^{-1} is captured exclusively at 0.0275° horizontal resolution. Comparing irrigated against not irrigated simulations, the irrigated simulations at 0.11° horizontal resolution exhibit higher precipitation rates exceeding 7.5 mm h^{-1}, with values up to 27.5 mm h^{-1}. At 0.0275 horizontal resolution, the differences between the irrigated and not irrigated simulation are less pronounced than at 0.11°. However, in the simulation at 0.0275° horizontal resolution, irrigation contributes to higher precipitation exceeding 17.5 mmh^{-1}. Interestingly, the highest precipitation values ($\geq$ 40 mmh^{-1}) are represented by the non-irrigated simulation at 0.0275° horizontal resolution.

3.1.2 Diurnal Cycle

In comparison to the observational station data, the mean diurnal cycle of the 2 m temperature is represented well (Figure 3a) by the simulations during MAMJJ. All simulations show a warm bias from midnight to 11:00 LT. Particularly, the simulations at 0.0275° horizontal resolution with the non-hydrostatic model version suffer from the highest warm bias in the not irrigated simulations and show overall higher temperatures than their corresponding simulations at 0.11° horizontal resolution. The warmer bias at convection-permitting scale might result from smaller-scale cloud cover leading to increased radiation. A similar warmer bias in the same area in summer was also found by Ban et al.

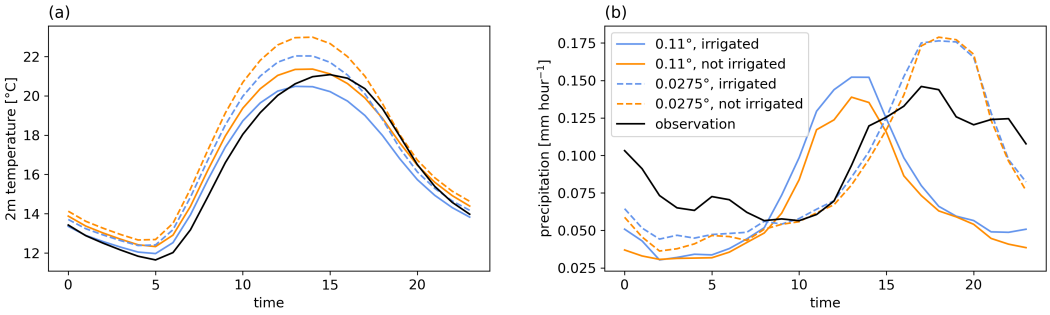

Figure 3. Diurnal cycle for simulations results at different resolutions and observational data in D0275-EVAL for (a) 2 m temperature and (b) precipitation during MAMJJ at the station locations.

(2014) when comparing simulations with convection parameterizations and explicitly resolved convection. Further, Halladay et al. (2024) described a warm and dry bias in convection-permitting simulations, which might be related to deficit in moisture availability from soil and vegetation. Both irrigated simulations reduce the temperature and decrease the warm bias in the first part of the day. However, at 0.11° horizontal resolution the temperature reduction by irrigation turns into the coldest bias from noon compared to the observational values. The timing of the observed maximum temperature at 15:00 LT is not matched by any simulations, which reach their peak at 13:00 LT. A detailed analysis of irrigation effects on the diurnal 2 m temperatures can be found in Section 3.2.2. In general, the not irrigated simulation at 0.11° horizontal resolution aligns the most with the observational data.

The mean diurnal cycle of precipitation in MAMJJ shows large differences between both simulations at 0.11° and 0.0275° resolutions, as well as when compared to observations (Figure 3b). In the simulations at 0.11° horizontal resolution, the diurnal cycle of precipitation peaks at noon with an intensity of 0.135 mmh^{-1} for the non-irrigated simulation and 0.15 mmh^{-1} for the irrigated simulation. These values closely match the observational peak intensity of 0.145 mm h^{-1}, although the observed peak occurs later in the afternoon, at 16:00 LT. This timing is captured better by the simulations at 0.0275° horizontal resolution with explicitly resolved convection, although they overestimate the peak of precipitation, regardless of the irrigation. During nighttime, all simulations underestimate precipitation. As in Figure 2d, the irrigated simulation at 0.11° horizontal resolution results in higher precipitation values than the non-irrigated simulation. At 0.0275° horizontal resolution, irrigation enhances slightly precipitation from midnight until the precipitation peak at 16:00 LT. During the peak, both simulations show a similar precipitation intensity, followed by a comparable decline thereafter. For precipitation, the simulations at 0.0275° horizontal resolution can be summarized as the best representation of the diurnal cycle of precipitation.

Irrigation increases soil moisture and, consequently, influences the surface energy balance. The mean diurnal cycle of the irrigated surface energy balance for irrigated grid cells with an irrigation fraction above 70% (based on the grid cell extraction in D0275) develops similarly in the simulations at 0.11° and 0.0275° horizontal resolution (Figure 4). In the irrigated simulations the turbulent sensible heat flux Qh) and the turbulent latent heat flux (Qe) as well as the net radiation (Rn) and the ground heat flux (G) calculated as residuum are slightly higher at 0.0275° resolution than at 0.11°, with maximum values reached at 13:00 LT. The latent heat flux is the dominant component in the surface energy balance (Figure 4a and b). The irrigation effects on the surface energy balance develop during the irrigation hours from 7:00 LT to 17:00 LT (Figure 4c). The

strongest irrigation effects on the turbulent heat fluxes develop around 13:00 LT, following the diurnal cycle of the surface energy balance. Irrigation leads to an increase of the latent heat flux by up to +190 Wm^{-2} at 0.11° and +200 Wm^{-2} at 0.0275° horizontal resolution caused by the increased soil moisture. Simultaneously, the sensible heat flux decreases by up to -120 Wm^{-2} at 0.11° and -150 Wm^{-2} at 0.0275° caused by lower surface temperatures. The reduction of the sensible heat flux through irrigation reaches negative values in the afternoon, a pattern usually occurring in the evening and nighttime, when the surface cools more intensely than the near-surface air temperature resulting in a reversed sensible heat flux. In the irrigated simulations at both resolutions, this feature occurs in the afternoon from 16:00 LT, likely associated with the strong cooling effect of irrigation on the surface temperatures. Irrigation decreases the ground heat flux until 14:00 LT indicating a smaller temperature gradient between the surface and deeper soil layers in the irrigated simulations than in the not irrigated simulations, as the the increased latent and decreased sensible heat flux lead to a less strong heating of the surface from radiation. The not-irrigated simulations show a larger, but faster decreasing ground heat flux towards the afternoon and evening hours. This follows the change in sign of the irrigation effect on the ground heat flux at 14:00 LT. From this moment, the irrigated simulations show a larger energy flux from the surface to the deeper soil layers than the not irrigated simulations, indicating a larger temperature gradient between the surface and deeper soil layers. Further, this can be linked to the delayed cooling effect of irrigation in deeper soil layers (Asmus et al., 2023). The effects of irrigation on the net radiation are rather small compared to the components of the surface energy balance. They are characterized by an increase by up to +20 Wm^{-2} during the irrigation hours at both resolutions. Comparing the two different resolutions reveal stronger irrigation effects on the turbulent heat fluxes, which are likely the result of the higher temperatures at the convection-permitting scale. However, it can be stated that the differences between the resolutions are small compared to the large differences between irrigated and not-irrigated simulations in our experiments.

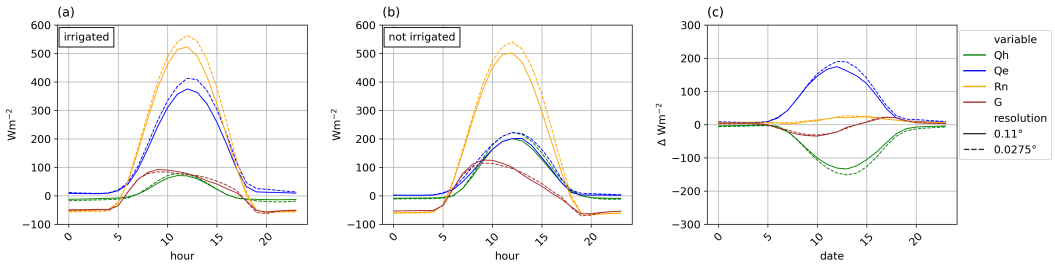

Figure 4. Mean diurnal surface energy balance of irrigated grid cells with irrigation fraction > 70% (based on the grid cell extraction in D0275) at 0.11° and 0.0275° resolution represented through turbulent sensible heat flux (Qh), turbulent latent heat flux (Qe), net-radiation (Rn) and ground heat flux (G) for a) irrigated simulations, b) non-irrigated simulations, c) difference between irrigated and non-irrigated simulations.

3.2 Representation of irrigation effects on different scales

3.2.1 Development of irrigation effects in a coupled soil-vegetation-atmosphere system

The interactive coupling of soil, vegetation and atmosphere processes enables the investigation of irrigation effects and feedbacks between these components of the regional cli-

mate system. For soil, vegetation, and surface variables, we investigate the impact of irrigation effects in the irrigated subgrid tiles. In this work, the authors refer to "relative soil moisture" as the fraction of the soil moisture of the maximum water holding capacity. This definition can be understood as filled proportion of the soil moisture bucket scheme used by REM2020-iMOVE (Section 2). A detailed description of the coupling of soil, vegetation and atmospheric processes can be found in Wilhelm et al. (2014), as well as in the Appendix A.

In our study irrigation is carried out mainly from mid of March until mid of July, when the harvest event occurs in our analysis region D0275. The irrigation settings result in daily irrigation and increase the soil moisture to the maximal water-holing capacity. In the non-irrigated simulations, the relative soil moisture decreases during the summer months reaching the lowest level of 0.4 in July, which marks the month with the highest differences in relative soil moisture between the irrigated and the non-irrigated simulations for both resolutions (Figure 5a and b). The increase of soil moisture in the irrigated simulations prevents cropland from water stress. This effect is evident in the response of the canopy conductance (Figure5c and d), which plays a key role in linking soil moisture with the development of vegetation (Appendix A) in REMO2020-iMOVE. The canopy conductance describes the opening of the stomata of leaves in a canopy and, therefore, drives the exchange of CO_2 and water vapor during the photosynthesis process. Under water stress, the canopy conductance reduces its opening, leading to less efficient photosynthesis. In REMO2020-iMOVE this process is calculated with the BETHY approach (Knorr, 1997) and the Farquhar model (Farquhar et al., 1980), which scales the canopy conductance under no water stress with the state of soil moisture (Appendix A, equation A2 and A3). The canopy conductance increases with irrigation (Figure 5c and d), as well as with the LAI (Figure 5i and j). Therefore, the irrigation effects on vegetational variables increase in the summer months until the end of the growing season. The canopy conductance is further dependent on the shortwave incoming radiation (Figure 5e), which drives the absorbed photosynthetically active radiation. The correlation of soil moisture changes and the changes in canopy conductance result in a Spearman's rank correlation coefficient ρ between 0.65 and 0.99 dependent on the month, or more precisely on the vegetation's state (Figure 6a-e). The correlation is very similar at both resolutions. The canopy conductance plays an important role in the photosynthesis process, which further produces the net primary production (NPP). While in March and April NPP is slightly smaller in the irrigated simulations compared to the non-irrigated simulations, it increases in the irrigated simulations in June by up to 12 $gCm^{-2}d^{-1}$ (Figure 5g and h). In addition, the correlation of the changes of soil moisture and NPP reaches the maximum of 1.0 in June (Figure 6i). The developments of the LAI are directly affected by the NPP, the soil moisture, and by a heat sum computed from the 2 m temperature, starting from the first of January each year. Similar to the NPP, the LAI is smaller values in the irrigated simulations compared to the non-irrigated simulations in March and April (Figure 5). This can be explained by the decrease of temperature caused by irrigation, which decreases the temperature sum, and therefore, slows down the LAI growth in the irrigated simulations (Appendix A). The soil moisture and LAI changes correlate with 0.48 at 0.11° resolution, and 0.84 at 0.0275° resolution in March. The higher correlation at 0.0275° resolution, as well as the slightly faster growth of the LAI in March and April in simulations at 0.0275° than in the simulations at 0.11° (Figure 5i) is most likely caused by the slightly higher temperatures in the simulations at 0.0275°. The calculation of the LAI as a temperature sum follows, that higher temperatures cause an earlier harvest in the model as presented in Figure 5i. Consequently, the irrigation effects on the LAI show not only an extended growing season and delayed harvest (Figure 5i and j), the increase of soil moisture and its positive effects on the stomatal conductance and NPP lead to a higher LAI maximum in the irrigated simulations for both resolutions - at 0.0275° resolution the LAI increases by up to +2.0 m^2m^{-2} at the 10 July, and at 0.11° resolution, one day later, with +1.6 m^2m^{-2}. The negative values in the end of July occur in grid cells, which show a higher LAI in the non-irrigated simulations than in the irrigated simula-

tions. This effect appears e.g. in grid cells where the LAI of cropland in the irrigated simulations is declining due to harvest, but not yet in the not irrigated simulation. This feature leads to the low correlation for July between the soil moisture changes and LAI changes (Figure 6o).

The impact of irrigation on vegetation processes is largly determined by the harvest event, which does not only stop the irrigation process, it also stopped NPP production and the LAI is declining. Consequently, the correlation with soil moisture changes decreases (Figure 6). The differences in the vegetation processes between both resolutions are rather small and mainly linked to the differences in the state of the atmosphere between both resolutions, such as slightly higher temperatures in the 0.0275° horizontal resolution.

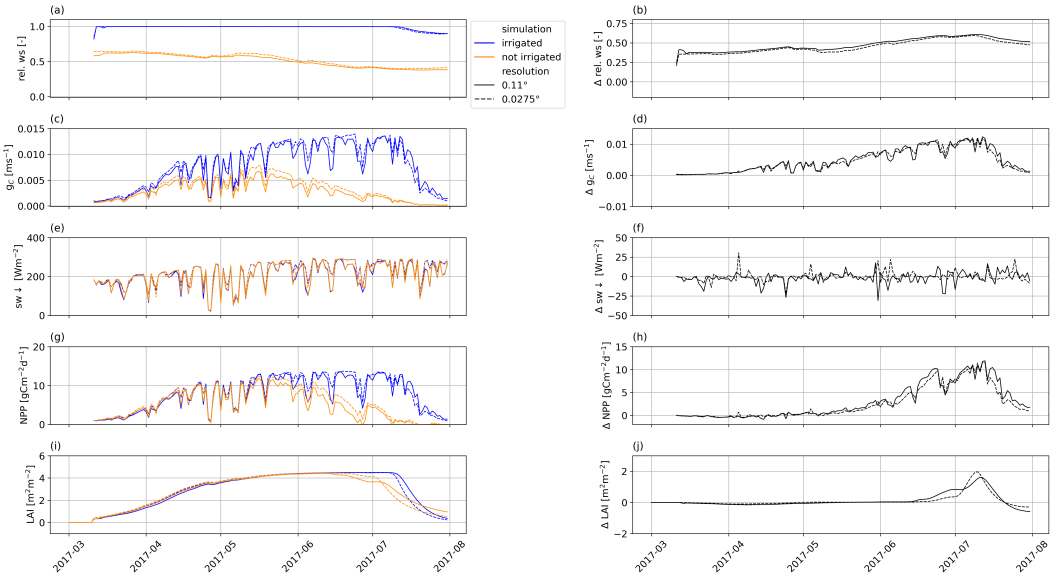

Figure 5. Timeseries of daily mean values during the growing season for a and b) relative soil moisture ($rel.ws$) of the irrigated fraction, c and d) canopy conductance (g_C) of the irrigated fraction, e and f) the shortwave radiation $sw\downarrow$, g and h) NPP of the irrigated fraction, and, i and j) LAI of the irrigated fraction. The left column shows the absolute values of the variable, while the right column presents the irrigation effect, as differences between the irrigated and non-irrigated simulations at both resolutions. Significance was tested with Wilcoxon sign-rank test for significant differences between irrigated and not irrigated distributions with respect to their resolution, as well as for 0.0275° resolution and 0.11° resolution with respect to the irrigation treatment. All tests found the differences between the distributions significant at a 5% significance level, except for $sw\downarrow$, and LAI, when comparing irrigated against not irrigated results.

For linking the irrigation effects on the vegetation to the atmospheric processes, we investigate a subset of meteorological variables (Figure 7). We select evapotranspiration, 2 m mean temperature (T2Mean), and 2 m relative humidity in irrigated grid cells with an irrigated fraction larger than 70% based on the grid cell extraction in D0275 and with the vegetation in growing state (LAI > 0.1). This extraction aims for a clearer representation of distinct irrigation effects in grid cells with active irrigation. Overall, the meteorological conditions in both resolutions are very similar. At both resolutions, irrigation increases evapotranspiration (Figure 7a and b) through the increase of soil moisture. In our coupled model system, the evapotranspiration is additionally driven by the dynamic canopy conductance. This linkage can explain the decrease of evapotranspiration in June and July in the not irrigated simulations (Figure 5c). The effects of irriga-

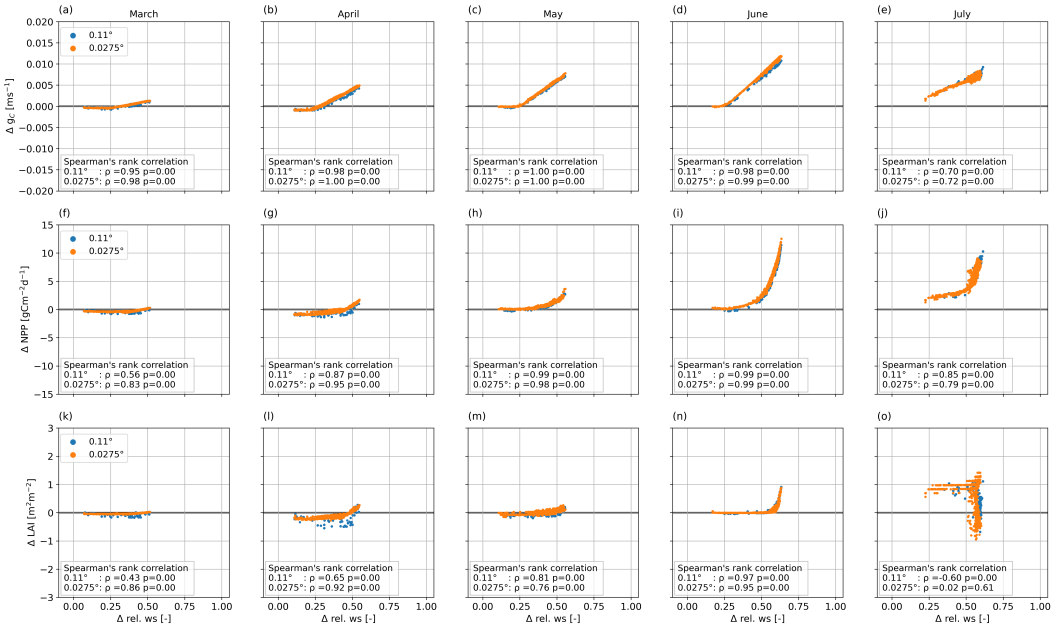

Figure 6. Correlation between irrigation effects of soil moisture and a - e) canopy conductance (g_C, f - j) NPP, and, k - p) LAI. The values are calculated as monthly means of daily values.

tion on evapotranspiration are similar at both resolutions and increase with higher temperatures, with a slightly larger effect on evapotranspiration rates at 0.0275° during the summer months (Figure 7d). Irrigation increases evapotranspiration by up to +6.5 mmday^{-1} at 0.11° and by up to +6.7 mmday^{-1} at 0.0275° resolution, with both maxima occurring in July, the warmest month with activated irrigation. Through land-atmosphere interaction, the changes in the surface fluxes with the reduced sensible heat flux and the increased latent heat flux and evapotranspiration lead to effects on the 2 m temperatures. Irrigation decreases T2Mean and prevents values exceeding 30 °C, which appear exclusively in the non-irrigated simulations in June and July. The irrigation effect is the strongest in July, towards the end of the growing season in both resolutions. The largest temperature reduction through irrigation reaches -4.0 K at 0.11° horizontal resolution and -4.38 K at 0.0275°, based on the spatial mean in grid cells with the irrigated fraction larger than 70% (based on the grid cell extraction in D0275) and the vegetation in growing state. In addition to the 2 m temperature, the increased evapotranspiration from irrigation affects the moisture content in the atmosphere. We calculate the relative humidity using the inverse Magnus formula (Magnus, 1844; Alduchov & Eskridge, 1996). The relative humidity shows lower values in the 0.0275° simulations than in the 0.11° simulations for both non-irrigated and irrigated simulations (Figure 7e). With the increasing temperature in summer (June and July), the relative humidity decreases in both resolutions, especially for the non-irrigated simulations. The effects of irrigation on relative humidity are the largest with the beginning of irrigation in March (Figure 7f), reaching an increases by up to +41% at 0.11° resolution and by up to +38% at 0.0275° resolution.

3.2.2 Irrigation effects on diurnal temperatures

For analyzing the effect on the diurnal temperature range, we selected June as it is the month with continuous irrigation and well-pronounced irrigation effects (section 3.2.1).

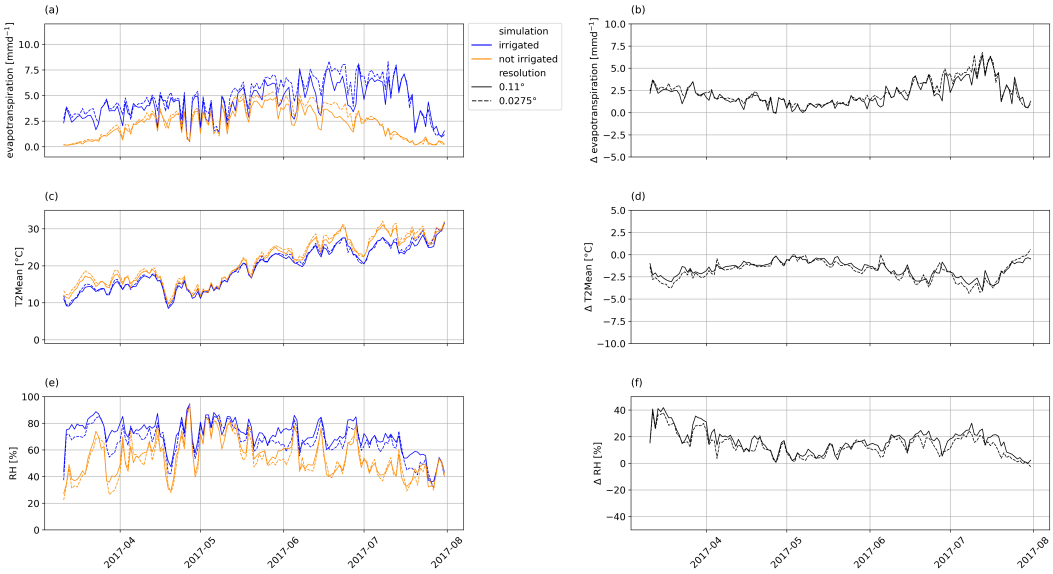

Figure 7. Timeseries daily mean values of grid cells with an irrigated fraction larger than 70% (based on the grid cell extraction in D0275) for a and b) evapotranspiration of the irrigated fraction, c and d) of T2Mean, and e and f) relative humidity in 2 m height. The left column shows the absolute values of the variable, while the right column presents the irrigation effect, as differences between the irrigated and non-irrigated simulations at both resolutions. Significance was tested with the Wilcoxon Sign-Rank test for significant differences between irrigated and not irrigated distributions with respect to their resolution, as well as for 0.0275° resolution and 0.11° resolution with respect to the irrigation treatment. All tests found the differences between the distributions significant at a 5% significance level.

For this analysis, we use the same extracted grid cells as in section 3.2.1. For the spatial average, we extract all values with an irrigation fraction exceeding 0.7 (based on the grid cell extraction in D0275) in order to differentiate and isolate the irrigation effect. We further use grid cells with vegetation in growing state. In Figure 8a, the irrigation effect on maximum temperature T2Max and minimum temperature T2Min as well as at daily mean temperature T2Mean is shown. In general, the effects exhibit a larger spread at 0.0275° resolution. The cooling effect is most pronounced for T2Max at both resolutions. At 0.0275° resolution, the majority of irrigation effects range from -1.6 K (5th percentile) to -6.5 K (95th percentile) with extreme outliers exceeding -10 K. At 0.11° resolution, the irrigation effect ranges from -0.9 K (5th percentile) to -5.1 K (95th percentile). For T2Mean, the irrigation effects are less pronounced than for T2Max. Again, at 0.0275°, the irrigation effects show a wider spread and stronger cooling effect compared to the 0.11° resolution. At 0.0275°, the cooling effect ranges from -0.4 K (95th percentile) to -3.8 K (5th percentile), while at 0.11° resolution, the irrigation effects predominatly spread from -0.6 K to -3.7 K. For T2Min, the cooling effect is least pronounced. At both resolution, the effects develop similarly, ranging from +0.5 K to -2.6 K at 0.11° and from +1 K to 2.1 K at 0.0275° resolution. It should be noted that for both resolutions, the irrigation effect on T2Min can develop as a warming effect, likely associated with the higher moisture content in the near-surface atmosphere. In this case, water vapor acts as a greenhouse gas absorbing longwave radiation from the surface, which can reverse the heat fluxes during nighttime. Another possible explanation was found by Chen and Jeong (2018) who attributed higher T2Min values in irrigated simulations with the higher soil moisture and an increased energy stored in the soil. In our simulations, an increase in tem-

perature values is also observed in the outliers of T2Max and T2Mean, although, they originate most likely from model internal variability and short-term, local effects. The intensity of the irrigation effects on the diurnal temperatures is correlated with the irrigation fraction (Figure 8b-d). The highest correlation can be found for T2Max with a Pearson's correlation coefficient (r) of 0.9 at 0.11° horizontal resolution and 0.85 at 0.0275° resolution. A lower correlation is found for the irrigation effect at T2Min, implying a smaller influence of the irrigation fraction on the T2Min effect. In general, the correlations are weaker for the simulations at 0.0275° horizontal resolution as the effects show a larger spread. The spatial distribution of irrigation effects at both horizontal resolutions for

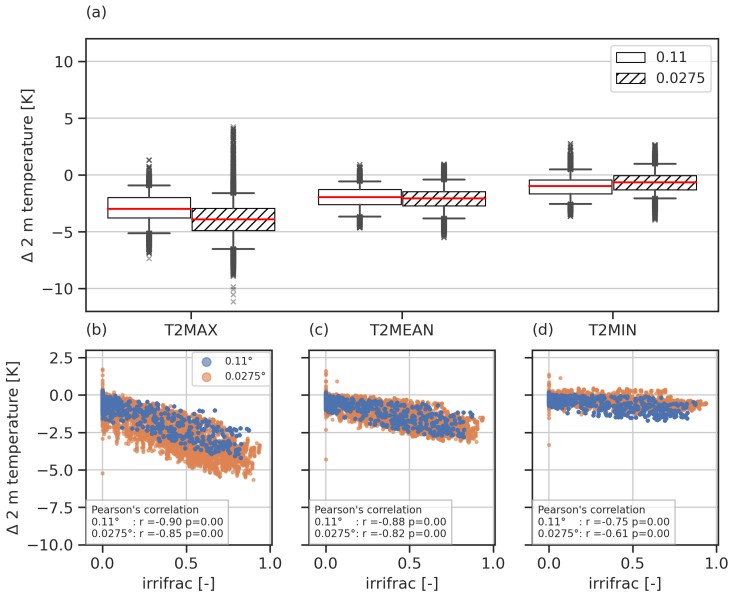

Figure 8. Irrigation effects on 2 m temperatures as a) boxplots of irrigation effect as the difference between the simulations with irrigation and the simulations without irrigation on 2 m temperature values during June at 0.11° and 0.0275° horizontal resolution averaged for grid cells with an irrigated fraction larger than 70% (based on the grid cell extraction in D0275). Whiskers indicate the 5th and 95th percentile, x indicates outliers, red line is the median, b) shows the correlation of the 2 m temperatures with the irrigated fraction at both resolutions. Significance was tested with a Wilcoxon-Sign-Rank test and found the differences for the distributions of irrigation effects on T2Max, T2Mean and T2Min of the different resolutions significant at a 5% significance level.

D0275-EVAL is shown in Figure 9. As in Figure 8, it is evident that the irrigation effects on T2Max and T2Mean are more pronounced at 0.0275° horizontal resolution than at 0.11° (Figure 9). For T2Max, the irrigation effects differ particularly in the northwest and west of the Po Valley, where they reach -5.7 K in single grid cells at 0.0275° and -4.2 K at 0.11°. This is where grid cells show a larger irrigated fraction at 0.0275° than at 0.11° (Figure 9c). However, in the north-eastern part of the Po Valley a larger irrigated fraction does not lead to stronger pronounced effects on the T2Max, indicating the dominance of other processes (Section 3.2.3). For T2Mean, the irrigation effects at 0.0275° horizontal resolution reaches -4.3 K in grid cells in the northwest and west of the Po Valley, where they cause a slightly stronger cooling than at 0.11°. However, for T2Min, the cooling due to irrigation at 0.0275° is less pronounced than at 0.11° resolution, particularly in the southern part of the Po Valley. In the simulations at 0.11°, the cooling ef-

fect on T2Min is stronger by -1.29 K than in the simulations at 0.0275°. Also, at 0.11° horizontal resolution, a larger area is affected by the cooling, while at 0.0275° less grid cells show an irrigation effect.

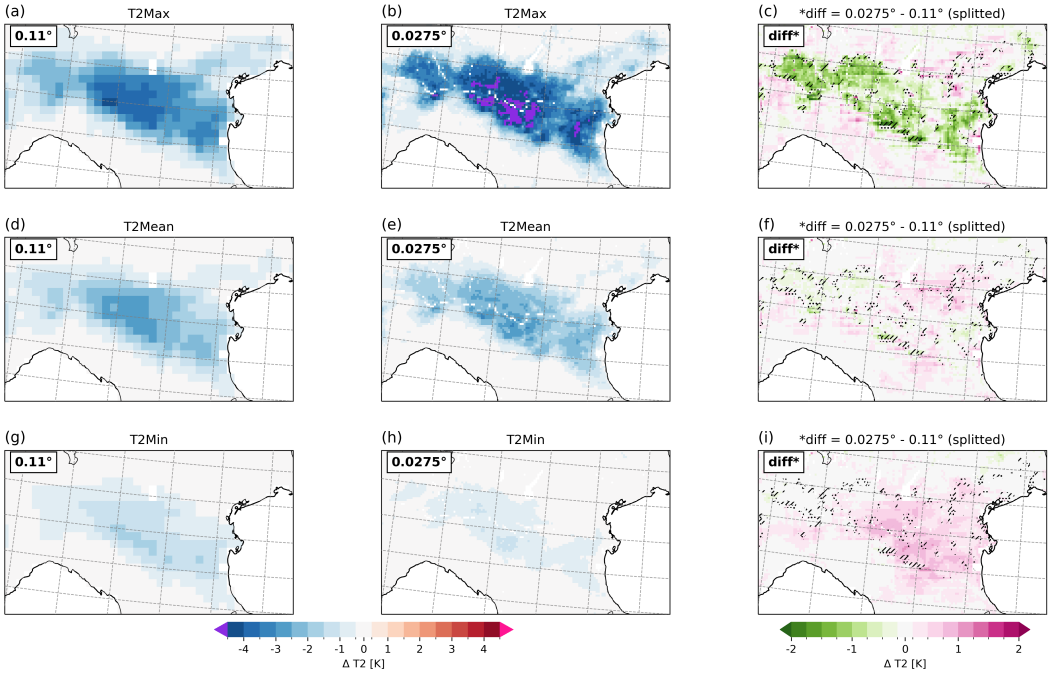

Figure 9. Spatial distribution of irrigation effects on the mean 2 m temperature values for June 2017 for a - c) T2Max, d - f) T2Mean and g - i) T2Min at 0.11° (first column, a, d, g) and 0.0275° (second column, b, e, h) and as difference of irrigation effects of both resolutions (third column, c, f, i). Hatches indicate a more than 10% larger irrigated fraction at 0.0275° than at 0.11° horizontal resolution, while dots indicate a 10% smaller irrigated fraction at 0.0275° than at 0.11° horizontal resolution.

As shown in Figure 8 the change in the irrigated fraction is less correlated with T2Min (r=-0.75 at 0.11° and r=-0.61 at 0.0275°) compared to the very strong correlation with T2Max (Figure 9). This suggests that different processes govern the varying intensity of irrigation effects at night. During nighttime, the irrigation can lead to higher air temperatures as (Figure 8). This effect was also found by Chen and Jeong (2018), who attributed it to the influence of the high soil moisture. In our simulations, the nighttime warming is less pronounced and shows a monthly averaged cooling effect (Figure 9). This can be explained by analyzing the planetary boundary layer (PBL) height and the turbulences in the lowest atmosphere level. Our results show a strong decrease of air temperature during the day (Figure 9), which persists into the night (Figure 9, Figure B2), most likely as residual of the strong daytime cooling. The daytime cooling effect (on T2Max) is particularly evident at 0.0275° horizontal resolution. However, at 0.0275° horizontal resolution, irrigation causes a strong reduction of turbulences occurs during daytime (Figure 10d-f), which reduces the vertical mixing of the irrigated effects to higher atmosphere levels, leading to less pronounced irrigation effects in the vertical extend compared to the simulations at 0.11° horizontal resolution (Figure B2, Figure B3). During nighttime, the near-surface TKE plays a less important role due to the overall reduced turbulences. In our results, the reduction of TKE is very similar at 0.11° and 0.0275° horizontal resolution and shows a very weak decrease (Figure 11). This underlines the theory that the nighttime cooling effect of irrigation in the vertical extent its persisting is a residual from

the daytime cooling, which can be observed at 0.11° horizontal resolution and leads to the more pronounced cooling effect at T2Min. Another factor influencing the development of irrigation effects in the atmosphere is the PBL height, which particularly decreases at 0.11° horizontal resolution by up to -500 m. This strong decrease together with the stronger surface fluxes at 0.0275° horizontal resolution (Figure 4) explain the more pronounced irrigation effects at 0.0275° horizontal resolution compared to 0.11° horizontal resolution.

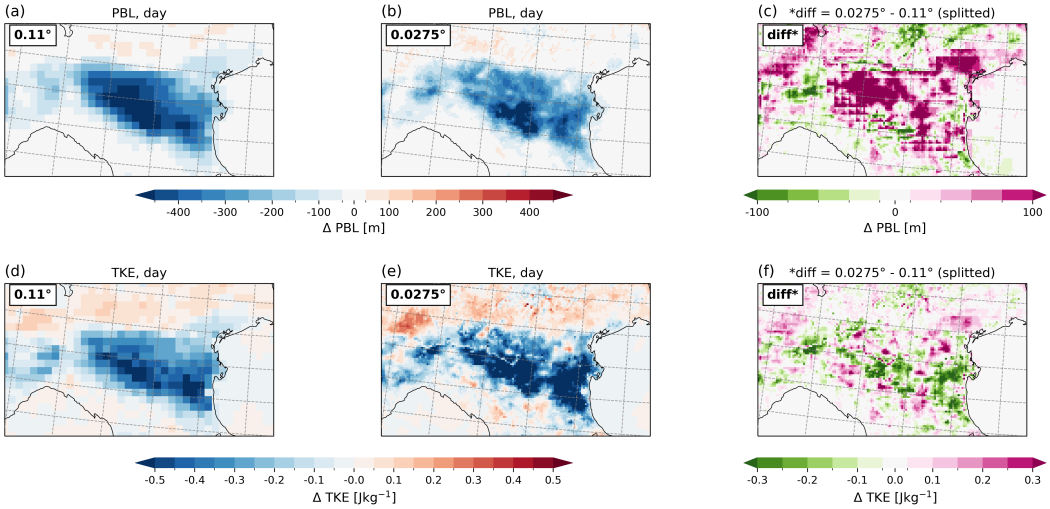

Figure 10. Spatial distribution of daytime irrigation effects in June 2017 for a - c) PBL height, and d - f) TKE at 0.11° (first column, a, d) and 0.0275° (second column, b, e), and as difference of irrigation effects of both resolutions (third column, c, f).

3.2.3 Irrigation effects on convective conditions

The different treatments of convection in the experiments of our study with parameterized convection and the explicitly resolved convection give reasons to investigate irrigation effects on convective conditions. As in section 3.2.2, we focus on irrigation effects developing in June 2017 in the D0275-EVAL region. As indicated in Section 3.1, the added value of explicitly resolving convection becomes clear in an improved diurnal cycle of precipitation (Figure 3b) and more high precipitation values in the simulations at 0.0275° horizontal resolution (Figure 2d). At 0.11° horizontal resolution, irrigation causes more frequently higher precipitation rates (Figure 2d), which is also shown by an increase of monthly accumulated precipitation by +26% in June in the analysis region (Figure 12a). However, the increase does not occur mainly above irrigated areas, but rather on the windward side of the Southern Alps, at the foot of the mountains, which represents the mean downwind direction in the simulation at 0.11° horizontal resolution (Figure 12c) in June. The strongest development of the convective available potential energy (CAPE) occurs at 18:00 LT, as hourly mean in June in our analysis domain. The precipitation increase at 0.11° horizontal resolution follows the increase of CAPE) (Figure 13a) and the decrease of convection inhibition (CIN) above the irrigated areas, resulting from the increased amount of moisture, and therefore, an increased amount of latent energy in the atmosphere originating from irrigation. Additionally, a strong reduction of the lifting condensation level (LCL) and the level of free convection (LFC) both by up to -1000 m occur above irrigated areas and facilitate the initiation of convection at 0.11° horizontal resolution (Fig-

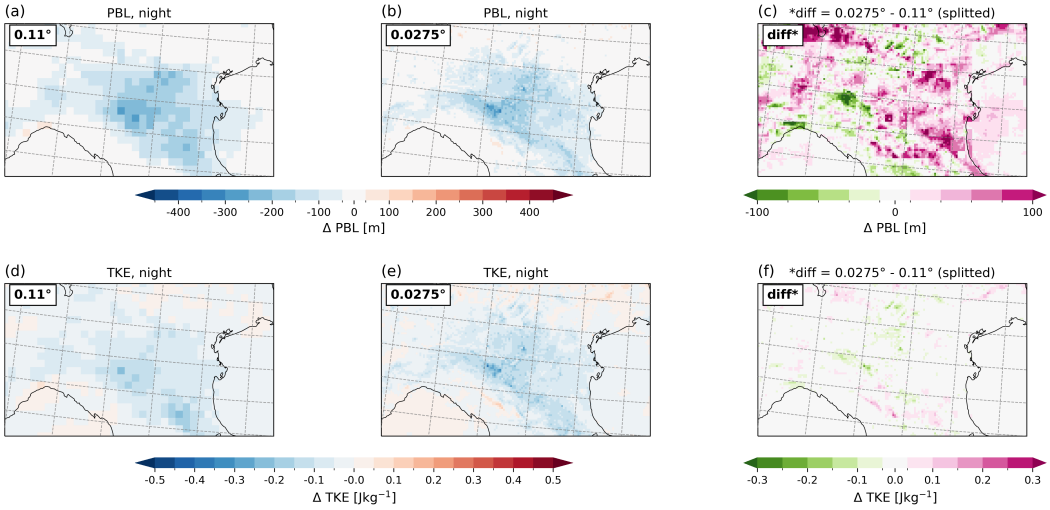

Figure 11. Spatial distribution of nighttime irrigation effects in June 2017 for a - c) PBL height, and d - f) TKE at 0.11° (first column, a, d) and 0.0275° (second column, b, e), and as difference of irrigation effects of both resolutions (third column, c, f).

ure 13e and g). The simulations at 0.0275° horizontal resolution show more mixed, small-scale changes in precipitation as irrigation effect with a total precipitation decrease by -5% above irrigated areas in the analysis region (Figure 12b). However, precipitation also increases at the windward side of the Southern Alps as in the simulations at 0.11° horizontal resolution. The irrigation effects in precipitation at 0.0275° horizontal resolution show small-scale patterns indicating development and suppression of convection. The different response to irrigation in precipitation of the experiments at 0.0275° horizontal resolution is further evident in the development of CAPE and CIN (Figure 13b and d). While CAPE strongly increases, and the LCL and LFC decrease similarly as at 0.11° horizontal resolution, CIN shows a mixed effect with areas of increased CIN, where convection is inhibited and precipitation is decreasing in the irrigated simulation at 0.0275°. Compared to the simulation at 0.11°, CIN is more frequently increased at 0.0275° horizontal resolution. However, also areas with decreased CIN occurs at 0.0275° and lead together with the increased CAPE and decreased condensation levels to a positive precipitation feedback from irrigation.

The developments of precipitation effects are related with the developments of the wind field. While the wind direction shows little response to irrigation in the monthly mean values of our experiments (Figure 12c and d), the monthly mean of the 10 m wind speed is reduced above the irrigated area and the Po delta at the Adriatic Coast (Figure 12e and f). In June 2017, a sea breeze occurs, but its intensity weakens due to irrigation. The reason is the cooling effect of irrigation on the surface and air temperature in the Po Valley (Figure 9), which leads to a reduced temperature gradient causing the sea breeze. A similar effect was also shown by Valmassoi et al. (2020b) and Udina et al. (2024). This impact develops particularly at 0.11° horizontal resolution leading to a wind speed reduction of -0.8 ms^{-1}. Linked with the wind speed reduction and cooling effect of the air temperature, the planetary boundary layer height (PBL) decreases with irrigation as well particularly at 0.11° horizontal resolution by up to -300 m above the irrigated areas.

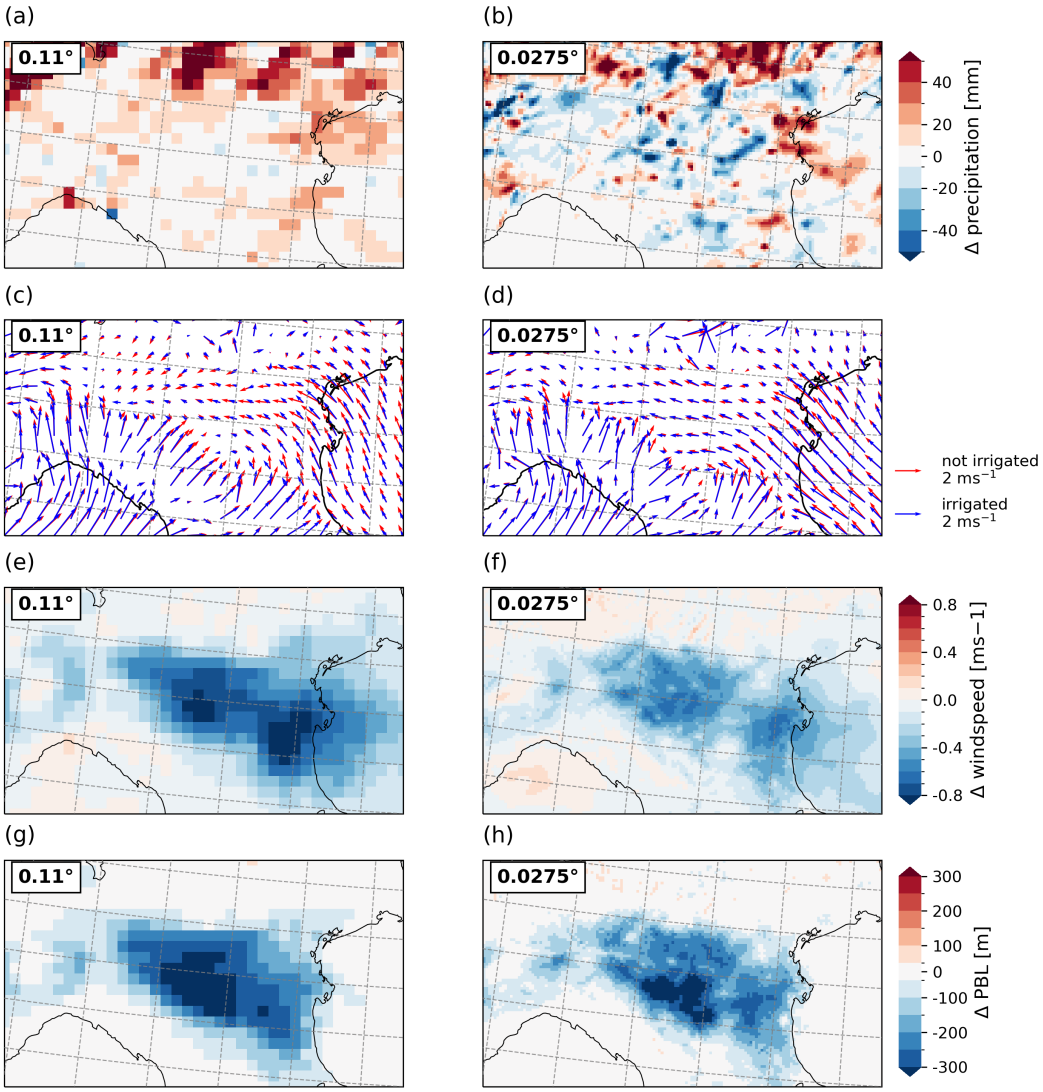

Figure 12. Spatial distribution of irrigation effects on a - b) accumulated precipitation, monthly mean values for c - d) 10 m wind vectors, e -f) 10 m wind speed, and g and h) PBL height at 0.11° (left column) and 0.0275° (right column) horizontal resolution for June 2017.

4 Discussion

Increasing the resolution and explicitly resolving convection in RCMs comes with many benefits and added values, as previously shown by e.g. (Prein et al., 2015; Lind et al., 2020; Langendijk et al., 2021; Soares et al., 2022; Adinolfi et al., 2023). The characteristics of the explicitly resolved vertical velocity and the higher resolution of the land surface influence various aspects and interconnected processes in regional climate model simulations. One key aspect is the higher resolution of the topography, which allows for a more realistic representation of mountains and valleys, thereby influencing the development of local meteorological conditions (Kendon et al., 2021). In our model domain, Northern Italy, climatic processes are strongly influenced by the Alps and, therefore, require a detailed representation of the elevation. Additionally, following a fractional approach, the representation of land cover at higher resolution is more heterogeneous than at lower resolution. For a separated irrigated fraction such as in our irrigation param-

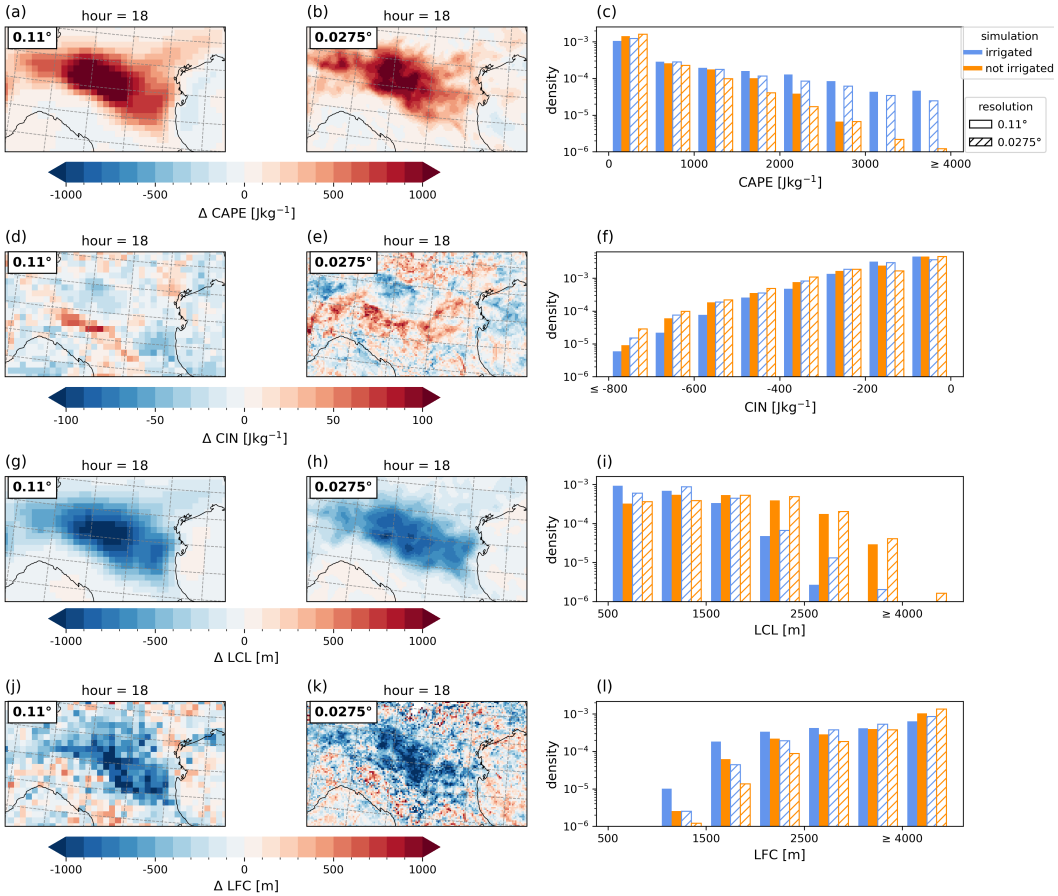

Figure 13. Irrigation effects on CAPE and CIN in June 2017, as a - b) and d - e) spatial distribution of hourly mean value at 1800 LT. The first two columns represent the spatial distribution of the hourly mean value at 1800 LT for the simulations at 0.11° and the simulations at 0.0275° horizontal resolution. The last column represents the normalized distribution of hourly values in grid cells with an irrigated fraction larger than 70% (based on the grid cell extraction in D0275).

eterization, the simulation results at 0.0275° lead to more grid cells with higher irrigated fractions than at 0.11° (Figure 2). Due to the weighted averaging of the turbulent surface fluxes with respect to different land cover tiles in the model grid cell in the lowest atmospheric layer (Kotlarski, 2007), the effects in the atmosphere are most pronounced in grid cells with high irrigated fractions. For both resolutions, a clear correlation between the irrigated fraction with the irrigation effect on temperature was found for T2Max (r=0.9 for 0.11° and r=0.85 for 0.0275° horizontal resolution). One example for this correlation is the stronger irrigation effect at 0.0275° horizontal resolution on T2Max in grid cells, which show a at least a 10% larger irrigated fraction at 0.0275° resolution compared to 0.11° located in the northwestern part of the Po Valley (Figure 9). The cooling effect on T2Max due to irrigation differs by up to -2 K in single grid cells of the monthly mean for June 2017 between the two resolutions. Beyond the changes in the irrigated fraction, the more pronounced cooling effect at the 2 m temperature at 0.0275° resolution is also influenced by a slightly stronger decrease in the sensible heat flux and a slightly stronger increase in the latent heat flux compared to the 0.11° resolution (Figure 8, Figure 9). However, in the eastern part of the Po Valley grid cells do show the clear correlation with

the intensity of the irrigation effect and the irrigated fraction. Here, other processes must be more dominant, such as local boundary conditions, strong wind speeds (Figure C1), leading to less pronounced irrigation effects despite a larger irrigated fraction. Further, the PBL height as well as TKE are important factors determining the vertical extent of irrigation effects. In our case study, a strongly decreased TKE at 0.0275° horizontal resolution during daytime leads to less pronounced irrigation effects in the vertical extent (Figure 10, Figure 11, Figure B2). This effect influences the irrigation effects in the nighttime, when the cooling signal persists as a residual. While (Chen & Jeong, 2018) found a warming effect of irrigation during nighttime, we find a less pronounced, but still a cooling effect. This can be explain by the fact, that our experiments are extreme experiments, and we use maximal irrigated until the maximal field capacity, which then leads to strong pronounced irrigation cooling effects such at T2Max by up to -4 K. Comparable studies found a cooling effect by up -3 K at T2Max as monthly mean of a grid cell in July (Valmassoi et al., 2020a). One of the most important benefits of convection-permitting resolution is the explicit treatment of the vertical velocity, which allows convection and cloud development processes to be resolved (Vergara-Temprado et al., 2020). Multiple studies have shown an improvement in the hourly precipitation intensity when using a non-hydrostatic model at convection-permitting scale, compared to convection-parameterized simulations at coarser scales (Ban et al., 2014; Prein et al., 2015). Despite a general underestimation of precipitation in our model compared to the point measurements of the ARPA stations, the distribution of hourly precipitation intensity is improved in the convection-permitting simulations (Figure 2 d), particularly in resolving higher precipitation intensities exceeding 2.5 mmh^{-1} and resolving heavy precipitation. The improvement of the representation of precipitation at 0.0275° horizontal resolution is also present in the diurnal cycle and the timing of the precipitation peaks, compared to precipitation on the station locations (Figure 3). The intensity however is overestimated during the peak and underestimated in the morning and at nighttime. At 0.11° resolution, precipitation peaks during noon, however, in terms of intensity it shows a good match with the precipitation maxima of the observational values. At 0.11° horizontal resolution, irrigation increases precipitation, not above the irrigated areas but rather at the windward side of the Southern Alps. Convection indicating variables such as a decreased LCL and LFC, a strongly increased CAPE and a decreased CIN show improved conditions for convection in the irrigated simulation at 0.11° horizontal resolution. In contrary, at 0.0275° irrigation causes a slight decrease of precipitation (-4 %) above the irrigated areas in the Po Valley, although similar conditions of CAPE, LCL and LFC exist as at 0.11°. However, CIN shows a mixed response to irrigation and increases in the areas, where precipitation decreases, and can therefore be understood as the factor leading to the precipitation differences caused by irrigation at 0.0275° horizontal resolution. As in our study, Valmassoi et al. (2020b) found a weaker effect of irrigation on precipitation at convection-permitting scale than using the convection parameterization. However, they found a total precipitation increase in the Po Valley by 9.5% for July 2015. The precipitation effect showed in the study by Valmassoi et al. (2020b) as well as in our study areas with convection-inducing conditions as well as areas with convection inhibiting conditions. For the irrigation effect on precipitation, Udina et al. (2024) found a change in sign when using the convection-permitting simulations compared to the convection parameterized simulations. Also here the parameterization of convection leads to a clear increase of precipitation while the convection-permitting simulations show a decrease of precipitation.

While the vegetation variables are not directly resolution dependent, due to the interactive coupling they are influenced by resolution-dependent developments in the atmosphere and soil. For example, changes in temperature affect directly the LAI development as well as the date of the harvest (Section 3.2.1). Therefore, changes in temperature caused by different simulations or caused by irrigation affect the development of vegetation, which then feeds back with atmospheric and soil processes. In our study, convection-permitting simulations are characterized by higher temperatures. Similar findings were reported by Ban et al. (2014) and Halladay et al. (2024) employing non-hydrostatic, re-

gional models for convection-permitting simulations over Europe. While Ban et al. (2014) find an increase in solar radiation through smaller-scale cloud cover as the reason for the higher temperatures, Halladay et al. (2024) links the warm and dry bias to the reduced precipitation frequency, which causes a lower soil moisture, and therefore, a decrease in evapotranspiration. In our coupled model system the higher temperatures at 0.0275° horizontal resolution accelerate the LAI growth and lead to an earlier harvest event. In turn, cooler temperatures, for instance caused by irrigation, slow down the LAI development in the first months. However, due to sufficient water and the high NPP rates, the LAI reaches higher values in the irrigated simulations compared to the not irrigated simulations. Furthermore, vegetation also reacts directly to soil moisture and shows an increased canopy conductance, which drives the evapotranspiration and, therefore, the cooling in the near-surface atmosphere as well as the increased relative humidity. These processes develop very similarly at both resolutions.

5 Conclusion

In our study, we employ for the first time the newly developed irrigation parameterization from Asmus et al. (2023) at convection-permitting scale (0.0275°) using REMO2020 with its non-hydrostatic dynamic core, interactively coupled to its mosaic-based vegetation module iMOVE. We compare the irrigation effects from these convection-permitting simulations with those from convection-parameterized simulations based on the hydrostatic dynamic core of REMO2020-iMOVE. In our setup, we consider the interaction between land, atmosphere and vegetation, as well as the effects and feedbacks between these components. The higher spatial resolution increases the heterogeneity of the surface, which is evident in the wider spread of the topography as well as in distribution of irrigated areas, with the irrigated fraction in grid cells represented by higher percentages At the two resolutions, the effects on irrigation on vegetation are similar at both resolutions. However, the interactive coupling leads to a feedback of vegetation to higher 2 m temperatures in the convection-permitting simulations, which cause an earlier harvest event. Irrigation has a counteracting effect and extends the growing season due to air temperature reduction and increases the maximum value of the LAI due to a larger canopy conduction, which increases the NPP and the evapotranspiration. The surface fluxes show a slightly stronger irrigation effect at 0.0275° horizontal resolution with a decrease of the sensible heat flux and an increase of the latent heat flux. Through the higher resolution in convection-permitting simulations, the fluxes lead to more distinct effects in the atmosphere, such as on near surface temperatures. The irrigation effect on T2Max is more localized and distinct at 0.0275° horizontal resolution. However, it has to be mentioned that the development of irrigation effects is strongly influenced by boundary layer processes like turbulences, which govern the irrigation effects in atmosphere. The largest differences between the two resolutions are found in the representation of precipitation due to the different treatment of convection. In our study, convection-permitting simulations improve the diurnal cycle of precipitation and the hourly values of the precipitation distribution for heavy precipitation. Irrigation effects on precipitation vary with resolution. At a 0.11° horizontal resolution, precipitation increases windward within the analysis domain but not directly above the irrigated areas. In contrast, at 0.0275° with explicitly resolved convection, precipitation decreases over the irrigated areas while still increasing windward. In our study, CIN is the important factor that inhibits convection at 0.0275° while it enables it at 0.11° horizontal resolution. A similar counteracting behavior has been observed in previous studies, highlighting the need for further research on the effects of irrigation on precipitation.

Appendix A Coupling of REMO and iMOVE

The vegetation processes are based on selected modules of JSBACH (Reick et al., 2021) and were implemented in REMO as iMOVE by (Wilhelm et al., 2014). The interactive coupling enables the interaction between atmospheric, soil and vegetation variables in every timestep. In the following and in Figure A1 the the key coupling processes are explained. For a more detailed descriptions can be found in (Wilhelm et al., 2014) and (Reick et al., 2021). The vegetation processes and growing conditions of plants are driven by the REMO variables soil moisture, 2 m temperature, surface and near-surface humidity, radiation, pressure, and atmospheric CO_2 concentration. Additionally, prescribed PFT-specific parameters determine the varying responses of different PFTs. The carbon assimilation by plants during the photosynthesis process and the transpiration of water vapor are linked through the stomata of the leaves, which open for CO_2 uptake, but in the same time loose water (transpiration) (Reick et al., 2021). For representing this link in the model, following JSBACH, iMOVE employs the Farquhar model (Farquhar et al., 1980) for the calculation of the photosynthesis process and the approach from the Biosphere Energy Transfer Hydrology (BETHY) model by (Knorr, 1997) for the stomata behavior. Applying this behavior to the canopy leads to the canopy conductance. According to Wilhelm et al. (2014) and Reick et al. (2021), in a first step, the photosynthesis is calculated under the assumption of unlimited water availability. This step derives the so-called "unstressed" canopy conductance for water vapor ($g_c^{H_2O}$) by setting it in relation to the canopy conductance of CO_2 using the equation

$$g_C^{H_2O} = \frac{1.6}{c_a - c_i} \frac{RT}{p} A_C \tag{A1}$$

with c_i and c_a as the CO_2 densities inside and outside the stomata, R as universal gas constant, T as leaf temperature, p as pressure, and A_C as assimilation rate over canopies. A_C takes into account the irradiation by including the fraction of absorbed photosynthetically active radiation when calculating the photoreaction of electrons, as well as by including the dark respiration (Reick et al., 2021). It has to be mentioned that the assimilation rate over canopies is highly temperature dependent (Reick et al., 2021). As in JSBACH (Reick et al., 2021), the water limitation from the available soil moisture leads to the "stressed" canopy conductance ($g_{c,stress}^{H_2O}$) using a scaling factor (f_{ws}) in equation A2 derived by equation A3

$$g_{C,stress}^{H_2O} = \begin{cases} f_{ws} g_C^{H_2O} & \text{for } q_a \leq q_s \\ 0 & \text{otherwise} \end{cases} \tag{A2}$$

$$f_{ws} = \begin{cases} 0 & \text{for } ws \leq ws_{pwp} \\ \frac{ws - ws_{pwp}}{ws_{crit} ws_{pwp}} & \text{for } ws_{pwp} < ws < ws_{crit} \\ 1 & \text{otherwise} \end{cases} \tag{A3}$$

withq_a as air humidity, q_s as surface humidity, ws_{pwp} as relative soil moisture at the wilting point (0.35), and ws_{crit} as relative soil moisture at critical point (0.75). From Equation A2 we can follow, that stressed canopy conductance depends not only at the soil moisture, but is also driven by the state of the humidity in the air and at the surface, leading to no canopy conductance, if air humidity exceeds surface humidity (Reick et al., 2021). The stressed canopy conductance is used in REMO-iMOVE for the calculation of the latent heat flux and evapotranspiration (Wilhelm et al., 2014). Further, the stressed canopy conductance calculates the stressed assimilation rate, also known as gross primary production (GPP) from which NPP can be derived by including the plant's respiration for maintenance and growth (Wilhelm et al., 2014). As in JSBACH, NPP, soil

moisture and air temperature are driving the phenology of PFTs in particular the development of the LAI (Λ) (Reick et al., 2021; Wilhelm et al., 2014). The LAI of crops is calculated with the Logistic Growth Phenology (LoGro-P) (Reick et al., 2021)

$$\frac{d\Lambda}{dt} = k\Lambda\left(1 - \frac{\Lambda}{\Lambda_{\max}}\right) - p\Lambda. \tag{A4}$$

$$k = \begin{cases} f_{\text{alloc}}\frac{\text{sla}\cdot\text{NPP}}{\Lambda}, & \text{for NPP} > 0 \\ 0, & \text{otherwise} \end{cases} \tag{A5}$$

with sla as the specific leaf area of crops (ratio of leaf area to carbon content), and $falloc$ the fraction of NPP allocated to leaf growth, and p as shedding shedding rate. Leaf shedding is represented with a reduction of the LAI and occurs if the temperature is too low, the soil moisture falls below the wilting point, the NPP of the previous day is negative, or if the growing season ended and harvest begins (Wilhelm et al., 2014). The harvest event for C3 crops in iMOVE is determined with a heat sum, and reduces the LAI to its minimum value of 0.1 (Wilhelm et al., 2014). For the coupling the LAI influences the transpiration, the albedo and the vegetation ratio in the model (Wilhelm et al., 2014).

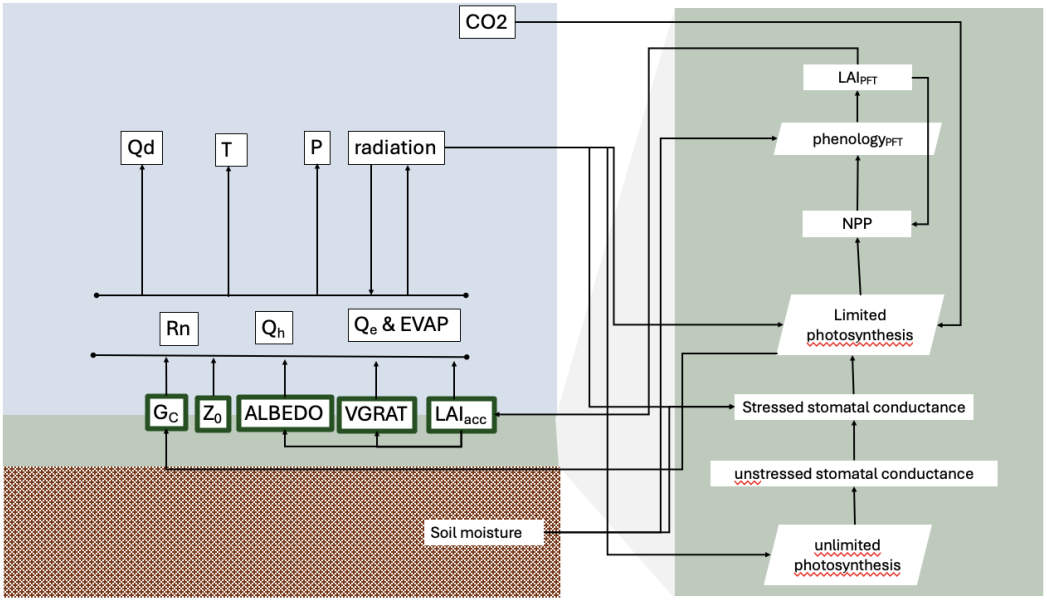

Figure A1. Coupling of soil, vegetation, and atmospheric processes in REMO-iMOVE. Adapted graphic from Wilhelm et al. (2014). G_C = canopy conductance, Z_0=surface roughness, $VGRAT$=vegetation ratio, R_n=net radiation, Q_s= turbulent sensible heat flux, Q_e=turbulent latent heat flux, $EVAP$=evaporation, Qd=specific humidity, T=air temperature, P=pressure. Green boxes are transferred from iMOVE to REMO.

Appendix B Irrigation effects in the boundary layer

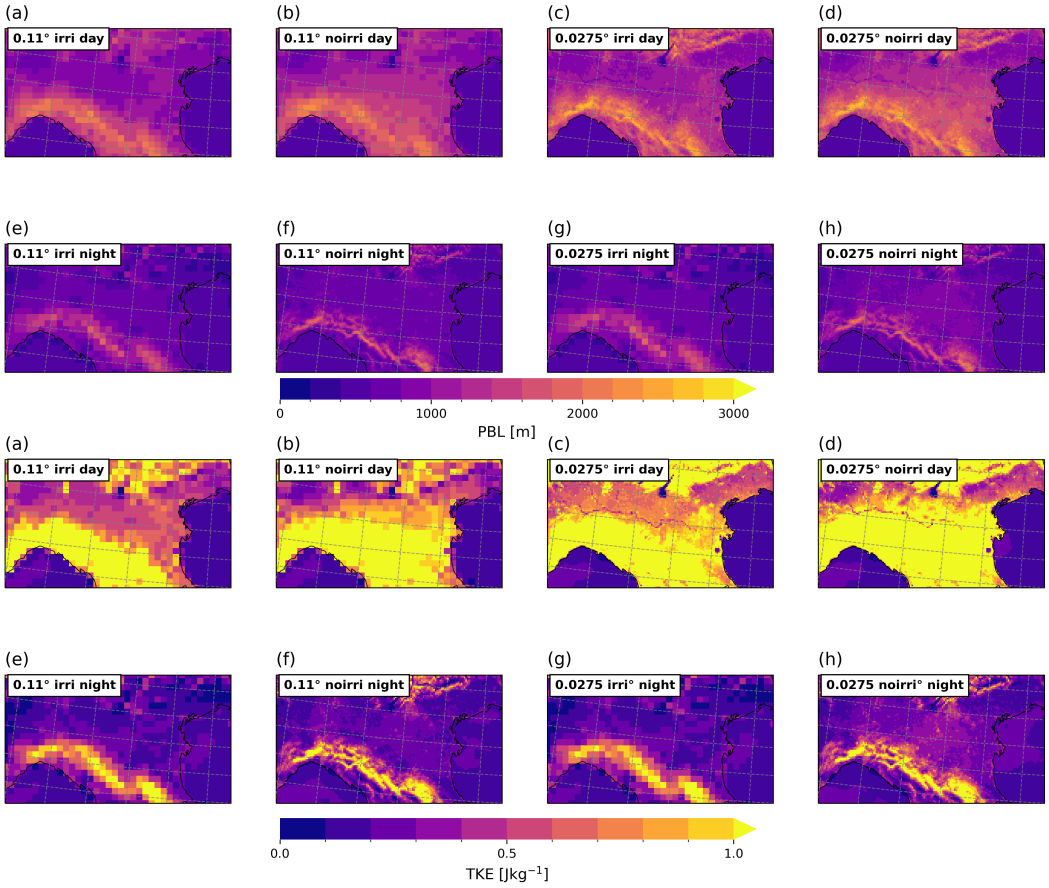

Figure B1. Spatial monthly mean values for June 2017 of (a-d) PBL height and (e-h) TKE, during daytime and nighttime for the irrigated and not irrigated simulations at 0.11° and 0.0275° horizontal resolution.

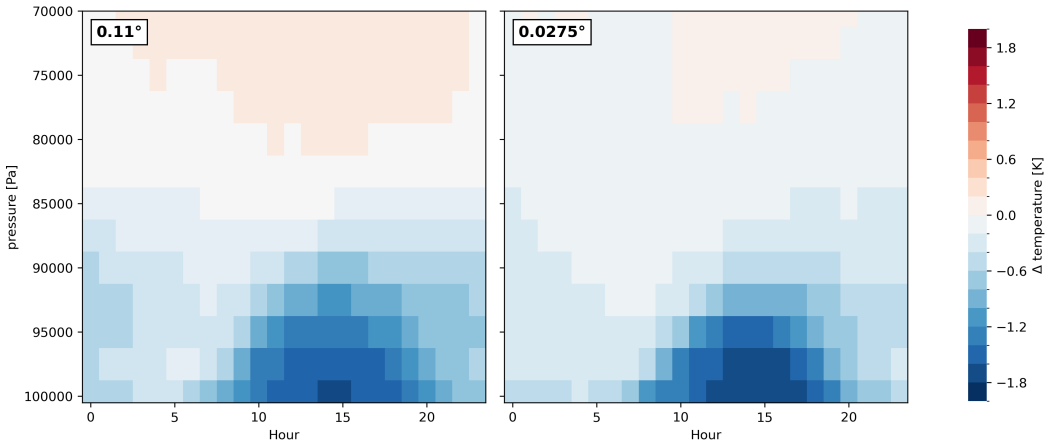

Figure B2. Vertical profile of the duration of irrigation effects on temperature at a) 0.11° horizontal resolution and b) 0.0275° horizontal resolution in grid cells showing different effects on T2Max and T2Min in Figure 9. The values represent hourly averages in June 2017.

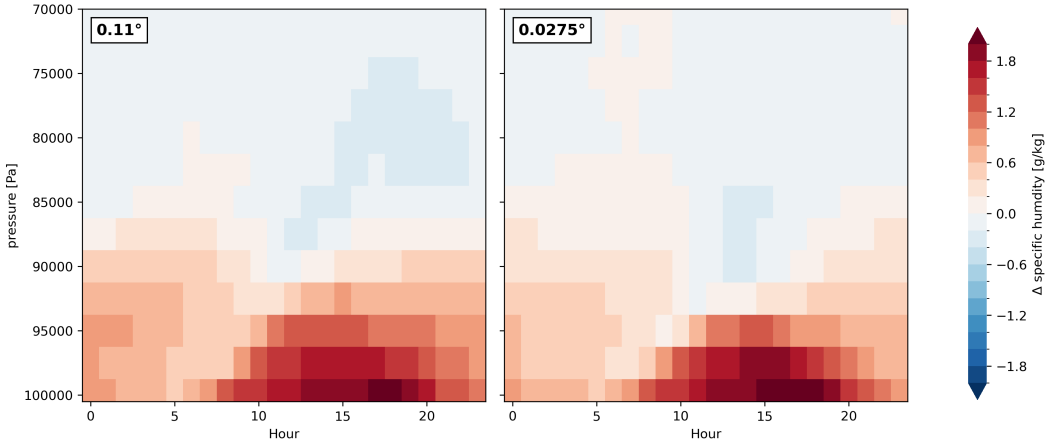

Figure B3. Vertical profile of the duration of irrigation effects on specific humidity at a) 0.11° horizontal resolution and b) 0.0275° horizontal resolution in grid cells showing different effects on T2Max and T2Min in Figure 9. The values represent hourly averages in June 2017.

Appendix C Precipitation and wind conditions

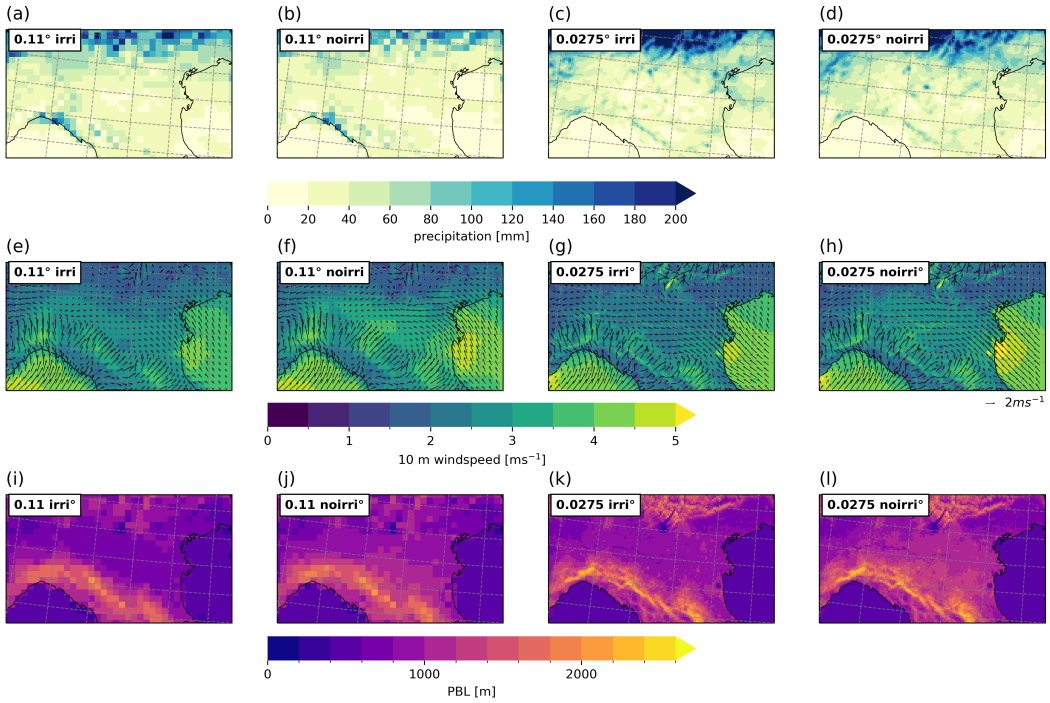

Figure C1. Spatial distribution of (a-d) accumulated precipitation, (e-h) mean wind conditions,(i-k) PBL height during June 2017 for the irrigated (a,c,e,g) and not irrigated (b,d,f,h) simulations at different resolution for the analysis region D0275-EVAL.

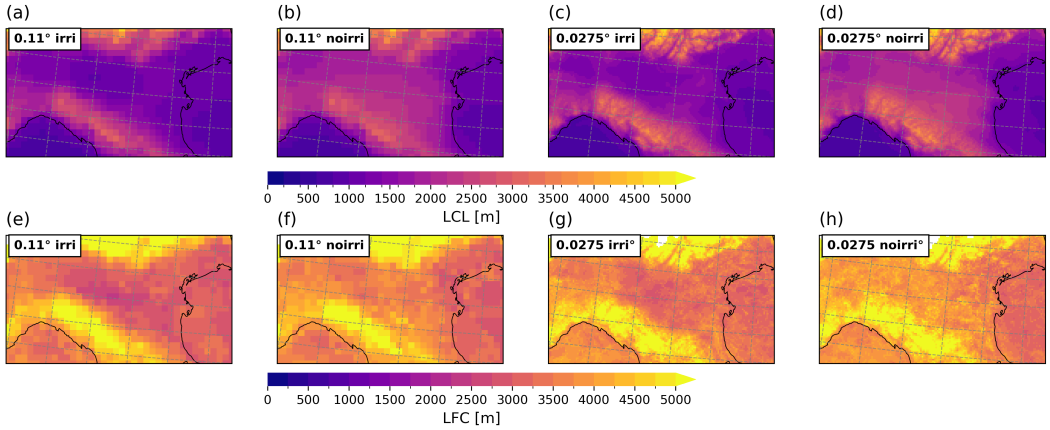

Figure C2. Spatial distribution of (a-d) LCL height and (e-h) LFC height as hourly mean of 1800 LT June 2017 for the irrigated (a,c,e,g) and not irrigated (b,d,f,h) simulations at different resolution for the analysis region D0275-EVAL.

Open Research Section

The shown model simulations were performed by the regional climate model REMO2020-iMOVE using the irrigation parameterization by Asmus et al. (2023) at the German Climate Computing Center (Deutsches Klimarechenzentrum, DKRZ). The data for this study is available at a zenodo repository (`https://doi.org/10.5281/zenodo.15144005`, Pop (2025a)), as well is the software for this study (`https://doi.org/10.5281/zenodo.15156272`,

Pop (2025b)). The observational data used for this analysis is publicly available from ARPA. The data for Emilia-Romagna is available at `https://simc.arpae.it/dext3r/` (Accessed on: 2023-12-22), the data for Lombardia is available at `https://idro.arpalombardia.it/manual/AnagraficaSensoriWEB.csv525` and `https://www.arpalombardia.it/temi-ambientali/meteo-e-clima/522form-richiesta-dati/` (Accessed on: 2023-12-22), and the data for Veneto is available at `https://www.ambienteveneto.it/datiorari/` (Accessed on: 2023-12-22).

Acknowledgments

We are grateful for the support and help of the REMO developer team located at GERICS. Here, we want to thank in particular Lars Buntemeyer for preparing the model forcing from ERA5 and from REMO-iMOVE simulations at 0.11°. We also thank Alain Tamoffo for internally reviewing our paper draft. We are grateful to DKRZ for providing the high computing capacity, with which we performed our simulations. Further, we want to thank ARPA for providing observational data. This work was financed within the framework of the Helmholtz Institute for Climate Service Science (HICSS), a cooperation between the Climate Service Center Germany (GERICS) and Universität Hamburg, Germany, and conducted as part of the LANDMATE (Modelling human LAND surface modifications and its feedbacks on local and regional cliMATE) project.

References

Adinolfi, M., Raffa, M., Reder, A., & Mercogliano, P. (2023). Investigation on potential and limitations of era5 reanalysis downscaled on italy by a convection-permitting model. *Climate Dynamics*, *61*, 4319-4342. doi: 10.1007/s00382-023-06803-w

Alduchov, O. A., & Eskridge, R. E. (1996). Improved magnus form approximation of saturation vapor pressure. *Journal of Applied Meteorology and Climatology*, *35*(4), 601 - 609. doi: https://doi.org/10.2172/548871

ARPA Emilia-Romagna. (2023). *Dext3r beta.* Arpae Emilia-Romagna. Retrieved from `https://simc.arpae.it/dext3r/` (Accessed on: 2023-12-22)

ARPA Lombardia. (2023a). *Dati sensori meteo 2017.* Arpa Lombardia. Retrieved from `https://www.arpalombardia.it/temi-ambientali/meteo-e-clima/form-richiesta-dati/` (Accessed on: 2023-12-22)

ARPA Lombardia. (2023b). *Stazioni meteorologiche.* Arpa Lombardia. Retrieved from `https://idro.arpalombardia.it/manual/AnagraficaSensoriWEB.csv` (Accessed on: 2023-12-22)

ARPAV Veneto. (2023). *dati meteorologici orari.* Arpa Veneto. Retrieved from `https://www.ambienteveneto.it/datiorari/` (Accessed on: 2023-12-22)

Asmus, C., Hoffmann, P., Pietikäinen, J.-P., Böhner, J., & Rechid, D. (2023, 12). Modeling and evaluating the effects of irrigation on land–atmosphere interaction in southwestern europe with the regional climate model remo2020–imove using a newly developed parameterization. *Geoscientific Model Development*, *16*, 7311-7337. Retrieved from `https://gmd.copernicus.org/articles/16/7311/2023/` doi: 10.5194/gmd-16-7311-2023

Ban, N., Caillaud, C., Coppola, E., Pichelli, E., Sobolowski, S., Adinolfi, M., ... Zander, M. J. (2021, Jul 01). The first multi-model ensemble of regional climate simulations at kilometer-scale resolution, part i: evaluation of precipitation. *Climate Dynamics*, *57*(1), 275-302. Retrieved from `https://doi.org/10.1007/s00382-021-05708-w` doi: 10.1007/s00382-021-05708-w

Ban, N., Schmidli, J., & Schär, C. (2014). Evaluation of the convection-resolving regional climate modeling approach in decade-long simulations. *Journal of Geophysical Research: Atmospheres*, *119*(13), 7889-7907. Retrieved from `https://agupubs.onlinelibrary.wiley.com/doi/abs/10.1002/2014JD021478` doi:

https://doi.org/10.1002/2014JD021478

Boucher, O., Myhre, G., & Myhre, A. (2004, 06). Direct influence of irrigation on atmospheric water vapour and climate. *Climate Dynamics*, *22*, 597-603. doi: 10.1007/s00382-004-0402-4

Broucke, S. V., & Lipzig, N. V. (2017, 10). Do convection-permitting models improve the representation of the impact of luc? *Climate Dynamics*, *49*, 2749-2763. doi: 10.1007/s00382-016-3489-5

Chen, X., & Jeong, S.-J. (2018, jan). Irrigation enhances local warming with greater nocturnal warming effects than daytime cooling effects. *Environmental Research Letters*, *13*(2), 024005. Retrieved from `https://dx.doi.org/10.1088/1748-9326/aa9dea` doi: 10.1088/1748-9326/aa9dea

Copernicus Climate Change Service. (2022, 11). *European state of the climate 2017.* https://climate.copernicus.eu/CopernicusESC. Copernicus Climate Change Service (C3S).

Cortés-Hernández, V. E., Caillaud, C., Bellon, G., Brisson, E., Alias, A., & Lucas-Picher, P. (2024). Evaluation of the convection permitting regional climate model cnrm-arome on the orographically complex island of corsica. *Climate Dynamics*. doi: 10.1007/s00382-024-07232-z

de Vrese, P., Hagemann, S., & Claussen, M. (2016, 4). Asian irrigation, african rain: Remote impacts of irrigation. *Geophysical Research Letters*, *43*, 3737-3745. doi: 10.1002/2016GL068146

Dominic, M., René, L., Julie M., T., & Philippe, L.-P. (2017). Spatial spin-up of fine scales in a regional climate model simulation driven by low-resolution boundary conditions. *Climate Dynamics*, *49*, 563-574. doi: 10.1007/s00382-016-3358-2

ESA. (2017). *Land cover cci product user guide version 2. tech. rep.* Author. Retrieved from `{maps.elie.ucl.ac.be/CCI/viewer/download/ESACCI-LC-Ph2-PUGv2_2.0.pdf}` (Accessed on: 14-12-2024)

Farquhar, G. D., Caemmerer, S., & Berry, J. A. (1980). A biochemical model of photosynthesis in leaves of c3 species. *Planta*, *149*, 78–90. doi: 10.1007/BF00386231

Fosser, G., Khodayar, S., & Berg, P. (2014). Benefit of convection permitting climate model simulations in the representation of convective precipitation. *Climate Dynamics*, *44*, 45-60. doi: 10.1007/s00382-014-2242-1

Goettel, H. (2009). *Einfluss der nichthydrostatischen Modellierung und der Niederschlagsverdriftung auf die Ergebnisse regionaler Klimamodellierung* (Doctoral dissertation, MPI für Meteorologie, Hamburg). doi: 10.17617/2.994076

Halladay, K., Berthou, S., & Kendon, E. (2024). Improving land surface feedbacks to the atmosphere in convection-permitting climate simulations for europe. *Climate Dynamics*. doi: 10.1007/s00382-024-07192-4

Heim, C., Panosetti, D., Schlemmer, L., Leuenberger, D., & Schär, C. (2020, 6). The influence of the resolution of orography on the simulation of orographic moist convection. *Monthly Weather Review*, *148*, 2391-2410. doi: 10.1175/MWR-D-19-0247.1

Hoffmann, P., Reinhart, V., Rechid, D., de Noblet, N., Davin, E., Asmus, C., ... Luyssaert, S. (2023, 08). High-resolution land use and land cover dataset for regional climate modelling: historical and future changes in europe. *Earth System Science Data*, *15*, 3819-3852. doi: 10.5194/essd-15-3819-2023

Hohenegger, C., Brockhaus, P., Bretherton, C. S., & Schär, C. (2009). The soil moisture-precipitation feedback in simulations with explicit and parameterized convection. *Journal of Climate*, *22*, 5003-5020. doi: 10.1175/2009JCLI2604.1

Jiménez-Esteve, B., Udina, M., Soler, M. R., Pepin, N., & Miró, J. R. (2018, 4). Land use and topography influence in a complex terrain area: A high resolution mesoscale modelling study over the eastern pyrenees using the wrf model. *Atmospheric Research*, *202*, 49-62. doi: 10.1016/j.atmosres.2017.11.012

Kendon, E. J., Prein, A. F., Senior, C. A., & Stirling, A. (2021, 4). *Challenges and outlook for convection-permitting climate modelling* (Vol. 379). Royal Society Publishing. doi: 10.1098/rsta.2019.0547

Knist, S., Goergen, K., & Simmer, C. (2019). Effects of land surface inhomogeneity on convection-permitting wrf simulations over central europe. *Meteorology and Atmospheric Physics*, *132*, 53-69. Retrieved from `https://doi.org/10.1007/s00703-019-00671-y` doi: 10.1007/s00703-019-00671-y

Knorr, W. (1997). *Satellitengestützte Fernerkundung und Modellierung des globalen CO_2-Austauschs der Landvegetation* (Examensarbeit). Max Planck Institute for Meteorology, Hamburg. (Also published as: Satellite remote sensing and modelling of the global CO_2 exchange of land vegetation: A synthesis study)

Kotlarski, S. (2007). A Subgrid Glacier Parameterisation for Use in Regional Climate Modelling. Dissertation. *Reports on Earth System Science*, *42*.

Langendijk, G. S., Rechid, D., Sieck, K., & Jacob, D. (2021). Added value of convection-permitting simulations for understanding future urban humidity extremes: case studies for berlin and its surroundings. *Weather and Climate Extremes*, *33*, 100367. Retrieved from `https://doi.org/10.1016/j.wace.2021.100367` doi: 10.1016/j.wace.2021.100367

Leng, G., Huang, M., Tang, Q., & Leung, L. R. (2015). A modeling study of irrigation effects on global surface water and groundwater resources under a changing climate. *Journal of Advances in Modeling Earth Systems*, *7*(3), 1285-1304. doi: 10.1002/2015MS000437

Leutwyler, D., Imamovic, A., & Schär, C. (2021). The continental-scale soil moisture-precipitation feedback in europe with parameterized and explicit convection. *Journal of Climate*, *34*, 5303-5320. doi: 10.1175/JCLI-D-20-0415.1

Lind, P., Belušić, D., Christensen, O. B., Dobler, A., Kjellström, E., Landgren, O., ... et al. (2020). Benefits and added value of convection-permitting climate modeling over fenno-scandinavia. *Climate Dynamics*, *55*, 1893–1912.

Liu, H., Meng, Z., Zhu, Y., & Huang, Y. (2023, 5). Convection initiation associated with a boundary layer convergence line over a real-world sharp vegetation-contrast area. *Monthly Weather Review*, *151*, 1189-1212. doi: 10.1175/MWR-D-22-0083.1

Lucas-Picher, P., Argüeso, D., Brisson, E., Tramblay, Y., Berg, P., Lemonsu, A., ... Caillaud, C. (2021). Convection-permitting modeling with regional climate models: Latest developments and next steps. *Wiley Interdisciplinary Reviews: Climate Change*, *12*, 1-59. doi: 10.1002/wcc.731

Magnus, G. (1844). Versuche über die Spannkräfte des Wasserdampfs. *Annalen der Physik*, *137*(2), 225-247. doi: https://doi.org/10.1002/andp.18441370202

Nordeng, T.-E. (1994, 09/1994). *Extended versions of the convective parametrization scheme at ecmwf and their impact on the mean and transient activity of the model in the tropics* (No. 206). Shinfield Park, Reading: ECMWF. Retrieved from `https://www.ecmwf.int/node/11393` doi: 10.21957/e34xwhysw

Ozdogan, M., Rodell, M., Beaudoing, H. K., & Toll, D. L. (2010). Simulating the effects of irrigation over the united states in a land surface model based on satellite-derived agricultural data. *Journal of Hydrometeorology*, *11*(1), 171 - 184. doi: 10.1175/2009JHM1116.1

Pietikäinen, J. P., Markkanen, T., Sieck, K., Jacob, D., Korhonen, J., Räisänen, P., ... Kaurola, J. (2018). The regional climate model REMO (v2015) coupled with the 1-D freshwater lake model FLake (v1): Fenno-Scandinavian climate and lakes. *Geoscientific Model Development*, *11*(4), 1321–1342. doi: 10.5194/gmd-11-1321-2018

Pietikäinen, J.-P., Sieck, K., Buntemeyer, L., Frisius, T., Nam, C., Hoffmann, P., ... Jacob, D. (n.d.). *Remo2020: a modernized modular regional climate model.* (in prep.)

Pop, C. (2025a, April). *Data supporting "the role of horizontal resolution in mod-*

eling irrigation effects with a coupled regional climate model system up to convection- permitting scale". Zenodo. Retrieved from https://doi.org/10.5281/zenodo.15144005 ([Dataset]) doi: 10.5281/zenodo.15144005

Pop, C. (2025b, April). *Scripts supporting the analysis of "the role of horizontal resolution in modeling irrigation effects with a coupled regional climate model system up to convection-permitting scale".* Zenodo. Retrieved from https://doi.org/10.5281/zenodo.15156272 ([Software]) doi: 10.5281/zenodo.15156272

Prein, A. F., Langhans, W., Fosser, G., Ferrone, A., Ban, N., Goergen, K., ... Leung, R. (2015). A review on regional convection-permitting climate modeling: Demonstrations, prospects, and challenges. *Reviews of Geophysics*, *53*, 323-361. doi: 10.1002/2014RG000475

Puma, M., & Cook, B. (2010, 08). Effects of irrigation on global climate during the 20th century. *J. Geophys. Res*, *115*. doi: 10.1029/2010JD014122

Qian, Y., Yang, Z., Feng, Z., & et al. (2020). Neglecting irrigation contributes to the simulated summertime warm-and-dry bias in the central united states. *npj Climate and Atmospheric Science*, *3*, 31. Retrieved from https://doi.org/10.1038/s41612-020-00135-w doi: 10.1038/s41612-020-00135-w

Reick, C. H., Gayler, V., Goll, D., Hagemann, S., Heidkamp, M., Nabel, J. E. M. S., ... Wilkenskjeld, S. (2021). *Jsbach 3 - the land component of the mpi earth system model: documentation of version 3.2* (Vol. 240; Tech. Rep.). Max Plack Institute for Meteorology. doi: 10.17617/2.3279802

Reinhart, V., Hoffmann, P., Rechid, D., Böhner, J., & Bechtel, B. (2022). High-resolution land use and land cover dataset for regional climate modelling: a plant functional type map for europe 2015. *Earth System Science Data*, *14*(4), 1735–1794. Retrieved from https://essd.copernicus.org/articles/14/1735/2022/ doi: 10.5194/essd-14-1735-2022

Sacks, W. J., Cook, B. I., Buenning, N., Levis, S., & Helkowski, J. H. (2009). Effects of global irrigation on the near-surface climate. *Clim. Dyn.*, *33*, 159–175. doi: 10.1007/s00382-008-0445-z

Saeed, F., Hagemann, S., & Jacob, D. (2009). Impact of irrigation on the south asian summer monsoon. *Geophysical Research Letters*, *36*(20).

Siebert, S., Henrich, V., Frenken, K., & Burke, J. (2013, 10). Update of the digital global map of irrigation areas to version 5. *Rheinische Friedrich-Wilhelms-Universituy, Bonn, Germany and Food and Agriculture Organization of the United Nations, Rome, Italy*. doi: 10.13140/2.1.2660.6728

Soares, P. M., Careto, J. A., Cardoso, R. M., Goergen, K., Katragkou, E., Sobolowski, S., ... et al. (2022). The added value of km-scale simulations to describe temperature over complex orography: the cordex fps-convection multi-model ensemble runs over the alps. *Climate dynamics*, 1–24. doi: 10.1007/s00382-022-06593-7

Thiery, W., Visser, A., Fischer, E., Hauser, M., Hirsch, A., Lawrence, D., ... Seneviratne, S. (2020, 01). Warming of hot extremes alleviated by expanding irrigation. *Nature Communications*, *11*. doi: 10.1038/s41467-019-14075-4

Tiedtke, M. (1989). A comprehensive mass flux scheme for cmulus parameterization in large-scale models. *Monthly Weather Review*, 1779-1800.

Tölle, M. H., & Churiulin, E. (2021, 10). Sensitivity of convection-permitting regional climate simulations to changes in land cover input data: Role of land surface characteristics for temperature and climate extremes. *Frontiers in Earth Science*, *9*. doi: 10.3389/feart.2021.722244

Udina, M., Peinó, E., Polls, F., Mercader, J., Guerrero, I., Valmassoi, A., ... Bech, J. (2024). Irrigation impact on boundary layer and precipitation characteristics in weather research and forecasting model simulations during liaise-2021. *Quarterly Journal of the Royal Meteorological Society*, *150*(763), 3251-3273. Retrieved from https://rmets.onlinelibrary.wiley.com/doi/abs/

10.1002/qj.4756 doi: https://doi.org/10.1002/qj.4756

Valmassoi, A., Dudhia, J., Di Sabatino, S., & Pilla, F. (2019, 09). Evaluation of three new surface irrigation parameterizations in the wrf-arw v3.8.1 model: the po valley (italy) case study. *Geoscientific Model Development Discussions*, 1-33. doi: 10.5194/gmd-2019-223

Valmassoi, A., Dudhia, J., Di Sabatino, S., & Pilla, F. (2020a, 03). Irrigation impact on precipitation during a heatwave event using wrf-arw: The summer 2015 po valley case. *Atmospheric Research*, *241*, 104951. doi: 10.1016/j.atmosres.2020.104951

Valmassoi, A., Dudhia, J., Di Sabatino, S., & Pilla, F. (2020b, 01). Regional climate impacts of irrigation in northern italy using a high resolution model. *Atmosphere*, *11*, 72. doi: 10.3390/atmos11010072

Valmassoi, A., & Keller, J. (2022, 11). A review on irrigation parameterizations in earth system models. *Frontiers in Water*, *4*, 906664. doi: 10.3389/frwa.2022.906664

Vanden Broucke, S., & Van Lipzig, N. (2017). Do convection-permitting models improve the representation of the impact of luc? *Climate Dynamics*, *49*, 2749–2763. doi: 10.1007/s00382-016-3489-5

Vergara-Temprado, J., Ban, N., Panosetti, D., Schlemmer, L., & Schär, C. (2020). Climate models permit convection at much coarser resolutions than previously considered. *Journal of Climate*, *33*, 1915-1933. doi: 10.1175/JCLI-D-19-0286.1

Wang, Y., Yang, B., Yang, Z., Feng, Z., Qiu, B., Dai, G., ... Zhang, Y. (2024, sep). Responses of summer mesoscale convective systems to irrigation over the north china plain based on convection-permitting model simulations. *Environmental Research Communications*, *6*(9), 091012. Retrieved from https://dx.doi.org/10.1088/2515-7620/ad78ba doi: 10.1088/2515-7620/ad78ba

Wilhelm, C., Rechid, D., & Jacob, D. (2014). Interactive coupling of regional atmosphere with biosphere in the new generation regional climate system model REMO-iMOVE. *Geoscientific Model Development*, *7*(3), 1093–1114. doi: 10.5194/gmd-7-1093-2014

Zhang, Z., He, C., Chen, F., Miguez-Macho, G., Liu, C., & Rasmussen, R. (2025). Us corn belt enhances regional precipitation recycling. *Proceedings of the National Academy of Sciences*, *122*(1), e2402656121. Retrieved from https://www.pnas.org/doi/abs/10.1073/pnas.2402656121 doi: 10.1073/pnas.2402656121

Eidesstattliche Versicherung | Declaration on Oath

Hiermit erkläre ich an Eides statt, dass ich die vorliegende Dissertationsschrift selbst verfasst und keine anderen als die angegebenen Quellen und Hilfsmittel benutzt habe.
Sofern im Zuge der Erstellung der vorliegenden Dissertationsschrift generative Künstliche Intelligenz (gKI) basierte elektronische Hilfsmittel verwendet wurden, versichere ich, dass meine eigene Leistung im Vordergrund stand und dass eine vollständige Dokumentation aller verwendeten Hilfsmittel gemäß der Guten wissenschaftlichen Praxis vorliegt. Ich trage die Verantwortung für eventuell durch die gKI generierte fehlerhafte oder verzerrte Inhalte, fehlerhafte Referenzen, Verstöße gegen das Datenschutz- und Urheberrecht oder Plagiate.

Ort, den | City, date
Hamburg, den 20.Mai 2025

Unterschrift | Signature
Christina Pop